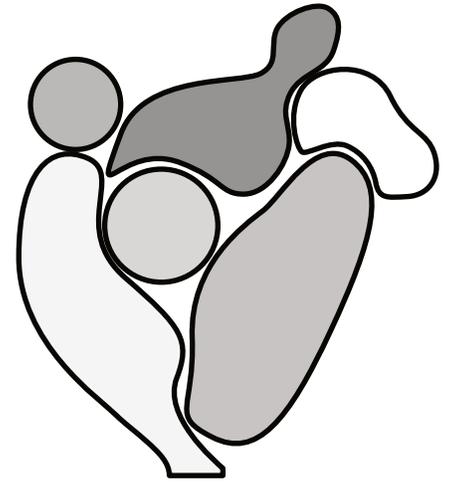# ENaC Isn't ASIC

A Study of Various Activating Mutations and Conditions of the Epithelial Sodium Channel

Presented by Richard Posert

to
the Biochemistry and Molecular Biology Graduate Program

and
Oregon Health and Science University School of Medicine

in partial fulfillment of the requirements for the degree of
Doctor of Philosophy

*For Lindsey, who shows me
that a better world is possible
by working to build it every day*

Table of contents

Frontmatter

Acknowledgements

It's impossible to acknowledge everyone who contributes to something like a PhD, and I won't attempt to do so. I will, however, mention people without whom and places without which I can be certain I would not have finished this whole thing.

First, my partner, Lindsey. My life is brighter and my path easier because you're in it.

Next, my dearest friends. I received some excellent advice when I was interviewing at graduate schools: "You only applied to places where the science interested you, and is of good quality. Now pay attention to the people who are here with you. You'll be spending six years with them." I decided to come to OHSU (which was *not* where I heard that advice) because I felt I could build a warm, kind, and supportive community here. I was right. So here is that community, presented in a computationally-randomized order.

I think I would have chased a more "prestigious" school without Tuck's guidance, and for that and everything else, I am ever grateful.

Ryan, what more is there to say after a literal dozen years of friendship. Thank you for being a steadfast companion, always willing to lend an ear or crack a window.

Casey and Ryan, you both mean the world to me and we miss you in Portland. I try to embody your Manic Host Energy whenever I'm entertaining. See you at thanksgiving.

Varchas, one of my favorite memories from the past six years is coming out into the dining room and seeing an empty box of Hi-Chews next to you at 6:30am, followed by an hour-long education in Indian politics. I cherish you.

Madeleine, what a joy it is to experience a conversion from "friend's partner" to "friend". I know I can rely on you and confide in you, and I hope you feel the same for me. Thank you for encouraging me to reach, and for pushing me over the finish line. See you at Vida.

John, not sure how you made it in this list. Can I still edit this?

Nigel, it's hard to make friends as an adult but you make it easy.

Sam and Becca (aka The Pod), you helped me survive 2020 and thrive since. Thank you for agreeing with me about Lindsey's pronunciation of /tʃeɪz ˈlɒ̃g/.

Thank you to Noah and Caz and especially Emlyn for some of the greatest Monday nights dice can dream of.

Alexis, you inspire me to keep trying new things and to trust I can learn to be creative.

Britt, the chaos you bring out in me is almost certainly good for me. Probably. I eagerly await your next midnight update on the home datacenter.

Gaelen, my number one hype man. I'm waiting in the wings to get you out the door too. I'm glad I tricked you into staying in Portland.

Liz, come on back to the West Coast. I'm glad you followed the science you're interested in, but I'm happier you're coming back.

Of course, to get a PhD in a lab science, you do unfortunately have to do some lab work. I did not enjoy this, but it was made bearable by my wonderful lab mates, Sigrid, Alex, and James. I also want to thank Nate, Zad, and Johannes from the Gouaux lab for helping me learn both how to do science and how to work in a high-pressure environment. Sarah, too, deserves some accolades for being an early guinea pig for me figuring out how to teach people cryoEM.

My cat, Nooch, certainly made this more difficult if anything, but it feels appropriate to at least mention her.

I consider myself lucky that as I approached a committee meeting I was more anxious about making Jonathan, Swetha, Dave, and Steve proud than about how they'd treat me. Thank you all for your kindness and guidance. Steve deserves special mention for helping me through the last year or so of the process and making sure I never read *too* deeply into my garbage TMD maps.

Finally, thank you to Shoofly and Honey Latte, where I wrote my dissertation and defense seminar. All told, it took me $624.43 of coffee, pastries, and breakfast burritos to write this document.

ENaC - An Overview

Structural biology is ultimately the study of particular domains and residues, but this knowledge most interesting and useful in the context of physiological processes. As such, it can be difficult to order the chapters of an introduction. Placing the structure before the function grounds discussion of mutations and disease, but leaves the structure unmoored from biomedical relevance. Conversely, placing function first leaves the reader without a clear understanding of which domains are important for which reasons, which is vital for a focused discussion of the protein.

To dodge the question of which is the cart and which is the course, I present here an exceedingly brief (and less heavily cited) discussion of ENaC structure and function. Everything covered here is covered in more detail in the Introduction. ENaC biology is discussed in Chapter 1, while details on the ENaC/DEG family and ENaC structure can be found in Chapter 2.

A bit of ion channel terminology

Ion channels are essential components of cellular life, present in everything from bacteria on up to humans. The minimal ion channel spans the lipid bilayer and allows ions to flow through a pore down their concentration gradient. We can measure the flow of ions through a single channel as a current (called the *unitary current*).

However, most ion channels have some mechanism by which the flow of ions can be controlled. We thus say an ion channel can be "open" or "closed", i.e., it can allow ions to flow through itself or not. This process is called *gating,* and is most often controlled by either voltage (voltage-gated ion channels) or some ligand (ligand-gated ion channels).

ENaC is a bit unique in that the ligand is a part of the channel itself, but that's beside the point

5

We can further quantify a channel's "openness" by how much time it spends in the open state vs. the closed state. A channel with an *open probability* (P_O) of 0.75 spends approximately 75% of its time in the open state and 25% of its time in the closed state.

Open probability and unitary currents are both properties of *single channels*. Groups of channels (for instance, all of the channels in a cell) do not have a measurable P_O, since the group will not be homogeneous.

For instance, say there is a collection of 100 ion channels. Twenty of those channels are bound to ligand, and seventeen of those channels are open. Eighty channels are not bound to ligand, and twenty-two of those channels are open. Do we only consider the ligand-bound channels, making the P_O $\frac{17}{20}$? Or maybe we should consider only the apo channels, making it $\frac{22}{80}$? Or perhaps we consider the whole population: $\frac{39}{100}$? Or is it maybe the mean P_O of both groups, $\frac{\frac{17}{20}+\frac{22}{80}}{2}$?

In practice, we'd probably describe this set of 100 channels as two populations: the open population with a P_O of 0.85 and the closed population with a P_O of 0.275. Ligand binding would move a channel from the closed to the open population, and ligand dissociation would move it back to the closed population.

Typical electrophysiology experiments measure the *macroscopic current*: how many ions flow through all of the channels of a given type in a cell. This is represented as *I*, with the current due to a particular ion, e.g., sodium as I_{Na^+}. Ion channels are often selective for a particular ion or set of ions. For instance, a sodium-specific ion channel will allow Na^+ but not other ions through, while a cation-selective channel will allow Ca^{2+} and K^+ but not Cl^-. Macroscopic current is affected by the number of channels in each gating state, the P_O of those states, the unitary current of the open channels, and the number of channels in the membrane (*N*). Further review is available from Hille or Ackerman and Clapham[1,2].

The ENaC/DEG family

The epithelial sodium channel (ENaC) is, perhaps obviously, a member of the ENaC/DEG family of ion channels. These channels are

trimeric, pass cationic currents, are voltage-insensitive, and are inhibited by the small molecule amiloride (and its derivatives). Amiloride blocks current through ENaC/DEG channels by binding a surface in the extracellular to the selectivity filter and blocking the pore.

The overall topology of these channels is similar, with the greatest sequence (and, presumably, structural) diversity found in the distal ECD (furthest from the membrane). Current structural study suggests a conserved overall gating mechanism as well.

Aside from ENaC, the best-studied members of the ENaC/DEG family are the eponymous degenerin (DEG) channel and the acid-sensing ion channel, ASIC. DEG is expressed in *C. elegans* and is involved in mechanosensation. ASIC is expressed in a variety of organisms (including humans) and opens in response to acidic extracellular conditions. ASIC has by far the best-described structure of the family.

ENaC Structure

ENaC is a triheteromeric ion channel comprising three subunits, the α, β, and γ subunits. Each subunit shares an overall similar topology, and so I describe them here without reference to a specific one.

For most figures in this document, I color the α subunit blue, the β subunit red, and the γ subunit magenta.

The transmembrane domain, or **TMD**, contains the pore and selectivity filter. The extracellular domain, or **ECD**, contains domains important for regulating open probability (P_O) and other functional characteristics. There are also short intracellular N- and C-terminal tails which regulate surface expression.

The ECD is further subdivided into six domains, named after the parts of a hand. The **palm** and **β-ball** form a rigid backbone and make the plurality of the contacts with the other subunits. The **knuckle**, **finger**, and **thumb** likely move during channel gating and contain important glycosylation sites.

The **GRIP** domain is unique to ENaC. ENaC opens when the GRIP domain is excised from the channel. The canonical proteases responsible for channel opening are: furin, which cuts the α subunit twice and γ subunit once; and prostasin, which cuts the γ subunit again.

Removal of the GRIP domain is thought to allow the finger and thumb to collapse together. This movement is coordinated with movement

Figure 1.: An overview of ENaC structure. Everything except the TMD is collectively called the ExtraCellular Domain (ECD).
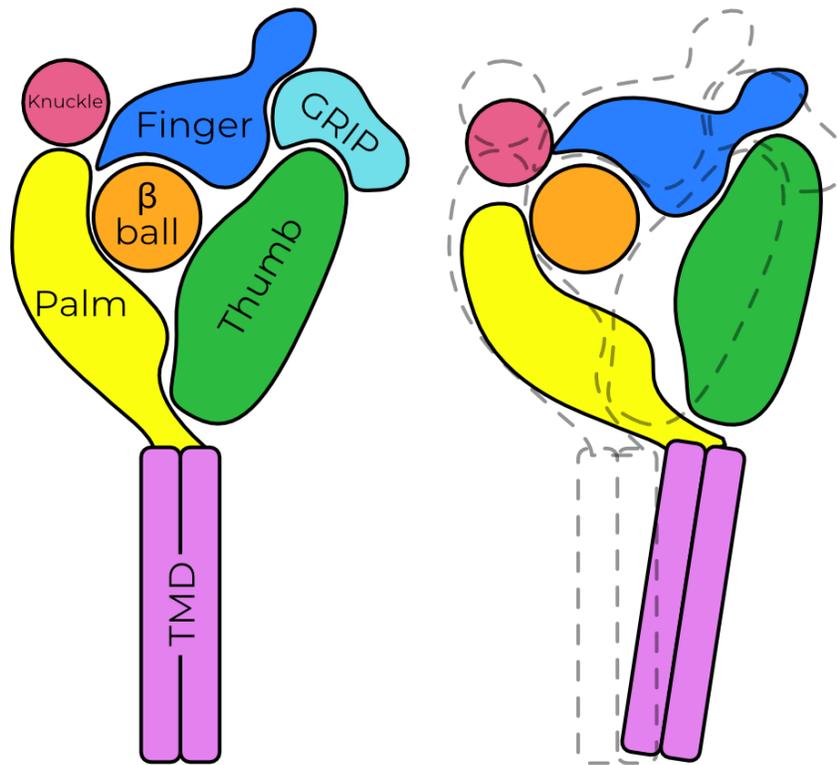
Figure 2.: An exaggerated model of ENaC opening. **Left**: an uncleaved subunit. **Right**: after GRIP is removed from the channel, the finger and thumb collapse together, pulling the TMD away from the pore axis and opening a fenestration.

of the palm away from the pore axis, which in turn opens a fenestration just above the membrane. Ions enter at this fenestration and pass down a pore formed by the second transmembrane helix, TM2.

Along this pore, ions larger than sodium are filtered out by size. It is thought that this selectivity filter is formed by a three-residue loop connecting swapped domains of TM2, but an un-swapped conformation is also possible.

The above summary of ENaC's presumed gating mechanism is based largely off cross-linking electrophysiology studies and ASIC's well-described gating mechanism. In ASIC, protons allow for finger/thumb collapse (recall that ASIC does not have a GRIP domain). However, ASIC rapidly desensitizes and ENaC does not.

ENaC Function and Regulation

The regulation and function of ENaC in the body is not entirely understood, but broadly, ENaC functions as the rate-limiting step of sodium reabsorption in tissues which express it. Thus, control of ENaC expression also controls water retention and reabsorption in those tissues.

ENaC is best studied in the kidney, where it plays a pivotal role in blood pressure regulation. When the kidney detects reduced blood pressure, it initiates a cascade which results in increased circulating levels of the mineralocorticoid hormone aldosterone. Aldosterone increases overall expression of ENaC, the proportion of ENaC at the cell surface, and the proportion of channels which are open (i.e., have an excised GRIP domain). For more detail on aldosterone and ENaC regulation in the kidney, see Section 1.2.1.
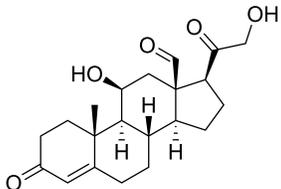
Figure 4.: Aldosterone

Cells with more ENaC at the surface allow more sodium to pass from the lumen to the interstitial fluid. This in turn results in increased water retention, thus raising blood volume and pressure.

Since the channel is activated primarily by proteolysis, ENaCs cannot close again once opened. Open channels are tagged for retrieval from the plasma membrane and degradation via ubiquitination on the N-termini each of the three subunits. Additionally, ENaC is sensitive to membrane composition and requires PIP_2 to open.
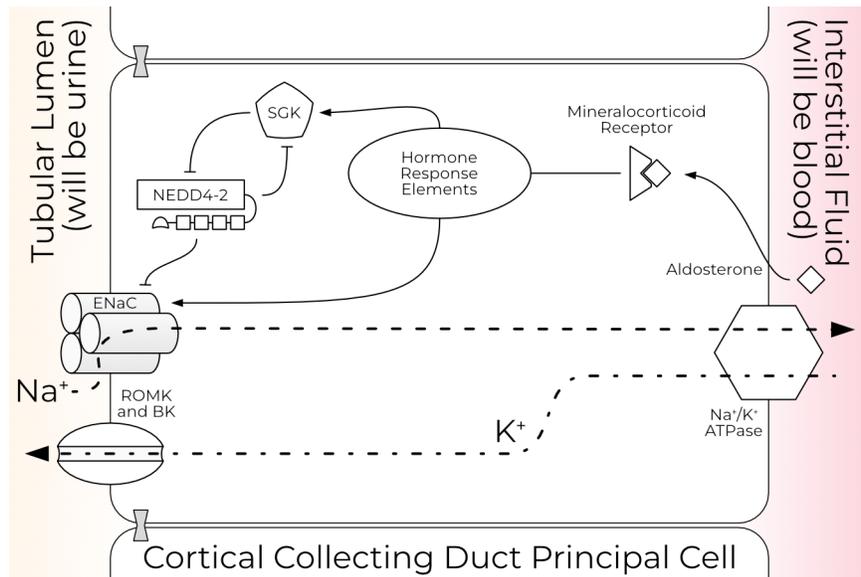
Figure 3.: Function and regulation of ENaC in the kidney. Each component is covered in more detail in Section 1.2, but the essential observation is that ENaC is the rate-limiting step in sodium reabsorption.

This is, I believe, enough of a background to move on to a full introduction of the topics covered in the remaining document. The reader is also encouraged to check the glossary for unfamiliar terms and abbreviations.

Part I.

Introduction

1. ENaC Physiology and Regulation

As a guide to the importance of ENaC for human health, I will begin with a background in the physiological functions of the channel. Chapter 2 provides a deeper investigation of ENaC's structure/function relationships. As a brief orientation, ENaC is a highly sodium-specific triheteromeric sodium channel expressed throughout the human body. The channel comprises one copy each of three paralogs: α-, β-, and γENaC. ENaC is thought to be activated by proteolytic removal of a portion of its extracellular domain and is potently inhibited by the small molecule amiloride and its derivatives.

I focus here on the systems in which we best understand ENaC's role: the lung and kidney. I next move on to other systems which provide important information about ENaC but have a smaller body of research. I will finish the chapter with an overview of the molecular mechanisms of ENaC regulation at the expression level.

While this chapter may seem unnecessarily detailed for our purposes, I believe it is important to understand both ENaC's role in several human diseases, the degree to which mouse models fail to recapitulate those diseases, and the shortcomings of viewing the channel only from the vantage of the kidney. This understanding is especially important when considering the limitations inherent to functional work performed in mouse tissue or on mouse proteins.

1.1. ENaC in the body

1.1.1. ENaC in the kidney

Blood pressure must be maintained within a narrow window of acceptable values. Too low, and vital organs do not receive sufficient oxygen and nutrients to function, but too high and blood vessels sustain damage. It is not surprising, then, that the human body has evolved several mechanisms for responding to changes in blood pressure, each with their own timescale ranging from milliseconds to weeks[3]. ENaC is the essential mechanism of the longest-term control, kidney excretion.
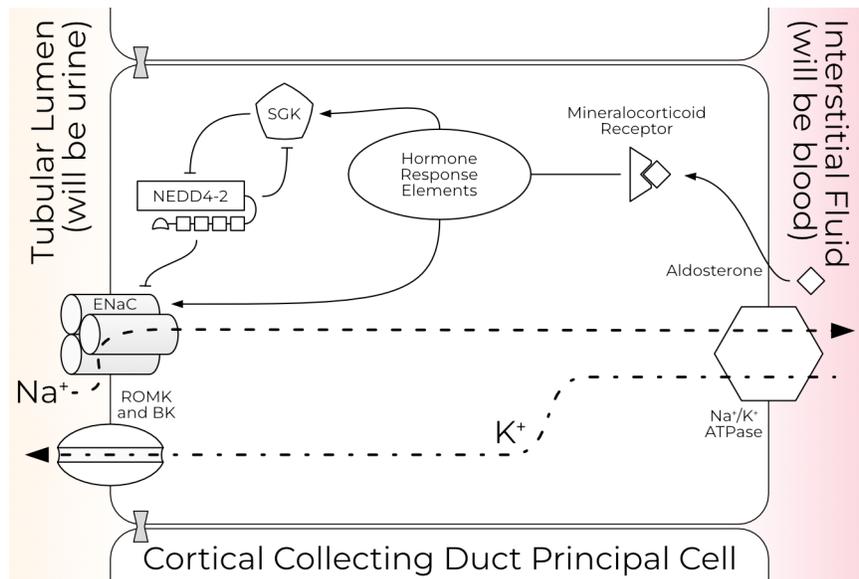
Figure 1.1.: Simplified model of ENaC regulation in a principal cell of the distal nephron in the kidney.

In the principal cells of the kidney, sodium travels down its concentration (into the cell) gradient across the apical membrane via ENaC (Figure 1.1). From there, it is transported across the basolateral membrane by the Na^+/K^+ ATPase. ENaC currents therefore induce retention of extra water to maintain the tightly controlled plasma sodium level. Thus, ENaC controls three essential functions of kidney filtration: first, the amount of sodium reabsorbed by the kidney; second,

blood volume (and therefore pressure); and third, the amount of potassium passed from the plasma into the urine.

A variety of ENaC mutations have dramatic effects on patients' blood pressure. One of the earliest described is Liddle syndrome[4]. Liddle syndrome (also called pseudoaldosteronism) results from an autosomal dominant gain-of-function mutation in ENaC. Hallmarks of the disease include severe hypertension, low potassium, high blood pH, low renin activity, and low aldosterone levels[5]. The disorder is thought to be rare, with only 72 families described as of 2018[6]. However, after excluding patients with other clear causes (primary aldosteronism, kidney or heart diseases, and obstructive sleep apnea), approximately one in one hundred hypertensive patients had Liddle syndrome, indicating that the prevalence may be higher than is currently thought[7,8].

All but one of the described cases involve mutation of the β or γ subunits[6,8]. A majority of these disrupt or remove entirely a proline-rich PY motif at the C-terminus of those channels[9]. This PY motif is the binding site for the E3 ubiquitin ligase Nedd4-2 (see Section 1.2.2). ENaC lacking the PY motif cannot be retrieved from the membrane, thus increasing sodium permeability by increasing N rather than the conductivity or P_O of the channels[10–12]. The remaining minority of described Liddle syndrome mutations (including the sole $ENaC_\alpha$ mutation) which do not affect PY-motif binding instead directly augment channel P_O[6]. Liddle syndrome is typically treated with small molecules that block ENaC (amiloride or triamterene) and a low-salt diet.

> The α subunit does have a PY motif, but no Liddle syndrome mutation of the α PY has been described. This is discussed further in Section 1.2.2.2.

Mouse models of Liddle syndrome complicate the situation somewhat. Mice with homozygous mutant Liddle βENaC fed a normal salt diet do not develop the characteristic high blood pressure, low potassium, and acidosis as humans do[13]. These phenotypes only develop with a high-salt diet. Moreover, these mice are still able to retrieve ENaC from the cell surface in the colon (unlike human Liddle patients)[14]. It is thus not clear that the mouse model of Liddle syndrome is fully applicable to the human disease.

Loss-of-function mutations also cause severe phenotypes. Type 1 pseudohypoaldosteronism (PHA1) was first described in a severely dehydrated infant who did not respond to aldosterone treatment[15]. There are two forms of PHA1: renal PHA1, which is milder and involves a mutation in the mineralocorticoid receptor; and systemic

> This may be due to incomplete penetrance of the mutant gene or differences in human and mouse Nedd4-2 function. For instance, if mouse Nedd4-2 does not require both the β and γ PY motifs, the channels could still be retrieved from the membrane.

17

PHA1, which involves a mutation in a gene for ENaC α, β, or γ[16,17]. Patients with systemic PHA1 are unable to retain any salt, and so become severely dehydrated and have high potassium, low sodium, and increased acidity in their blood[5]. This makes the disease particularly deadly to newborns. Treatment typically includes life-long supplementation with sodium and the potassium elimination drug Kayexalate[18].

Contrary to the pattern observed for Liddle Syndrome, most systemic PHA1 mutations occur in the gene encoding $ENaC_\alpha$[18]. The majority of described PHA1 mutations are nonsense mutations, although three missense mutations have been described[17–19]. One of these mutations occurs in the palm domain, one in the transmembrane domain, and one likely in the intracellular domain.

Although the genes for the β and γ subunits are both on chromosome 16 and the gene for $ENaC_\alpha$ is on chromosome 12, no difference in the rates of mutation for the affected genes are seen between patients and control groups[18].

1.1.2. ENaC in the lung

Cystic fibrosis (CF) is a recessive genetic disorder which affects many organs, most prominently the lungs. Patients with CF have thick airway mucus they are unable to clear, causing chronic airway infections and lung damage. Patients with CF also lose salt but, unlike patients with PHA1, the causative mutation is in the *CFTR* gene rather than an ENaC gene.

CFTR encodes a cAMP-regulated chloride channel, CFTR[20]. Pathogenic CFTR mutations dramatically reduce chloride permeability, resulting in poor reabsorption of Cl$^-$ in the lungs[21]. Reduced chloride absorption increases the absorption of sodium to maintain electrostatic balance. The cells then absorb more water to maintain osmolarity. This, in turn, dehydrates and thickens the airway surface liquid (ASL), which damages the underlying tissue and prevents mucous clearance[22–24].

The interplay between CFTR and ENaC in CF patients is complicated and not fully understood. Treatment of normal, but not CF, lung epithelia with amiloride augments Cl$^-$ transport[25]. Cells co-expressing CFTR and ENaC show smaller ENaC currents than do cells expressing only ENaC, but this effect depends on both CFTR's ability to pass Cl$^-$ and ENaC's intracellular termini[26]. Mice which overexpress βENaC in the airway show CF-like symptoms, including reduced airway liquid height and mucous clearance[27]. It would seem that the function of

Interestingly, mice overexpressing the α or γ subunits did not show CF-like symptoms. The authors point to prior research showing that αβ-only channels have a higher P_O than αβγ[28].

18

the two ion channels is linked both by electrochemical gradients and potentially other regulatory partners.

The relationship between ENaC-mediated Na^+ absorption and CF or CF-like disease turns out not to be so neat. In mice which overexpress βENaC and CFTR, one would expect the CF-like symptoms from increased βENaC expression to be rescued by increased Cl^- secretion. In actuality, said mice exhibit neither of these traits[29]. Additionally, Liddle syndrome patients have increased sodium absorption in all ENaC-expressing tissues but neither they nor Liddle syndrome mice develop CF-like lung disease[30]. In the opposite pattern of the mouse models, human patients with *reduced* βENaC function develop CF-like phenotypes of lung infection and elevated sweat chloride[31]. More confusingly, PHA1 patients (which have reduced ENaC expression in all tissues) produce excessive airway liquid as in CF-like disease, but this liquid does not become infected[32].

There are many hypotheses as to how these contradictions may be resolved, reviewed well by Collawn and colleagues, but more work on the subject is desperately needed[33]. The important point for our purposes is that, as with Liddle syndrome, the mouse CF model does not recapitulate human disease well. Indeed, mice with CFTR mutations which are pathogenic in humans do not develop lung disease at all[34].

For instance, it could be that βENaC and/or CFTR are being knocked into the wrong cell types, or that the time scale of the effect is longer than is currently thought.

1.1.3. ENaC in the tongue

As one might expect for a sodium-specific ion channel, ENaC is also implicated in taste. Although it may seem a less clinically essential tissue, ENaC function and expression in the tongue differs significantly from what is expected based on the better-studied kidney. It is therefore useful as a spotlight on how little we still know about the very basic stoichiometry and function of the ENaC subunits.

The organization of taste in the mammalian tongue is complex, but well-reviewed by Yarmolinsnky and colleagues[35]. Briefly, taste buds comprise 50–100 taste receptor cells (TRCs). Each TRC expresses receptors for and responds to just one of the five basic tastes: salty, sweet, sour, bitter, and umami[36,37]. These receptors are highly diverse, with closely related species having widely varying taste responses to the same molecule.

For instance, hamsters do not taste aspartame as sweet[38].

19

1. ENaC Physiology and Regulation

Salt sensation is further divided into an appetitive taste (e.g., a potato chip) and an aversive taste (sea water). Amiloride blocks rats' ability to taste the difference between KCl and NaCl and reduces their voluntary NaCl (but not KCl) consumption[39,40]. Thus, the appetitive taste is taken to result from Na^+ currents in amiloride-sensitive TRCs, while the aversive NaCl taste results from Cl^- currents in amiloride-insensitive TRCs[41]. ENaC seems a prime candidate for the amiloride-sensitive Na^+ current; indeed, all three subunits are detected in taste buds but not the surrounding epithelia[42]. Mice with αENaC specifically knocked-out in mature TRCs lost their preference for salt, and those TRCs no longer responded to low Na^+ concentrations[43]. However, recent work has significantly complicated the role of αβγ ENaC in salt taste.

Investigation of ENaC expression patterns in mouse taste buds show that no taste bud cell expresses both the α and β subunits[44]. αENaC homomeric channels pass small (100 times smaller than αβγ) currents when expressed alone in oocytes[45]. Homomeric α channels may, therefore, carry the amiloride-sensitive salt taste. However, amiloride-sensitive salt perception depends on the mouse line, and the line used in the expression pattern study has a low amiloride sensitivity[46]. Thus the possibility remains that salt taste in mice is mediated by αβγENaC and is simply harder to detect with this experimental setup. Homomeric α channels may instead carry the amiloride-sensitive salt taste.

Perhaps more importantly, salt taste in humans is insensitive to amiloride[47]. Additionally, humans express δENaC (a fourth subunit which is a pseudogene in rats and mice) in the taste bud, rather than αENaC[48]. As with CF and Liddle syndrome, the mouse model of taste is a poor facsimile of the process in humans.

Despite this fact, salty taste illustrates an important unanswered question regarding ENaC: what is the full complement of physiologically relevant, functional ENaC channels? Canonical ENaCs are composed of one each of the β, γ, and either α or δ subunits. However, the combination of αENaC knock-out mice and ENaC expression patterns makes it likely that channels with only one or two ENaC subunit types, while rare, are physiologically relevant.

I note here that we cannot say these channels are homomeric αENaC channels. They may be assemblies of ENaC with other ENaC/DEG family members or as-yet unknown other proteins. Regardless of the

The composition of the channel likely affects their sensitivity to amiloride as well, although since the entire ENaC/DEG family is blocked by amiloride at one concentration or another one would expect that these combinations would be as well.

20

ultimate identity of the amiloride-sensitive salt taste receptor, the patterns observed in taste are difficult to explain if the only physiologically relevant ENaC is the (α/δ)βγ triheteromer, which makes it an interesting and valuable system for further study.

1.1.4. ENaC in blood vessels

Myogenic vasoconstriction is an important component of blood pressure regulation in which the diameter of a blood vessel decreases in response to increased blood pressure. This response is essential for maintaining proper blood flow. ENaC is expressed in the vascular smooth muscle cells responsible for the constriction of blood vessels[49,50]. Treatment with amiloride or its derivatives reduces myogenic tone in a dose-dependent manner. This fact, combined with the knowledge that channels related to ENaC are mechanosensitive in worms, makes ENaC a likely candidate for the pressure sensor responsible for myogenic vasoconstriction[51].

Not to belabor an earlier point, but only β and γ ENaC are detected in *ex vivo* preparations of vascular smooth muscle cells, while those subunits plus α are detected in cultured cells.

Similarly, systemic blood pressure is monitored by the central nervous system via baroreceptors. Baroreceptors keep mean arterial pressure at a steady level on a short time scale[52]. These neurons express β and γ, but not α, ENaC[53]. Treatment with amiloride or its derivatives blocks both the response of these neurons to physical stimulation and blood pressure regulation. It therefore seems likely that ENaC is used by baroreceptors to sense blood pressure, but further research is necessary to strictly define this role.

1.1.5. ENaC in the colon

ENaC plays an important role in sodium reabsorption in the colon. Colon expression of the β and γ subunits increases in response to aldosterone treatment, while α expression remains constant[14,54]. Patients with Crohn's disease, a chronic inflammatory bowel disease, have reduced sodium reabsorption in the colon, which leads to diarrhea[55,56]. Similarly, patients with ulcerative colitis have reduced ENaC expression due to inflammatory cytokines, resulting in water loss and diarrhea[57]. To be clear, the colon relies on a wide array of systems to reabsorb ions and water. These results indicate that ENaC is one of the players in this process.

1.2. Regulation

It should come as no surprise that expression of ENaC is under tight control, given the number of important processes ENaC is implicated in. In this section I provide a general, by no means exhaustive review of proteins known to regulate ENaC at the expression level. A discussion of molecular mechanisms by which ENaC P_O is modulated benefits from further background in ENaC structure and is therefore covered in Section 2.4.

This overview of ENaC regulation is necessarily brief and limited to the kidney (Figure 1.1), since that system is best understood. Fortunately, the patterns observed in the kidney largely hold in other tissues with the notable exception of aldosterone-induced expression.

1.2.1. Aldosterone

Aldosterone is the primary mineralocorticoid hormone and the main mechanism by which the body regulates plasma sodium levels. When the kidney is not receiving enough salt, it initiates a cascade to (among many other effects) increase activity of ENaC via the hormone aldosterone. ENaC is also regulated by other hormonal signals, including vasopressin and insulin, but a review of those mechanisms is outside the scope of this work. For the interested reader, Garty and Palmer's review of the complete picture of ENaC regulation is quite thorough if a bit old[60].

For a review of the Renin-Angiotensin-Aldosterone System consider Weir and Dzau[58]. For a review more focused on aldosterone alone, Stockand's is quite thorough and readable[59].

Aldosterone response is divided into two phases, aptly named the early and late phases. In the early phase, aldosterone increases ENaC P_O in part via increased activity of serum and glucocorticoid-regulated kinase (SGK, Section 1.2.3)[61,62]. SGK's effect has mainly been attributed to inhibition of Nedd4-2 (Section 1.2.2), while some labs also report a direct increase in ENaC P_O[63,64]. Aldosterone also stimulates phosphatidylinositol 3-kinase (PI3K) and K-Ras, which promotes the physical interaction of ENaC and PI3K[65,66]. Phospholipids have both short- and long-term effects on ENaC currents and are discussed further in Section 2.4.2.1. The majority of aldosterone's early-phase effect on sodium currents is due to increased P_O of existing channels, rather than delivery of new channels to the cell surface[67].

Aldosterone's late phase increase of sodium permeability is mediated both by direct increase of ENaC gene expression and movement of ENaC from an internal pool to the apical membrane[68–71]. In some studies, aldosterone increases transcription of the β- and γ- (but not α-) ENaC genes[14,68,72–74]. In others, increases in αENaC transcription are also (or exclusively) observed[71,75–79]. The effect of aldosterone does seem to be consistent within tissue types: most studies demonstrating an increase in αENaC transcription are performed in the kidney, while aldosterone increases β and γ transcription in the colon. ENaC transcription in the lung is less dependent on circulating aldosterone levels than other tissues[80].

1.2.2. Nedd4-2

Nedd4-2, also known as Nedd4L, is a HECT E3 ubiquitin ligase. E3 ligases perform the final step in the ubiquitination cascade: the transfer of an activated ubiquitin (Ub) from an E2 to the substrate. Nedd4-2 is the cognate E3 ligase for ENaC in humans, rats, and mice (but not *Xenopus*). Ubiquitination of ENaC by Nedd4-2 results in internalization and degradation of the channel, reducing the cell's Na^+ permeability. Study of ENaC surface dwell time is complicated by a reserve pool maintained by the cells to be cycled up to the membrane, but there is a consensus that ENaC is recycled quickly; surface half life estimates range from fifteen minutes to three hours, with the low end having more support[81]. Disruption of this mechanism is the most common cause of Liddle syndrome (Section 1.1.1), indicating the essential role Nedd4-2 plays in regulation of ENaC surface expression.

In older literature, this process is called "Sodium Feedback Inhibition".

1.2.2.1. Nedd4-2 Structure

Like many members of the HECT ligase family, Nedd4-2 has an N-terminal C2 domain, three or four (depending on the species) WW domains, and a C-terminal HECT domain (Figure 1.2). As the astute reader has already guessed, humans also express a paralogous HECT E3 ligase, Nedd4, which does not regulate ENaC *in vivo*[82,83]. It is important to note that expressing *either* of these two ligases heterologously *does* reduce ENaC currents. This makes evaluation

WW Domains bind PY motifs on ENaC

C2 Domain
Protein-protein
and lipid
interactions

C-lobe is flexible to
pick up Ub from the
N-lobe (grey) and move
it to the substrate (white)

HECT Domain
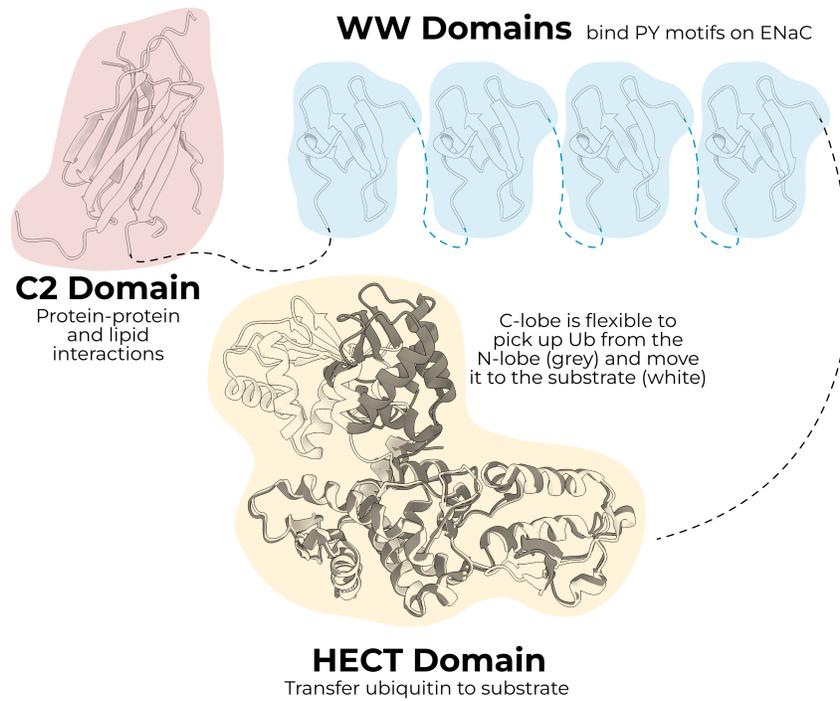Transfer ubiquitin to substrate

Figure 1.2.: The domains of Nedd4-2. Crystal structures for the C2
domain, WW domain, and the two flexible positions of
the HECT domain from PDBs 3M7F, 4N7H, 2XBB, and
2XBF respectively.

of the Nedd4-2/ENaC literature complicated, as conclusions drawn from heterologous systems may not hold in the organism.

In any case, the two proteins are 63% identical, and although there are differences in substrate affinity, the function of the domains in an abstract sense is quite similar. As such, I will present research on both proteins, preferring results from Nedd4-2 when possible, and highlighting points where the findings may not be fully generalizable.

The C2 domain is a Ca^{2+}-dependent phospholipid and protein-binding domain. Increased intracellular Ca^{2+} induces translocation of Nedd4 from the cytosol to the membrane[85]. This apical targeting is the result of an interaction between the C2 domain and Annexin XIIIb[86].

For a good review of general C2 domain evolution, structure, and function see Rizo and Südhof[84].

WW domains are protein-protein interaction domains comprising a three-stranded β-sheet. These small domains bind PY-motifs (PPXY), including those found in each ENaC subunit (PPAY, PPNY, PPKY in human α, β, and γ respectively). It is the removal of these domains that causes Liddle syndrome in truncation mutants[87]. Nedd4-2 cannot bind the Liddle mutants, and so the cell cannot pull the open channels from the surface, resulting in a gain of function. Interestingly, mice and rat Nedd4-2 have three WW domains, while human Nedd4-2 has four.

The HECT domain is the business end of the protein. Unlike RING ligases, HECT ligases form a thioester bond with Ub before transferring it to the substrate. The domain itself is split into the N-lobe, which is larger and interacts with the E2 enzyme, and the C-lobe, which contains the catalytic cysteine.

Buetow and Huang's review of E3 ligase structure is very good, and includes HECT ligases[88].

HECT ligases have several auto-inhibitory functions to prevent inappropriate ubiquitination. The C2 domain intramolecularly binds the HECT domain near the catalytic cysteine, blocking function[89]. The HECT domain also has an internal PY motif which is bound by its own WW domain[90]. Nedd4-2 remains bound this way until it encounters a substrate, at which point it binds and ubiquitinates the target. The enzyme then ubiquitinates itself, targeting it for degradation. Finally, the linker between WW domains 2 and 3 blocks function of the HECT domain in Nedd4[91].

It is not currently known which WW domain binds this internal PY motif, or if the association is intra- or intermolecular.

1.2.2.2. Nedd4-2 and ENaC

Nedd4-2 is expressed throughout the body but is most abundant in the kidney and lung[92]. In a high-salt diet (i.e., low-aldosterone), the WW domains bind ENaC's PY motifs and ubiquitinate the channels, causing them to be internalized and degraded[63,93–95].

The functional importance of lipid binding by the C2 domain is unclear. In heterologous systems, both Nedd4 and Nedd4-2 inhibit ENaC currents with or without a C2 domain, and both rats and humans express splice variants of Nedd4-2 which is missing the C2 domain[96–99]. In fact, C2-less Nedd4 suppresses ENaC currents more than WT Nedd4 in heterologous systems[96,100]. This may indicate that the C2 domain is more important as a regulatory, rather than functional, domain. However, mice expressing Nedd4-2 without a C2 domain fail to regulate ENaC in response to a high-salt diet and develop hypertension, leaving open the possibility that the membrane-binding functionality is more important *in vivo*[101].

Nedd4-2 relies on a subset of its WW domains to bind and regulate ENaC. In humans, only WW3 and WW4 of Nedd4-2 are required to reduce ENaC currents[102]. Human WW2 does bind ENaC weakly, while WW1 does not seem to interact with any ENaC subunit. Differential affinity among the WW domains is observed in other species as well[96,103].

Nedd4-2 does regulate many other proteins — it is possible that WW1 is required to regulate these other targets.

Once ENaC is bound, the HECT domain begins ubiquitinating N-terminal lysines on the channel[95]. Although lysines in each subunit are ubiquitinated, the γ subunit lysines are required for ubiquitination of α- and βENaC.

Several constitutively-expressed deubiquitinating enzymes (DUBs) oppose ENaC ubiquitination[104–106]. Interestingly, DUBs increase the relative amount of cleaved (i.e., active; see Section 2.4.1) ENaC at the cell surface. It is not known whether this effect is a direct result of DUB binding and action, or a simple follow-on effect of longer surface dwell time due to reduced recycling.

HECT domains are capable of serial ubiquitin addition, in which the C-terminus of ubiquitin is connected to the N-terminus or one of several lysines on the nascent chain[107]. Different chains determine the fate of the tagged protein; Nedd4-2 preferentially produces chains of

ubiquitin connected by lysine 63 (K63 chains)[108]. K63 chains most often send substrates somewhere other than the proteasome for degradation or recycling. In the specific case of ENaC, some groups have reported lysosomal degradation, while others report a combination of proteasomal and lysosomal targeting[94,95,110]. Regardless of ubiquitinated ENaC's ultimate destination, the interplay of Nedd4-2 and ENaC is critical to the overall sodium permeability of the cell.

For a review of the roles different ubiquitin chains play, I recommend Komander and Rape[109].

1.2.3. SGK and 14-3-3

Serum- and glucocorticoid-induced kinase (SGK) is a serine/threonine kinase expressed in several tissues including heart, brain, lung, and kidney[111]. Transcription of SGK is directly induced by a multitude of signals, including aldosterone[62,64,112].

Mice lacking SGK present a salt-wasting phenotype and high serum aldosterone, similar to the symptoms seen in PHA1 patients (Section 1.1.1)[113]. SGK increases ENaC surface expression and currents by disrupting the Nedd4-2/ENaC interaction by phosphorylating Nedd4-2[79,83,114]. SGK is itself, in turn, ubiquitinated by Nedd4-2[116]. This establishes a tight negative feedback loop which imparts a sharper temporal dependence of SGK expression on aldosterone.

SGK also directly interacts with and phosphorylates αENaC[117,118]. This association increases ENaC activity even in channels lacking the C-terminal PY motif[119].

Interestingly, SGK has an internal PY motif which is critical for Nedd4-2 binding[115]. It's not known whether this PY motif, 14-3-3 bridging, or both are necessary for Nedd4-2 ubiquitination of SGK.

Phosphorylated Nedd4-2 is bound and inhibited by 14-3-3, which is a protein that binds other phosphorylated regulatory proteins[120,121]. Humans express seven isoforms of 14-3-3; at least the β, ε, and η isoforms are known to dimerize and regulate Nedd4-2[122,123]. 14-3-3 binds with a high affinity to Nedd4-2 phosphorylated at serines 342 and 448.

14-3-3 binding rearranges and reduces the solvent accessibility of WW domains 3 and 4 (which are essential for ENaC binding) and the catalytic cysteine[123,124]. It is likely, then, that 14-3-3 regulates Nedd4-2 both by blocking its catalytic activity and sterically preventing Nedd4-2/ENaC.

Pohl and colleagues demonstrate that all seven isoforms are able to bind at least one of the two 14-3-3 binding sites in Nedd4-2, but this does not necessarily translate to inhibition of Nedd4-2 function[123].

1.3. Conclusion

ENaC is a tightly regulated ion channel implicated in a vast array of biological functions, from blood pressure control to the pleasurable taste of salty food. I have provided here a brief overview of the tissues in which ENaC expression is responsive to aldosterone (the body's main salt regulatory hormone) as well as the proteins involved in coordinating its expression.

I hope I have also highlighted the great amount we do not know about the channel. ENaC's function and regulation in the kidney is well-studied, but the trends observed in that tissue do not translate well to the lung (in which Liddle syndrome patients do not develop disease) or tongue (in which no heterotrimeric channels seem to exist). Additionally, the transcriptional and translational responses to aldosterone differ in different tissues.

Regardless, a deeper understanding of ENaC is necessary for a deeper understanding of the disorders and diseases covered in this chapter. To that end, I next present some background on what we know about ENaC currents and what we can infer about its molecular mechanism of gating based on related channels.

2. ENaC Currents, Structure, and Gating

In this chapter I begin with an overview of ENaC electrophysiology. From there, I move into a discussion of current knowledge about ENaC's structure/function relationships. Finally, I provide a brief overview of proteins which directly modify ENaC's electrophysiological properties (rather than expression levels, which are covered in Section 1.2).

2.1. ASIC

ENaC is a member of the ENaC/DEG superfamily of sodium-selective ion channels. These ion channels share a common ancestor as far back as Cnidaria and, as their long evolutionary history might imply, fill a wide variety of roles in the organisms that express them[125]. The structures of ENaC/DEG family members solved so far also hold to a common topology: the ion channels are trimeric, with large extracellular domains, two transmembrane helices per subunit, and short intracellular tails.

The member of this family of which we have the greatest structural understanding is the acid-sensing ion channel (ASIC). All of the gating states of this channel have been solved, and a great deal is known about its gating mechanism and the conformational changes associated with channel opening, desensitization, and closing. Since existing functional study of ENaC suggests similar conformational changes, most researchers assume that the conformational changes associated with ENaC's gating mechanism will be similar. In this section I provide the reader with a brief introduction to ASIC and important similarities and differences between it and ENaC.

The ASICs are themselves a family of ion channels, and the properties of each channel differ slightly from the others. There is also evidence

29

that different ASIC proteins can form heterotrimeric ASIC channels. However, the only ASIC for which we have structural information is ASIC1a, and so I refer to that channel as ASIC for the rest of this document. I will explicitly refer to the ASIC family as necessary.

2.1.1. Gating

ASIC's gating cycle involves three states: resting, open, and desensitized (Figure 2.1). ASIC opens when its extracellular domain is exposed to acidic solution, with a half-maximum activation at pH 5.8[126]. This peak current then desensitizes with a time constant of 0.64 — a marked difference from ENaC currents, which do not desensitize.

Protons open the channel by binding an acidic pocket located between the finger, thumb, and β-ball domains (Figure 2.2). Binding of protons to titratable residues in this pocket result in the collapse of the finger and thumb. This collapse is in turn propagated through the thumb and palm to the TMD, which rotates and translates about the pore axis (Figure 2.3). This movement opens a fenestration just above the cell membrane, through which ions enter the pore (Figure 2.4).

The pore is lined by the second transmembrane helix from each subunit. Approximately two-thirds of the way down the pore, the helix breaks and short loop connects a domain swap to the adjacent TM2 helix (Figure 2.5). This loop, called the GAS belt due to its one-letter code sequence, forms the selectivity filter of ASIC.

Unlike ENaC, ASIC desensitizes. Rapidly upon opening, a short loop in ASIC's palm flips to a desensitized conformation, which decouples the ECD and TMD. Thus, the ECD remains proton-bound and open, while the TMD returns to a closed conformation and obstructs the fenestration, preventing ions from passing through.

2.2. ENaC Electrophysiology

ENaC currents are characterized by high Na^+/K^+ selectivity, high affinity for amiloride, and a desensitization-like process called sodium self-inhibition (SSI). Here I cover each of these facets and connect them to the following discussion of ENaC structure.

Resting

Proton binding site

Knuckle Finger

β ball

Palm

Thumb

H+

H+

TMD

ECD and TMD rearrange to accommodate proton

H+

Palm reorganization uncouples ECD and TMD conformations, closing the fenestration

Movement of lower palm and TMD opens fenestration

Desensitized
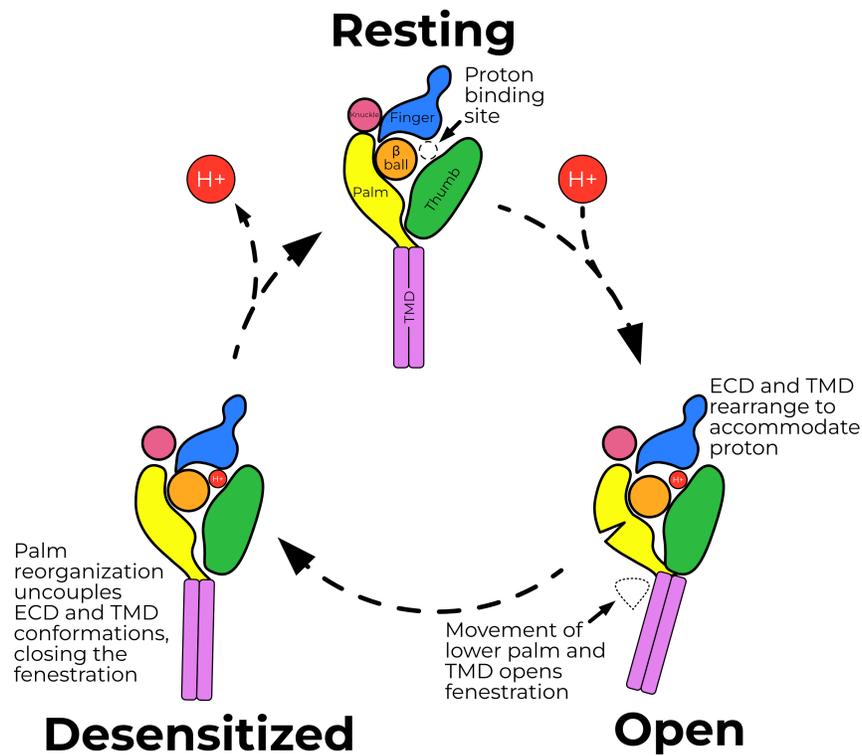
Open

Figure 2.1.: An overview of ASIC's gating mechanism. The channel starts in a resting state (top), with a de-protonated acidic pocket. This conformation holds the finger and thumb apart. When a proton bonds, the channel enters the open state (bottom right). Collapse of the finger and thumb causes conformational shifts of the palm and TMD, opening the fenestration and allowing the channel to pass current. The channel rapidly desensitizes (bottom left). The palm and TMD return to a closed conformation, while the finger and thumb remain protonated and in the same conformation as the open state.
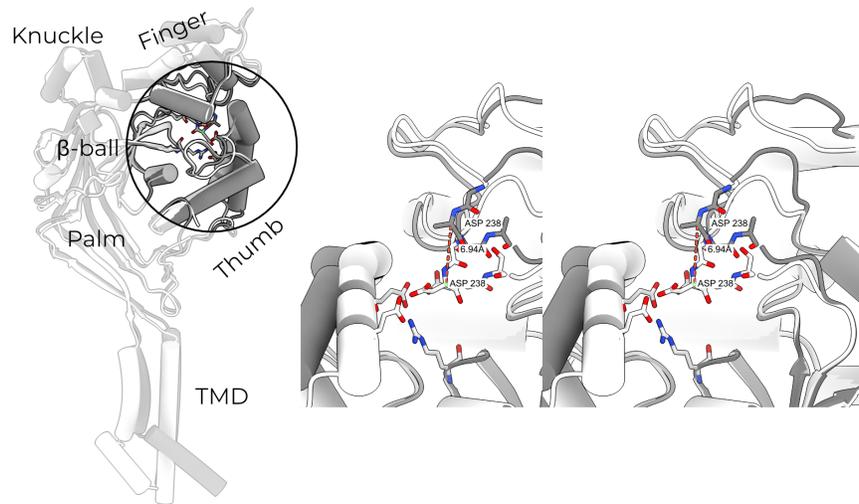
Figure 2.2.: ASIC's acidic pocket. Protonation of the acidic pocket collapses the finger and thumb, which propagates to an opening of the fenestration. **Left**: an overview of ASIC, with the acidic pocket highlighted. **Right**: a stereo view comparison of the acidic pocket between resting (grey, 5WKV) and open (white, 4NTW) states. Note that, once protonated, Asp 238 moves 7 Å to form interactions with the thumb.

Knuckle

Finger

Palm

Thumb

The palm and
TMD move away
from the pore
axis

The finger and
thumb collapse

TMD
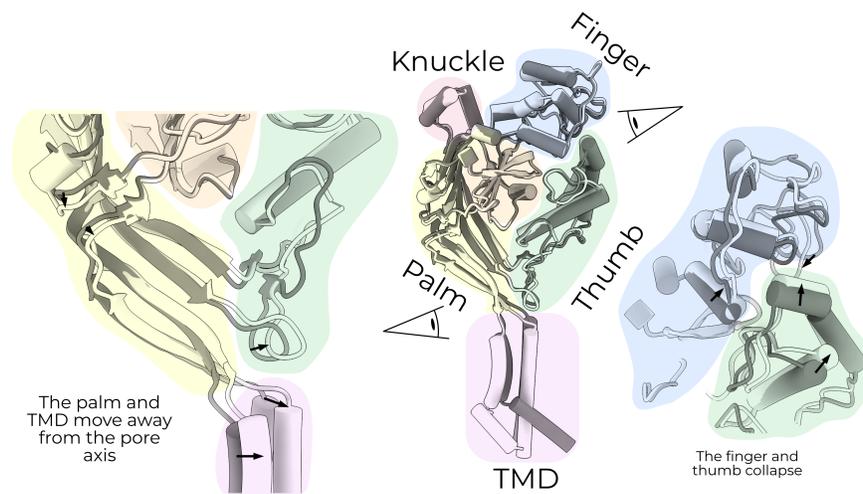
Figure 2.3.: A diagram of ASIC's gating conformational changes. When resting ASIC (grey)are protonated (white), the finger and thumb collapse (right). This movement is coordinated with the movement of the lower palm and TMD away from the pore axis, which opens the extracellular fenestration (left).
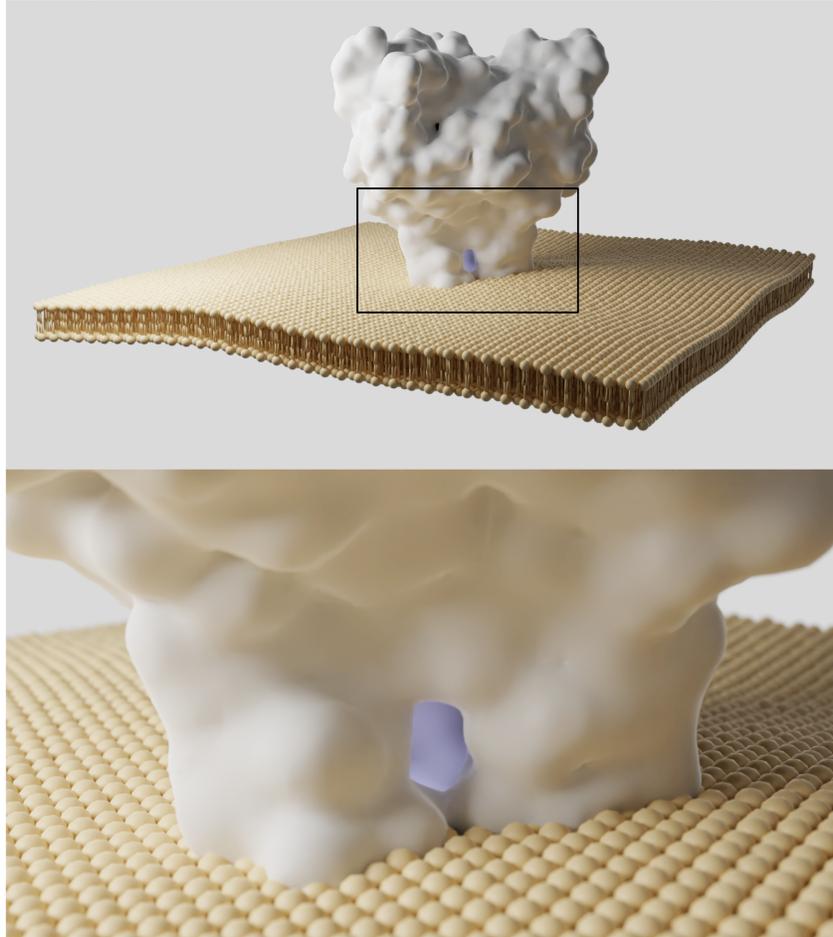
Figure 2.4.: The fenestration in ASIC. Membrane is for illustration purposes only and is not based on actual structural data. PDB: 4NTW.
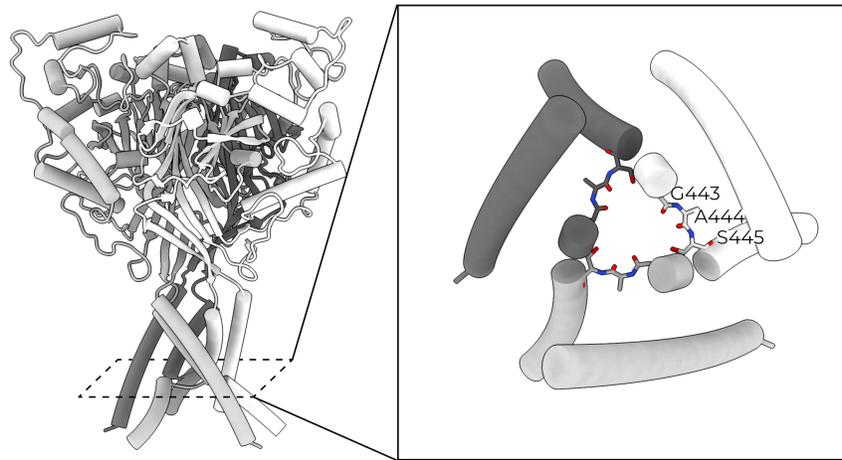
Figure 2.5.: The GAS belt of ASIC. **Left**: an overview of ASIC highlighting the domain swap. The three subunits are identical, but colored in shades of grey for clarity. **Right**: the GAS belt viewed from the extracellular side. Note that the alanine side chain points away from the pore. Only the final residue for the TM2 helix before the swap is shown to improve visibility of the GAS belt, but observe that the swapped TM2 helix continues the same trajectory as the upper half.
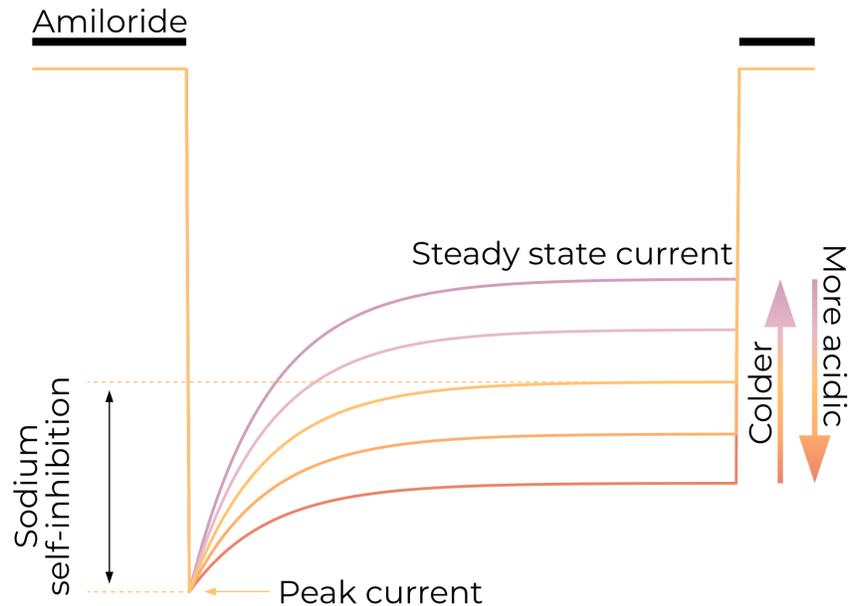
Figure 2.6.: Model ENaC Currents

2.2.1. The pore and selectivity filter

For comparison, ASIC's I_{Na}/I_K is typically estimated at around 10.

ENaC is highly selective for Na^+ over K^+, with an estimated I_{Na^+}/I_{K^+} well over 100[127,128]. The precise number depends on the study, since potassium currents through ENaC are often difficult to detect at all. ENaC does not pass appreciable H^+ currents until the extracellular solution reaches a pH of 5 or lower[129].

Ions enter the channel through a fenestration just outside the membrane and travel down a pore formed by the second transmembrane helices of all three subunits, just as in ASIC[128,130]. As discussed further in Section 2.3.2.3, ENaC's selectivity filter is composed of a triplet of residues in a domain-swapping loop between adjacent transmembrane helices. Based on structures of related channels, this domain swap is expected to occur approximately halfway through the membrane[131]. The third residue of the α loop (a serine) plays an outsize role in determining channel selectivity[132].

ENaC achieves high specificity for sodium by "sieving" ions, physically preventing larger cations from moving down the pore. The selectivity filter is so small that Na^+ ions must be dehydrated before passing

through[132]. Because ENaC separates by size, Li^+ currents are slightly larger than Na^+ currents ($I_{Li^+}/I_{Na^+} \cong 1.5$). The energetic cost of this sieving results in a low single-channel conductance (approximately 5 pS)[127].

2.2.2. Amiloride and other inhibitors

The ENaC/DEG family of ion channels are all inhibited (to varying degrees) by the small molecule amiloride. Amiloride has the highest affinity for ENaC, with an IC_{50} of about 100 nM. More hydrophobic derivatives (e.g., benzamil or phenamil) bind approximately ten times tighter, indicating that amiloride binds ENaC at a hydrophobic patch (amiloride derivatives are reviewed well by Kleyman and Cragoe[133]).

Amiloride binds just above (i.e., extracellular to) the selectivity filter in a voltage-dependent manner[128,134]. Some mutagenesis studies indicate that amiloride interacts primarily with the β and γ subunits, while others (and evolutionary analysis) are more consistent with an extended interaction surface including the α subunit[128,130,135]. Studies with sulfhydryl reagents suggest that the binding surface is only accessible when the channel is in the open state[130].

Amiloride binding is reduced in high-K^+ solutions, perhaps due to K^+ getting "stuck" at the selectivity filter[129].

2.2.3. P_O and sodium self-inhibition

ENaCs are characterized by long dwell times in both the open and closed states and a low likelihood of switching states[127]. Proteolytic cleavage of the extracellular domain of the channel pushes the channel from a state with a P_O of nearly zero to a constitutively open state[136]. Conversely, intracellular acidification and Ca^{2+} both reduce channel P_O[137,138]. Unlike the related Acid Sensing Ion Channel (ASIC), ENaC is not directly opened by changes in extracellular pH.

As they do not have a ligand *per se*, ENaCs do not desensitize in the traditional sense. Steady-state macroscopic currents are, however, lower than peak currents[139]. This reduction in sodium current on the scale of seconds is called sodium self-inhibition (SSI) and is an important characteristic of ENaC electrophysiology.

SSI is not to be confused with the term "sodium feedback inhibition", which refers to reduction in ENaC at the cell surface via the action of Nedd4-2 and other regulatory partners.

37

SSI reduces ENaC currents as a direct result of extracellular Na^+ concentrations, not the currents themselves[140]. Lower temperatures reduce the magnitude of SSI, resulting in greater steady-state ENaC currents[140,141]. ENaC is believed to have only a single open and single closed state[127,142].

As discussed in Section 2.4.1, ENaC is activated by proteolytic removal of a portion of its extracellular domain called the Gating Relief of Inhibition by Proteolysis (GRIP) domain. This increase in current is a result of SSI relief[140,143]. It is reasonable to expect, then, that the sodium-binding site is composed at least in part by the GRIP domain. Indeed, an acidic pocket fits this description and binds as-yet-unidentified ions[144,145]. While extracellular pH does not open ENaC, more acidic extracellular solutions reduce SSI magnitude, resulting in a larger steady-state current[146]. More basic extracellular solutions result in greater SSI magnitude and therefore lower steady-state currents.

Surprisingly, despite its effect on SSI magnitude, pH does not influence Na^+ K_i. If solvent-exposed acidic residues do participate in sodium-binding for SSI, one would expect their protonation to reduce the affinity for sodium. Additionally, the effect of pH on SSI magnitude seems to be species-dependent, further complicating the role of the acidic pocket.

2.3. ENaC Structure

ENaC is a heterotrimeric protein comprising one copy each of αENaC, βENaC, and γENaC arranged counterclockwise when viewed from the extracellular side (Figure 2.7)[45,147]. Each subunit is approximately 30% identical to the others, and all three share a topology common to the entire ENaC/DEG family. In this section, I will cover structure/function relationships for the two main sections of ENaC: the extracellular and transmembrane domains (ECD and TMD, respectively).

This is only marginally higher than the approximately 25% identity they each have with related channel ASIC1. The subunits are approximately 50% similar to each other and 30% similar to ASIC1.

I will also make extensive analogy to a closely related channel, the acid-sensing ion channel (ASIC). Throughout this document, when I refer to ASIC, I specifically mean ASIC1 unless I specify a different paralog. ASIC is another member of the ENaC/DEG family which is
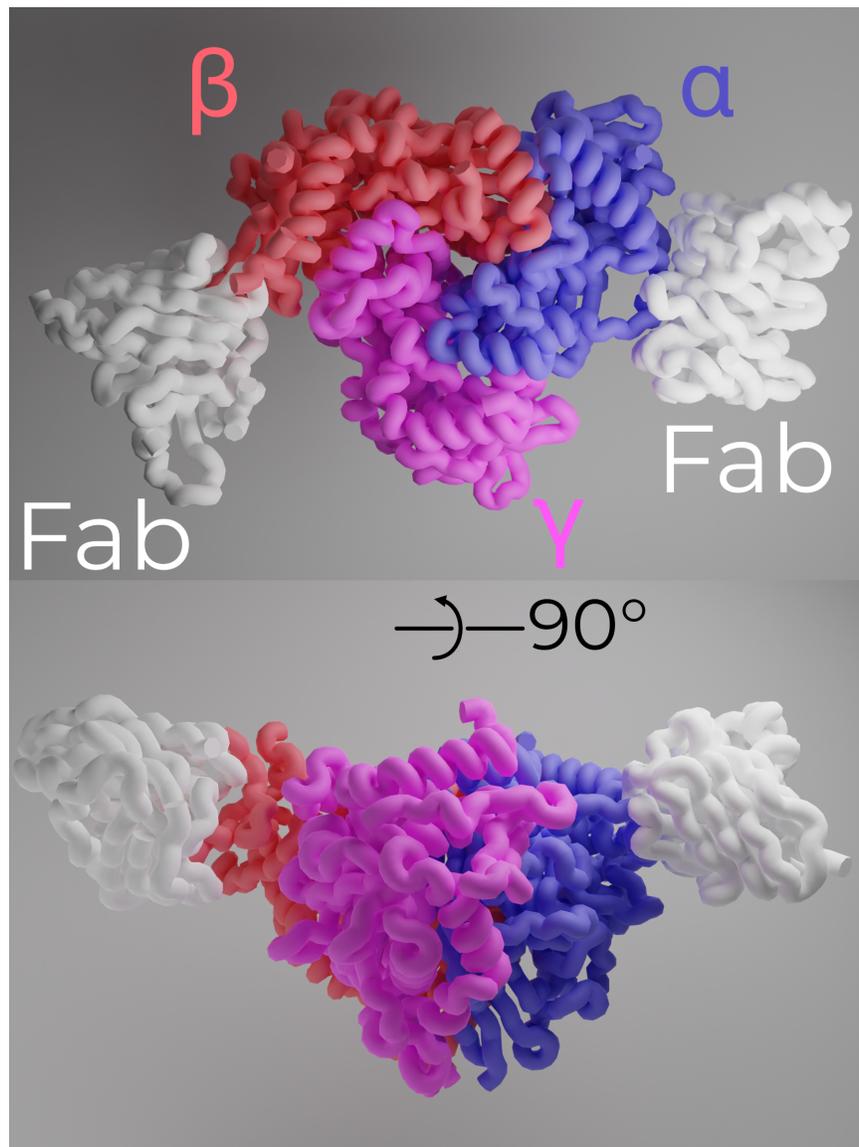
Figure 2.7.: ENaC viewed from outside the cell (top) and parallel to the membrane (bottom). The TMD is not modeled here. This model includes two Fabs used to break the channel pseudosymmetry, one which binds α ENaC and one which binds β. They are not part of ENaC. PDB: 6WTH.

activated by protons. I recommend Yoder and colleagues' excellent overview of ASIC's gating mechanism to interested readers[148].

The first structures of a third ENaC/DEG family member, FMRFamide-gated sodium channel 1 (FaNaC 1; hereafter FaNaC), were published during the production of this document[149]. This is exciting for two reasons. First, FaNaC is much more closely related to ENaC than is ASIC[125]. Second, FaNaC shares its overall architecture with ENaC and ASIC, aside from divergence at the ligand-recognition region of the distal finger. These similarities further support a shared overall gating mechanism among the ENaC/DEG family.

2.3.1. Stoichiometry

To date, all solved structures of the ENaC/DEG family are trimeric. Prior to the first structure of ASIC, functional studies of the channel suggested a tetrameric, ααβγ channel — Kashlan and Kleyman discuss the abandonment of the tetrameric hypothesis well[150]. Although homomeric αENaC channels are competent to pass very small amiloride-sensitive currents, expressing all three subunits results in currents over 100 times larger than the α-only channels[45]. Thus, the canonical ENaC channel is the αβγ heterotrimer.

More exotic channel compositions, like 3α:3β:3γ, were also suggested.

As discussed in Section 1.1, it is not clear that this canonical channel is the only one expressed in the body. No tissue assayed thus far expresses all three subunits in equal amounts (in some cases, one or more subunits are not expressed at all). Aldosterone rarely induces expression of all three channels equally. More strikingly, the regulatory protein SPLUNC1 binds to βENaC in the lumen and induces internalization of α- and γ- (but *not* β-) ENaC[151]. It is not clear how a small (26 kDa), secreted protein could separate βENaC from the α and γ subunits on its own. Indeed, the same study indicates that βENaC becomes less mobile upon SPLUNC1 binding, suggesting coupling to other, larger proteins. A deeper investigation of the various chaperones and processes involved in ENaC assembly and dissociation would be interesting but, unfortunately, there is only a small body of existing literature on the topic. For our purposes, ENaC is the αβγ heterotrimer.
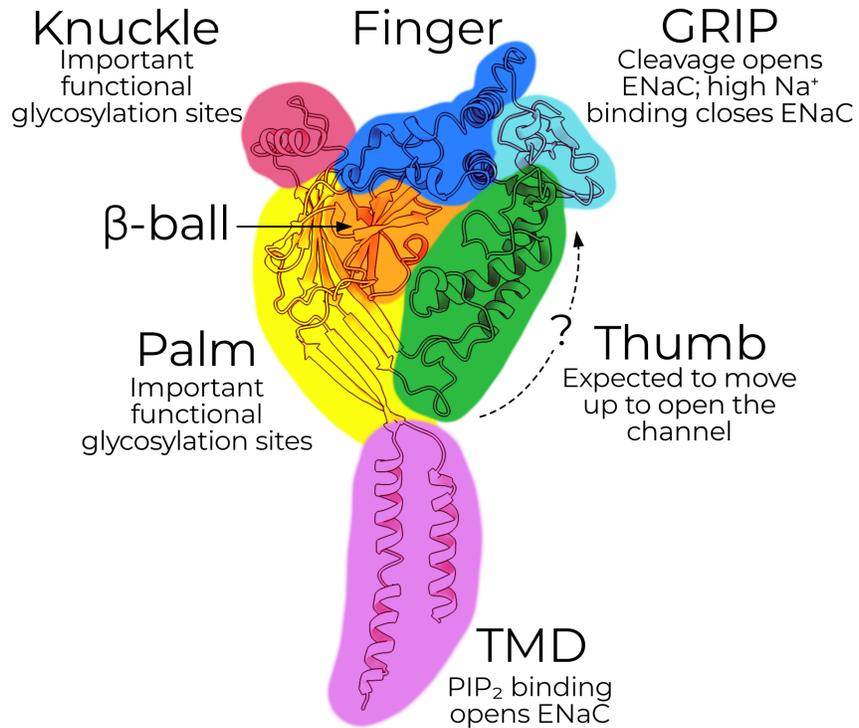
Figure 2.8.: Cartoon representation of an ENaC subunit. Each domain is labeled, and important functions are noted next to the labels.

2.3.2. Functional Domains

Each subunit has a mass of approximately 75 kDa, with short intracellular N- and C-terminal tails and two transmembrane helices (TM1 and TM2, which together form the transmembrane domain, TMD). The extracellular domain (ECD) comprises the bulk of the protein (approximately 50 kDa), which is further subdivided into domains named for their vague resemblance to a left hand grasping a ball (Figure 2.8). Uncleaved channels typically run a bit higher (between 90 and 120 kDa) on SDS-PAGE due to SDS binding and extensive glycosylation (Section 2.3.3).

The α, β, and γ subunits are 75, 72, and 74 kDa respectively.

2.3.2.1. Scaffolding — the palm, β-ball, and knuckle

The palm (yellow) comprises a twisted β-sheet of seven β-strands (β1, 3, 6, and 9–12). The β-ball forms (as one might expect) a tightly twisted ball of four β-strands: β2, 4, 5, and 7. The knuckle, comprising only a single α-helix (α6) is connected to the extracellular end of the palm.

Although the palm does lie along the pseudo-threefold symmetry axis, the ion permeation pathway of ASIC suggests that it is probably not involved in passing Na^+ currents[152]. The palm instead forms the structural scaffold of each subunit, connecting the finger and knuckle at the extracellular edge of the domain to the thumb at the membrane-adjacent end. About a third of each subunit's buried surface area (1,667 out of 4,662 $Å^2$ for αENaC) is in the palm, despite it containing only about a fifth of the modeled residues. Given this outsize role in establishing channel topology, it is no surprise that the palm is highly conserved among the ENaC/DEG family and plays a pivotal role in channel gating.

When ASIC opens, the palm pivots around the β-ball (orange) and moves inward by approximately 4 $Å$[131]. This movement is coupled to the TMD, opening the pore. The same overall mechanism is expected in ENaC and has support from cross-linking studies[153]. The α and β palm domains and the α knuckle also host glycosylation sites which are required for mechanosensitive gating (Section 2.4.3). Unfortunately, the research on ENaC glycosylation is relatively scant, and not much is known about tissue- or organism-specific glycosylation patterns.

In ASIC, the knuckle is largely uninvolved in gating and is considered a rather inert part of the palm/knuckle scaffold. In contrast, ENaC's knuckle is an important source of heterogeneity between the three subunits. The carboxyl terminus of α6 differs between the three subunits, and its interface with the adjacent subunit's finger domain may contribute to the enforcement of a clockwise subunit arrangement[145].

2.3.2.2. Gating — the finger, thumb, and GRIP

The finger, thumb, and gating relief of inhibition by proteolysis (GRIP) domains form the essential regulatory machinery of the channel. The finger domain (blue) comprises three α-helices (α1–3). The thumb domain (green) comprises two large helices, α4 and 5.

The α- and γGRIP domains (cyan) are, as the name painstakingly makes clear, expected to block channel opening until they are proteolytically excised (see Section 2.4.1). The βGRIP is not cleaved during canonical channel opening and is, perhaps relatedly, the GRIP for which we have the best structural information. We can model a sheet of two anti-parallel pairs of β-strands in βGRIP. The GRIP domain shrouds the interface between the finger and thumb, forming extensive contacts between the two.

When we were publishing the first structure of ENaC, we struggled to find a good backronym for GRIP. My suggestion of Good, Really Important Part was rejected.

In ASIC, protonation of an acidic pocket formed by the β-ball, finger, and thumb of a single subunit causes collapse of the thumb toward the finger. This pulls the palm (and therefore the TMD) away from the symmetry axis, opening the channel. In ENaC, no such acidic residues exist. Instead, an aromatic pocket is formed by the finger, thumb, and GRIP domains. Based on this similar architecture and a slew of cross linking studies, it is thought that the GRIP domain forms a wedge between the finger and thumb, preventing their collapse[154–156].

Indeed, the Kleyman laboratory has identified short segments of the GRIP domain (eight and eleven amino acids in α and γENaC, respectively) which, when flowed over open channels, close them (Figure 2.9)[157–159]. These peptides are part of the P1 strand of the GRIP domain and pack tightly against the remaining GRIP domain, α2 of the finger domain, and the upper edge of the thumb.

The α peptide is LPHPLQRL, and RFSHRIPLLIF that of the γ subunit.
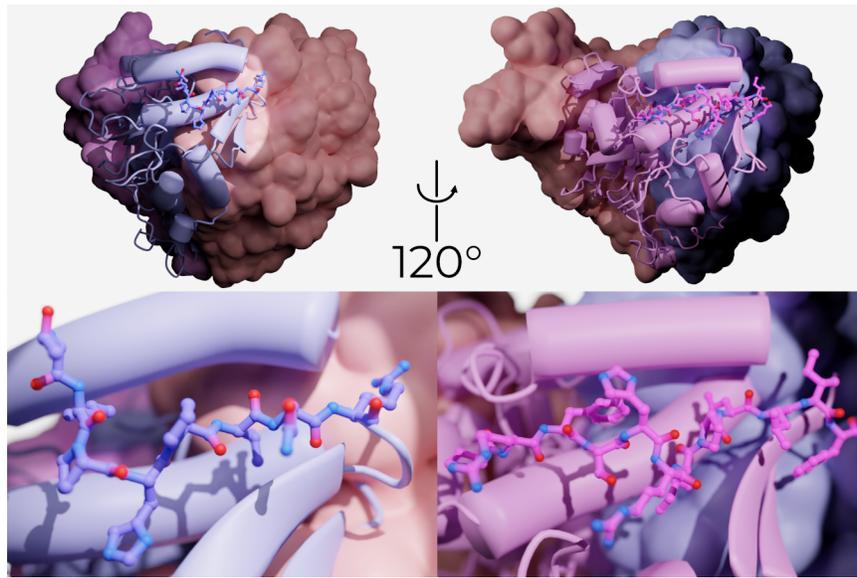
Figure 2.9.: The inhibitory peptides of the α (left) and γ subunits. PDB: 6WTH.

We have hypothesized that cleavage and subsequent removal of the P3 strand releases P1 and, therefore, decouples the finger and thumb[145]. From here, we and others have assumed that the gating mechanism is more-or-less that of ASIC: the finger and thumb collapse, and their movement pulls the palm and TMD away from the pore axis (Figure 2.3). However, without a map and model of the open and closed channels, we cannot rule out other mechanisms.

The new results from FaNaC call this assumption into question[149]. The finger and thumb do *not* collapse in FaNaC. Rather, they move in a concerted action up and away from the membrane, toward the α6 helix of the adjacent knuckle domain.

It is worth noting here that while FaNaC is gated by peptide binding (as is ENaC, after a fashion), FaNaC's ligand binding pocket is distinct from ENaC's. The FaNaC peptide binds a pocket comprising α2, the β6-β7 linker, and α6 from the adjacent subunit, i.e., the finger and knuckle. ENaC's GRIP domain interacts instead with the thumb and finger. Since the FaNaC pocket is on "the other side" of the finger, it would not be entirely surprising if the movement of the finger in the two channels is different.

A histidine in the β9-α4 loop of FaNaC (which connects the palm and thumb) points down between TM1 and TM2. Mutation of this histidine to serine results in constitutively active channels, implying that the energy gained by ligand binding is used to overcome the interaction of this histidine with the TMs. ASIC and ENaC both have bulky residues (tryptophan and tyrosine, respectively) in this position.

2.3.2.3. Conduction — what we expect for the TMD

No map of ENaC has reliable density for the transmembrane domain. Nevertheless, we can infer a great deal from electrophysiological studies of ENaC and maps of other members of the ENaC/DEG family, mostly the well-studied ASIC.

ASIC's gating cycle comprises three states: resting, open, and desensitized (Figure 2.1). The pore of the first solved structure of ASIC was asymmetric, but this truncated crystallization construct did not conduct sodium currents[160]. Subsequent structures of ASIC show symmetric pores throughout its gating cycle.

In the resting state of ASIC, negative charges clustered in the acidic pocket (formed by the finger, thumb, and β-ball) hold the finger and thumb apart. The separation of the thumb from the finger pushes the palm inward, holding the channel in a position which obstructs its lateral gate.

When ASIC encounters low extracellular pH, the residues in the acidic pocket are protonated. This relieves electrostatic repulsion and allows the finger/thumb interface to collapse, pulling the palm and TMD inward and opening a lateral fenestration just above the membrane (Figure 2.4)[131].

Mutating a residue just above the second transmembrane helix in βENaC holds the channel open, likely by holding open a similar fenestration[161]. This βS520K is known as the DEG mutation, named after the *C. elegans* channel from which the mutation is derived.

Interestingly, TM2 is split halfway through the membrane, with the C-terminal side swapping to complete the TM2 of the adjacent (clockwise) subunit. This domain swap forms a triangular arrangement of short Gly-Ala-Ser loops, called the GAS belt. The GAS belt forms ASIC's selectivity filter[163]. The homologous residues in the α-, β-, and

Evolutionary analysis suggests that a non-swapped conformation may have some physiological relevance, but no functional structure of this state has been solved[162].

45
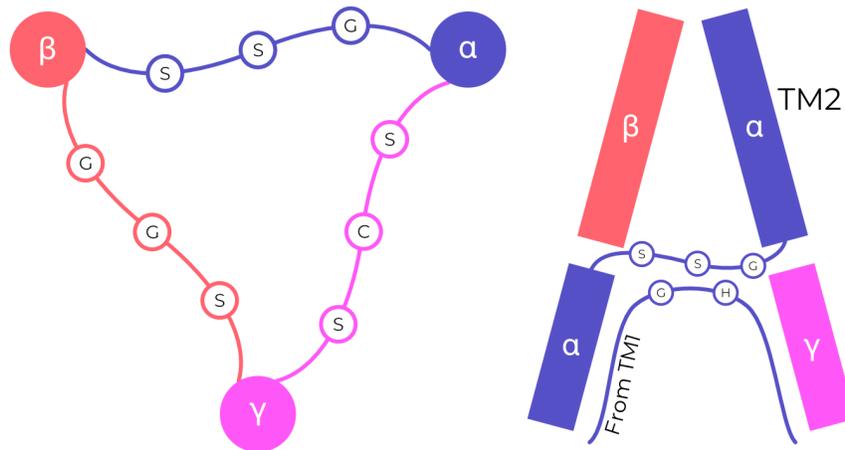
Figure 2.10.: A cartoon of ENaC's selectivity filter. **Left**: a top-down view of the domain swap loop. **Right**: a schematic illustration of αTM2 breaking and completing βTM2. The concept of a domain swap is supported by structures of other ENaC/DEG channels and studies of ENaC mutants.

γENaC (GSS, GGS, and SCS respectively, Figure 2.10) play a significant role in that channel's selectivity, implying the same pore structure and domain swap[128,130,164–166].

In the open state, the ions pass from the extracellular fenestration down a negatively-charged pore through the GAS belt, and into the intracellular fenestration. The GAS belt selects for Na^+ over other cations by a "sieving mechanism", physically preventing the passage of ions with hydrated radii too large for the filter. It is worth noting here that ENaC's significantly higher Na^+ selectivity and lower unitary currents suggest that, unlike ASIC, Na^+ ions are dehydrated before passing through ENaC[167]. We thus expect that ENaC's selectivity filter will be significantly narrower than that of ASIC[168].

The conical region below the GAS belt and between TMs was believed to be filled with unstructured lipids. However, a recent structure of ASIC revealed that the N-terminus re-enters the membrane to buttress the GAS belt (Figure 2.11)[169]. The re-entrant loop also houses the highly conserved N-terminal two-residue His-Gly pair (the HG motif). The HG motif is critically important in gating and selectivity of ENaC, and likely plays a similar role in other ENaC/DEG fam-
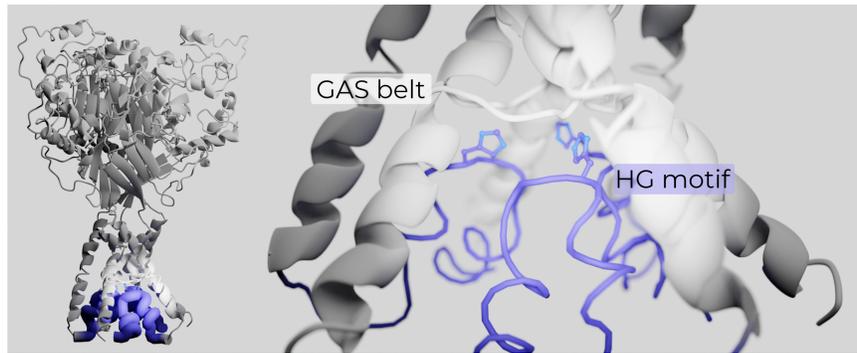
Figure 2.11.: The HG motif in ASIC. The re-entrant loop is highlighted in blue, and the highly-conserved histidine is represented with sticks. PDB: 6VTL.

ily members[17,170,171]. The HG motif supports the GAS belt through several hydrogen bonds and hydrophobic interactions with adjacent TM2s, stabilizing this otherwise-fragile structure.

Unlike ENaC, ASIC desensitizes. In desensitized ASICs, the β11-β12 linker in the palm domain is flipped toward the channel center[152]. This decouples the still-collapsed finger and thumb domains from the lower palm and TMD, allowing the fenestration to close (Figure 2.1). In essence, the desensitized channels have an open ECD but a closed TMD. As ENaCs do not desensitize, the role of this linker is likely different. However, the linker sequence is highly conserved between ASIC and ENaCs, and an L→Q mutation results in a significant increase in current[172].

2.3.3. Glycosylation

Glycans play an essential role in channel trafficking and maturation. The β subunit is heavily glycosylated, with eleven predicted sites in human compared to α and γ's six and five, respectively. Prior to this work, four sites on βENaC, two on αENaC, and one on γENaC had been modeled[145]. Deletion of all glycosylation sites on any of the three subunits significantly decreases both total and surface expression of ENaC[173]. The same dependence of expression on glycosylation is seen in ASIC[174].

There is a conspicuous A→D/E mutation between ASIC and ENaC, but this acidic residue does not form any obvious associations in models solved thus far.

ENaC glycosylation has functional implications beyond surface expression. Glycan maturation and proteolytic processing appear to happen in a concerted fashion, but they are not interdependent[175]. SSI is significantly reduced in ENaCs without glycans on any of the three subunits[173]. ASIC also depends on glycans for proper channel function — deletion of specific glycans changes current magnitude or proton affinity[174].

To my knowledge, investigation of ENaC glycosylation has thus far been limited to knock-out of all predicted glycosylation sites in a single subunit or the entire channel. A study of single-glycan knock-outs, as has been performed in ASIC, would be invaluable in determining the specific contribution of glycosylation of each ECD domain.

2.4. Direct regulation of ENaC

2.4.1. Proteases

Proteolytic activation of ENaC was discovered shortly after the channel itself. Overnight treatment of *Xenopus laevis* bladder with aprotinin (a serine protease inhibitor) dramatically reduced ENaC currents; the same effect was observed in an *X. laevis* cell line[176,177]. ENaC currents were quickly rescued by treatment with the serine protease trypsin. Thus, an activating role for proteases was established.

ENaC exists in two populations at the cell surface: "near-silent" channels with a low P_O (less than 0.02) and activated channels which are essentially constitutively open ($P_O \cong 0.9$)[178,179]. Treatment with exogenous trypsin activates the near-silent channels, and cleaved and uncleaved ENaC is found in cells and extracellular vesicles (making a secondary messenger unlikely)[180–183].

The ortholog of prostasin in *X. laevis* was discovered before this evolutionary connection was known. Tt is still named Channel Activating Protease 1 (CAP1) in that organism for this reason.

Prostasin was the first protease found to activate ENaC[177]. Furin's role in channel activation was reported shortly thereafter[181]. Prostasin is a membrane-associate serine protease, expressed highly in prostate and seminal fluid and moderately in other tissues including colon, lung, and kidney[184]. In contrast to prostasin's relatively circumscribed expression, furin (also a serine protease) is expressed in essentially all human tissues. Furin plays a role in a vast array of

biological processes including ENaC activation and is well-reviewed by Thomas[185].

Both furin and prostasin are enteropeptidases which cleave following polybasic tracts (i.e., stretches of amino acids with multiple Lys or Arg residues). Both αENaC and γENaC have canonical cleavage sites in their GRIP domains which open the channel (Section 2.3.2.2)[181]. Current research suggests that, during channel activation, furin cuts α twice and γ once, while prostasin cuts γ once.

Unfortunately, these sites are in regions we have not yet been able to resolve. The relative changes in P_O resulting from each cleavage event is still unclear, and seems to be tissue dependent[136,181,186]. In addition to prostasin, γENaC is also cleaved and activated by a wide repertoire of different proteases in different tissues[186–196].
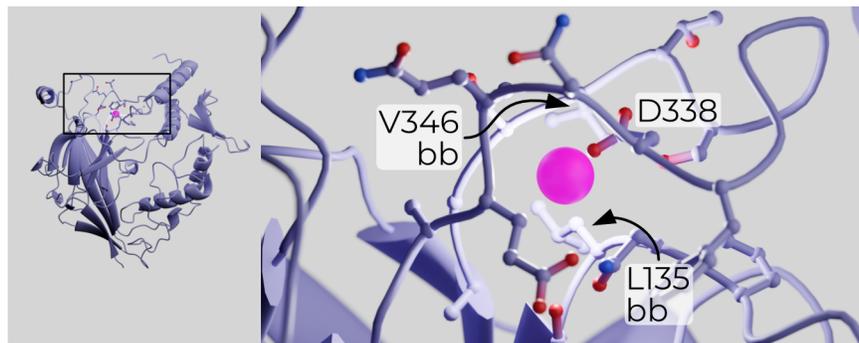
Figure 2.12.: The acidic pocket of αENaC. Residues close enough to bind the putative Na^+ ion are labeled. A residue label including "bb" indicates that the carbonyl oxygen of the main chain binds the ion. PDB: 6WTH.

Removal of the inhibitory peptides is thought to open ENaC by relieving SSI[143]. Mutagenesis and structural work identified a putative Na^+-binding "acidic pocket" formed by the finger and β-ball (Figure 2.12)[144,145]. If the GRIP domain does indeed prevent collapse of the finger and thumb toward each other, Na^+ binding to a low-affinity site on the other side of α1 may pull the finger up and away from the thumb. Structures demonstrating such movement have yet to be captured — indeed, all structures solved before this work were in high-Na^+ buffers.

Recall that sodium self-inhibition describes the tendency of steady-state ENaC currents to be smaller than peak currents, somewhat resembling desensitization.

Proteolytic activation has been described in great detail in a wide

range of *in vitro* systems, but the link is not quite so obvious *in vivo*. For instance, mice treated with aprotinin show reduced ENaC activity as expected[197]. However, when mice are fed a low-sodium diet, the appearance of cleaved ENaC and increases in amiloride-sensitive current are largely independent[198]. It is thus not obvious that the direct cleavage/current relationship observed *in vitro* is true *in vivo*. What's more, while proteolytic cleavage may be the main pathway by which ENaC is opened, ENaC is also sensitive to other signals.

2.4.2. The membrane

2.4.2.1. Phospholipids

Like many ion channels, ENaC is modulated by phospholipids. For instance, ENaC is known to segregate into lipid rafts[199,200]. Cholesterol alone does not activate the channel, but it does facilitate the interaction between phosphatidylinositol and binding sites in the β and γ subunits[202,203]. This interaction is absolutely required for ENaC opening.

Lipid rafts are proposed regions of the cell membrane enriched in cholesterol and sphingolipids. While there is clearly some kind of spatial-compositional heterogeneity in cell membranes, the existence of lipid rafts in particular is still an open question[200,201].

Treatment of inside-out patches with phosphatidylinositol bisphosphate (PIP$_2$) increases ENaC P_O within seconds, and P_O is reduced again upon PIP$_2$ removal, ruling out the possibility of PIP$_2$-induced proteolytic cleavage[204,205]. Similarly, no change in channel number is observed in these experiments. A correlation between ENaC currents and PIP$_2$ levels is also observed in mouse trachea[206]. Note that PIP$_2$ only augments ENaC currents up to a point — more PIP$_2$ than is necessary does not result in greater ENaC currents. Put another way, a lack of PIP$_2$ reduces ENaC currents but PIP$_2$ does not itself potentiate them[207].

Unlike PIP$_2$, phosphatidylinositol triphosphate (PIP$_3$) does augment ENaC currents both directly and via a signaling cascade. In its immediate effect, PIP$_3$ binds γENaC just after the second transmembrane domain to rapidly open the channel[207–209]. PIP$_3$ also increases the number of channels at the cell surface in a longer cascade mediated by SGK (Section 1.2.3)[65]. In fact, aldosterone's effect on SGK is mediated by PI3K and PIP$_3$[210].

Interestingly, mutation of negatively-charged residues in the γENaC PIP$_3$ binding site increases ENaC currents both with *and* without PIP$_3$[209].

ENaC's dependence on phosphatidylinositols presents a problem. PIPs are rare enough in the membrane that, if the lipids and channel

50

were both freely diffusing, the expected P_O of ENaC would be far lower than what is observed[211,212]. MARCKS is a lipid-binding protein which sequesters PIP_2 and PIP_3 into regions of high local concentration[213]. MARCKS also binds ENaC, potentially anchoring the channel in a region of the membrane with a high enough local concentration PIPs for the proper channel P_O[214].

MARCKS is itself subject to regulation by a wide range of signals, which in turn affect ENaC currents, e.g., Ca^{2+} and (in an amusing symmetry) proteolysis of MARCKS itself[215,216].

2.4.2.2. Palmitoylation

Palmitoylation is a reversible process in which hydrophobic chains are attached to cysteine residues, anchoring them in the membrane. Multiple cysteines in β- and γENaC (but none in αENaC) are palmitoylated, with varying effects[217–219].

Blocking palmitoylation of two cysteines in βENaC (in mouse: C43 and C557) significantly reduces ENaC currents[217]. This effect is not mediated by differences in trafficking or cleavage but by changes in channel P_O, specifically increased SSI. C43 is suggestively close to the HG motif; it may be that membrane anchoring of this cysteine aids in proper folding of the re-entrant loop and therefore the pore.

γENaC also has two palmitoylated cysteines, C33 and C41, which straddle that subunit's HG motif[219]. Again, C→A mutation of these cysteines increase SSI without affecting surface exposure or channel cleavage. Surprisingly, addition of a β palmitoylation mutant to a mutant γ background does not further reduce currents — put another way, the γ mutations are dominant.

2.4.3. Mechanosensation

Whether or not ENaC directly senses membrane stretch has long been a point of contention, but decades of careful research indicate that laminar sheer stress (LSS) opens the channel regardless of proteolytic state. Bath perfusion of *X. laevis* oocytes or CHO cells expressing ENaC produces amiloride-sensitive Na^+ currents without changing their cleavage state[220,221].

Single channel recordings indicate that LSS currents result from directly increased P_O[50]. Although LSS can open uncleaved channels, pre-treatment of human ENaC with trypsin significantly primed LSS

The same study reported an opposite effect — inhibition of LSS currents by trypsin treatment — for *X. laevis* ENaC[50].

response[50,222]. Over the course of minutes, ENaC becomes less sensitive to repeated stimulation with LSS[223]. Mutant ENaCs with truncated C-termini did not show this response, indicating that it may be mediated by Nedd4-2 (Section 1.2.2.2).

Multiple domains may participate in LSS sensation. Genetic deletion of the GRIP domain slows response to LSS, although this may be an artifact of differences in finger/thumb coupling rather than a true measure of the GRIP domain's participation in gating[224]. Work on human and rat ENaC demonstrated a strong dependence of LSS currents on glycosylation of the αENaC palm and knuckle; in another study, deletion of any single subunit's glycans has no effect on LSS currents[173,225]. The former study makes a compelling argument that the glycans influence LSS by interacting with the extracellular matrix — a difference in oocyte preparation may therefore explain this discrepancy.

2.5. Conclusion

I've demonstrated that although we can make some assumptions about how changes in the ENaC ECD are coupled to pore opening, much of the channel's gating mechanism remains unknown. For instance: which glycans are involved in which aspects of channel gating? How does sodium inhibit the channel, and where does it bind? Does ENaC contain a GAS belt and a lateral fenestration like ASIC?

Moreover, the existence of several, semi-overlapping means of modulating channel P_O indicates that there may be multiple, physiologically relevant means of opening ENaC that cells use to fine-tune their Na^+ permeability. At a more basic level, structures of ENaC's TMD, pore, and selectivity filter would contribute to our understanding of the important ENaC/DEG family more broadly. It is with this in mind that I set out on the goals of this project: to solve the structure of the ENaC TMD, and to solve high-resolution structures of the channel in various salts.

Part II.

Results and Discussion

3. The Transmembrane Domain Remains Elusive

One of the long-standing goals of our lab is to solve the structure of the ENaC TMD. Such a structure would provide valuable insight into the source of ENaC's spectacular selectivity for sodium over potassium. It would also inform our view on the similarities and differences between ENaC and ASIC, such as whether ENaC also has an HG-motif, whether ENaC's gating mechanism follows that of ASIC, and what conformational changes cause sodium self-inhibition.

Unfortunately, that goal will stand a while longer. None of my maps produce TMD density with resolutions better than 6 Å, and few of them even reach that threshold. Additionally, no map has density for all six transmembrane helices (TMs). Finally, and most damning, the arrangement of the TMs we do see is not consistent with what is known about their arrangement around the pore. We must conclude that the TMD of my maps is significantly disrupted, and analysis of these results will not bear fruit. I reproduce them in the first section of this chapter in case they are ever of interest. Perhaps of more value will be the following sections in which I cover experiments that produced no valuable results so that future researchers do not retread the same ground.

3.1. Constructs

To tackle the problem of the ENaC TMD, I solved the structure of six different combinations of condition and construct. These conditions are summarized in Table A.1, but I will present them in greater detail here, along with their models. In addition to the mutations I discuss here, all human constructs had the canonical furin sites knocked out: αR178A, R204A and γR138A. It was our hope that knocking out furin

sites would lead to a more defined ECD composition by preventing our expression system from cleaving the ECD.

It is important to note that the described mutations were only applied to the human constructs we discuss. All mouse models are wild-type (with the exception of a few residues left from cleavage of GFP off the γ subunit).

3.1.1. Cysteine Knock-Out
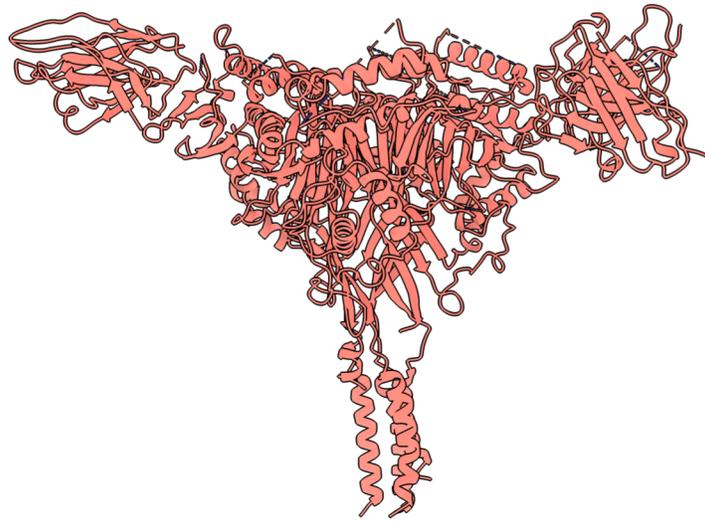
CKO Digitonin

Figure 3.1.: The CKO model.

The cysteine knock-out (CKO) mutant had four C→A mutations: αC63A, βC30A, and γC33A,C41A (Figure 3.1). We mutated these positions because some (but not all) intracellular cysteine residues are known to be palmitoylated[217–219].

We wondered if previous difficulty in solving the structure of the TMD may have been the result of aberrant palmitoylation, given that ENaC in our expression system exists at far higher concentration than would exist in a typical cell. CKO mutants did indeed express at

higher levels than WT, and their peaks on SEC appeared more homogeneous.

3.1.2. DEG
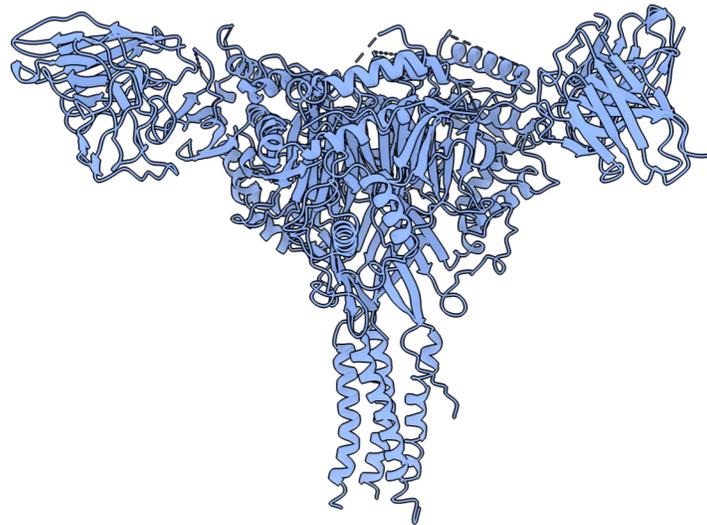
CKO/DEG Difab

Figure 3.2.: The CKO/DEG model.

The DEG mutation replaces serine 520 in human ENaC with the equivalent lysine from *C. elegans*'s DEG channel. This mutation keeps the channel in an open state regardless of whether the GRIP domain is cleaved or not[161]. In channels to which we apply the DEG mutation, we also apply a mutation in the GRIP domain which reduces the affinity of the channel for its inhibitory peptide, αT240W[158].

The DEG and GRIP mutations were applied to a background of human CKO channels. We thus call these channels, which we expect to be constitutively open, CKO/DEG channels (Figure 3.2).

3.1.3. Acid-shock

For two maps (CKO digitonin and CKO/DEG difab), I briefly "shocked" the material by desalting it into a pH 6.0 solution (as opposed to our typical purification pH of 7.4). I did this to test if poorly-folded material from internal membranes might be more susceptible to cashing out in less-favored conditions. I did not end up detecting any difference in either the final yield, the yield before and after acid-shock, or the map quality. I therefore discontinued this practice after these two maps.

3.1.4. PIP$_2$

CKO/DEG Monofab/PIP$_2$
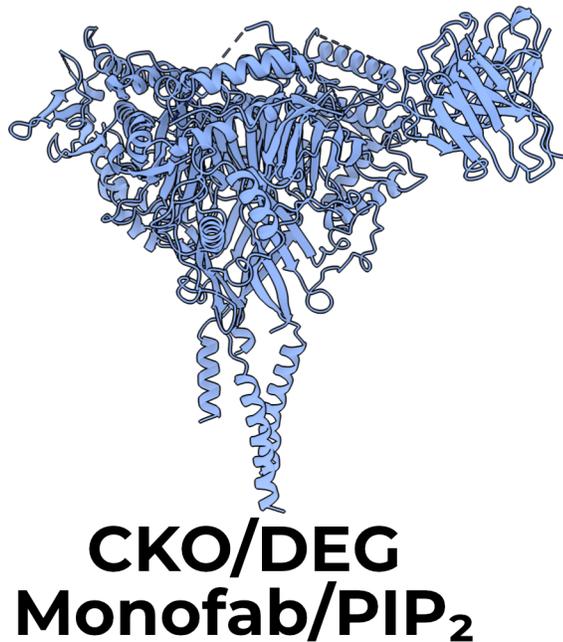
Figure 3.3.: The CKO/DEG monofab PIP$_2$ model.

As discussed in Section 2.4.2.1, ENaC requires PIP$_2$ to open. I thus added 1 mM C8 PIP$_2$ to the CKO/DEG monofab samples just before grid preparation (Figure 3.3). I did not notice any difference in TMD quality or conformation compared with the CKO/DEG difab map (which did not have PIP$_2$ added), and so did not add the lipid to any other preparations in this work.

3.1.5. Nanodiscs
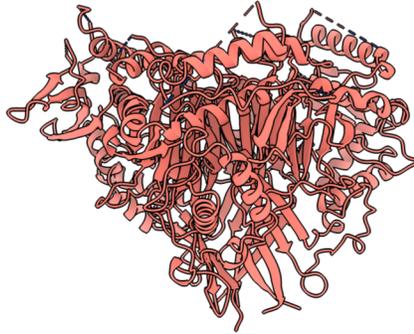
CKO Nanodiscs

Figure 3.4.: The CKO nanodisc model. Note that I was not able to resolve any features in the TMD.

ENaC seems to interact significantly with the membrane (Section 2.4.2). I thus wondered if making grids with protein in lipids, as opposed to detergent, might improve the map quality. I thus solved a map of CKO protein in nanodiscs composed of POPC to test this hypothesis (Figure 3.4).

This map had the worst TMD density of any of the conditions I tested. My nanodisc prep had very low yields (approximately 5%), and so there may be some issue that causes the material to unfold during nanodisc reconstitution. Another possibility is that the nanodisc is more ordered than a micelle, and so dominates the alignment of the TMD, blurring out TM helices.

It is possible that other lipid combinations or reconstitution pipelines might improve results. This could be a promising avenue for future research, but I did not pursue that here.

We had also been concerned that our use of Fabs might make it dif-

ficult or impossible to align our particles to the TMD, or that they may be changing the conformation of the ECD in some way. This protein preparation therefore did not include either of the fabs we use to break pseudosymmetry. Using the extensive ECD glycosylation I was still able to break pseudosymmetry, but did not detect any differences with and without Fabs (discussed more in Chapter 4).

3.1.6. Mouse ENaC and trypsin

Mouse Uncleaved   **Mouse Trypsin**
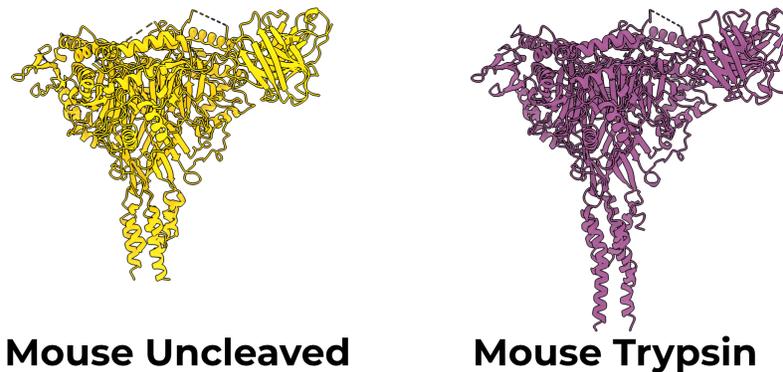
Figure 3.5.: The models of uncleaved (left) and trypsin-treated (right) mouse ENaC.

Finally, I investigated another homologue, mouse ENaC (Figure 3.5). Like human ENaC, mouse ENaC is an αβγ heterotrimer. This material was treated in largely the same way as human ENaC, and the results are presented together.

I treated one of the two mouse maps presented here with trypsin. We expected this to induce a conformational change from the closed to open states, but did not see any significant difference in the ECD or TMD. This is discussed further in Chapter 4.

3.2. The TMD is misfolded

Our previous structural work was focused on wild-type-like channels, with undefined gating states[145]. I wondered if channels with

a defined open state might provide a more consistent, and therefore higher resolution, TMD. To this end, I created mutant channels (CKO/DEG) which contained two mutations expected to increase channel P_O. The first, βS520K, holds the channel open regardless of proteolytic cleavage state[161]. The second, αT240W, which reduces the affinity of the channel for the α inhibitory peptide[158]. I solved maps of the CKO/DEG channels with and without C8 PIP_2, a ligand known to open ENaC without proteolysis[226].
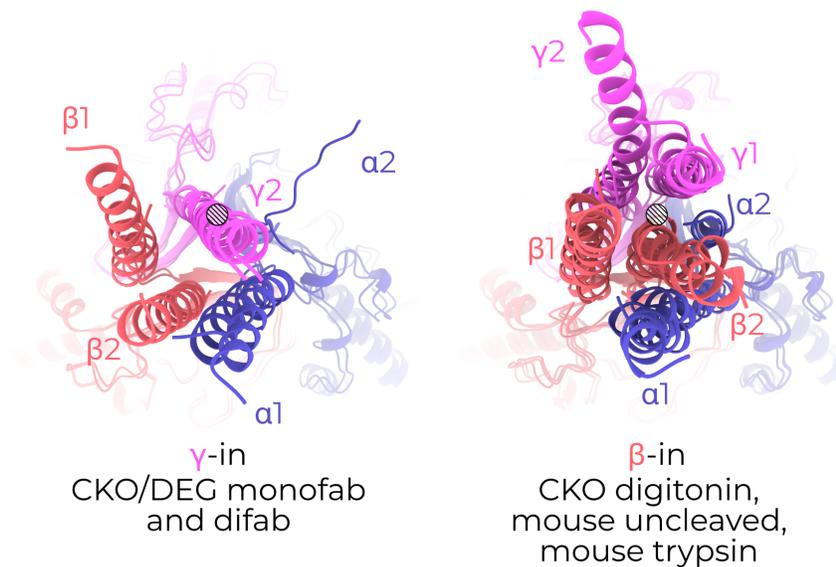
Figure 3.6.: The ENaC transmembrane domain adopts two conformations. TMDs of all six ENaC models separated by TM conformation, viewed from the intracellular side. Models are in the same position and at the same scale in each image, so positions are directly comparable. A grated circle is added in the same position to aid comparison between panels.

In all six of our models, the visible TMs are arranged in a roughly triangular fashion around a central helix (Figure 3.6 A). In CKO/DEG channels this helix is γ TM2. In all other models, the central helix is β TM2. I thus name the two conformations γ-in or β-in, respectively. I observe no change in the TMD open addition of PIP_2. Unfortunately, αTM2 and γTM1 are only visible in the β-in conformation. The arrangement of and great distance between pore-forming TM2

helices observed in our maps (Figure 3.7) also runs counter to existing knowledge of ENaC's pore[135]. Given this surprising state and the low quality of the maps' TMDs, I limit technical discussion of the TMD and hope that future studies will better resolve this critical channel domain. I do also note that although our cryoEM maps support the presence of the αT240W mutation, I observe no significant rearrangement of the nearby residues (Figure 3.8).

3.3. Functional Assays

I will cover my work on developing functional assays here, since they would be most useful in assessing the quality of purified ENaC's TMD. For the most part, I worked on two functional assays: the scintillation proximity assay (SPA) and the flux assay. Much of the work I present on SPA was performed alongside Alex Houser and especially James Cahill.

3.3.1. The scintillation proximity assay does not show promise for ENaC/DEG family members

In a SPA assay, the protein of interest is bound to beads which contain a scintillant. Radiolabeled ligand is then added to the mixture. If the ligand binds the protein, it is close enough to the beads that the β-particles can interact with the scintillant, emitting light. These counts can be taken as a measurement of binding affinity. Some argue that measuring affinity for a pore-binding ligand is a proxy for measuring proper folding of the pore[227].

Our main issue was non-specific binding. We could never measure the non-specific binding in its entirety, and so any signal that may potentially have been present was swamped out in noise. Changing from detergent sample to nanodiscs did not improve signal. Neither did changing from standard SPA beads to smaller, higher SNR nanoSPA beads.

One possible explanation of this is that none of our ENaC has a properly folded TMD and therefore cannot bind amiloride or its derivatives. Indeed, that is what our maps seem to suggest. However, experiments performed with human ASIC show the same result: ever-
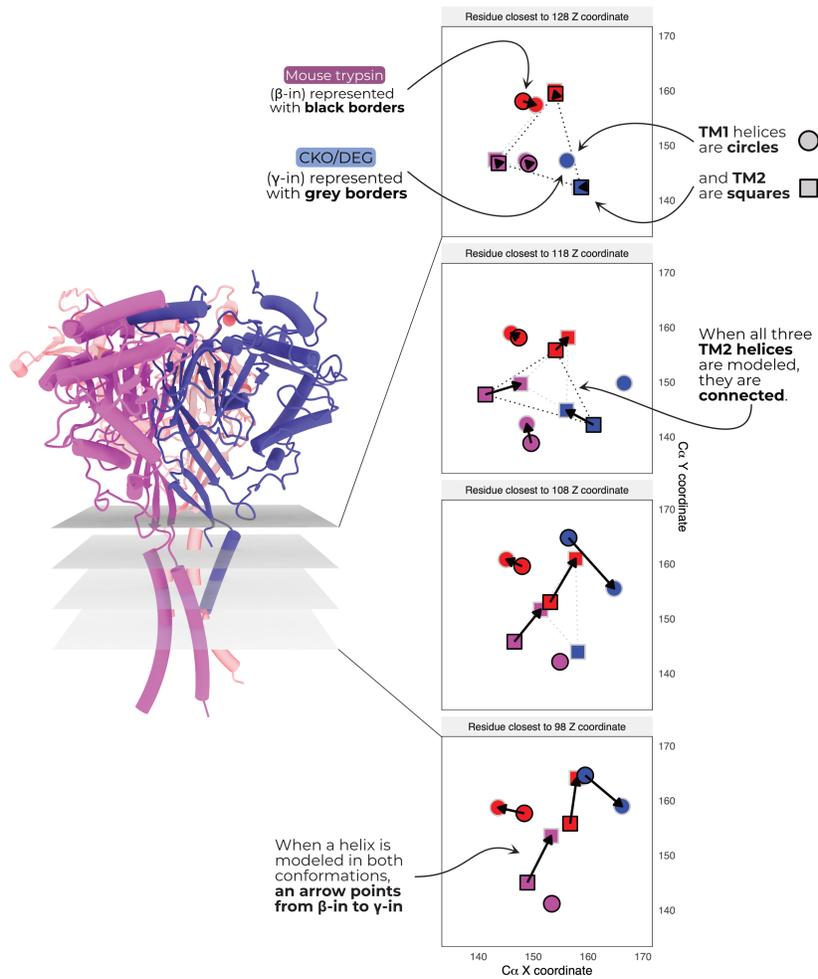
Figure 3.7.: Slices through the ENaC TMD reveal a non-physiological arrangement. Slices of the models with the best TMD density for both of β-in and γ-in (mouse trypsin and CKO/DEG difab, respectively) are displayed at four Z co-ordinates. The Cα of the residue closest to each Z coordinate is plotted in the horizontal XY plane and assigned a symbol to aid viewing. TM1 residues are circles; TM2 residues are squares. β-in residues have black borders, while γ-in residues have grey borders. Arrows connect the β-in residue to its cognate γ-in residue. If all three TM2 helices are modeled, they are connected by a triangle to represent the size of the pore at that Z slice.
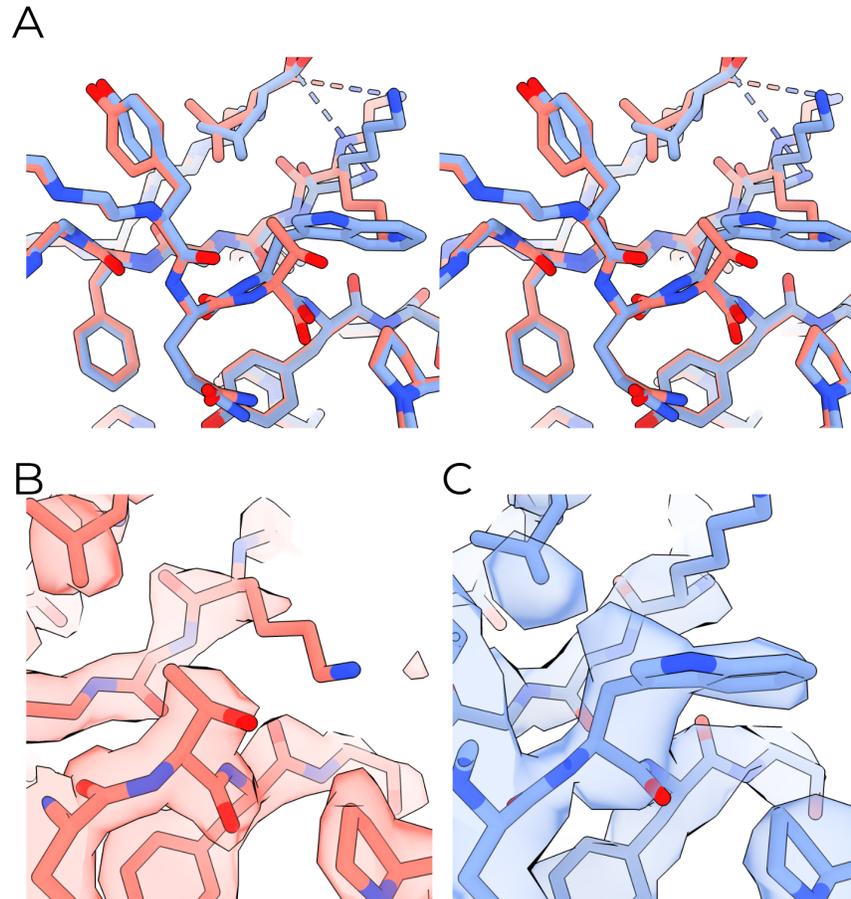
Figure 3.8.: The αT240W mutation does not modify ECD conformation. **A**: Stereo view of the GRIP domain near αT240. Red: CKO, blue: CKO/DEG monofab. **B** and **C**: CryoEM map potential surrounding α240 in CKO and CKO/DEG monofab, respectively.
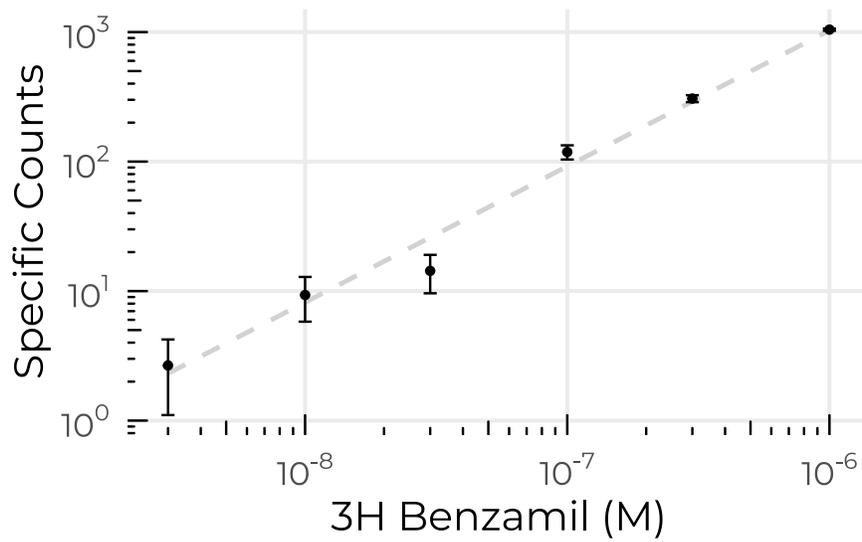
Figure 3.9.: An example of SPA, in this case of CKO/DEG nanodiscs. Note that although the background counts have been subtracted, the relationship between ligand and counts is still linear.

increasing linear "specific" counts no matter the conditions (James Cahill, personal communication). However, this same ASIC protein has properly folded TMs as assessed by cryoEM maps.

These problems are not seen when other labs use the same reagents on different targets. Typically, when SPA doesn't work, there are zero specific counts rather than some linearly increasing unaccounted-for background. It may, then, be that SPA with tritiated amiloride derivatives does not work with, or is significantly more difficult for, members of the ENaC/DEG family.

3.3.2. A sodium flux assay shows promise

After abandoning SPA I went in search of a new, more direct means of assessing ENaC function. I had previously used a K^+ flux assay when working on GIRK and decided to try adapting it to Na^+ flux. For an example of this assay, see Figure 1C of Whorton and McKinnon[228].

In the canonical K^+ flux assay, the protein of interest is incorporated into small unilamellar vesicles with potassium buffer inside
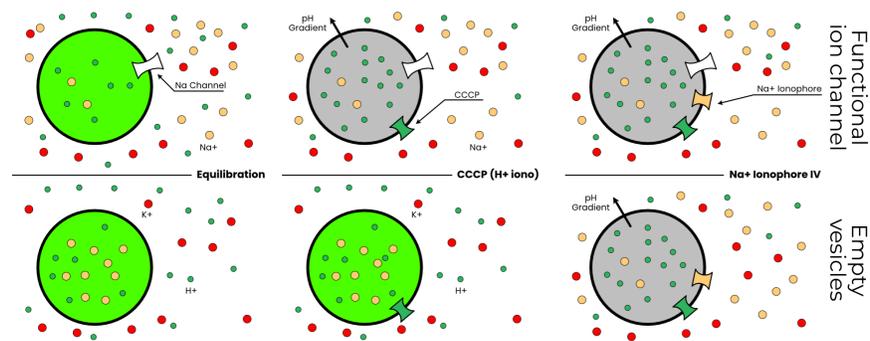
Figure 3.10.: A cartoon of a sodium flux assay. Red, yellow, and green circles are K$^+$, Na$^+$, and H$^+$ respectively. White, green, and beige hyperbolae are sodium channels, CCCP, and Na$^+$ ionophores respectively. **Left**: Vesicles with (top) or without (bottom) sodium channels are equilibrated in a buffer containing ACMA. Both are fluorescent because no pH gradient exists. **Middle**: CCCP is added to both mixtures. This quenches fluorescence in the ion channel vesicles by establishing a pH gradient. **Right**: Na$^+$ ionophore is added to both mixtures. This measures the maximum fluorescence quenching possible in the prep.

and sodium outside (Figure 3.10). Thus, in vesicles with functional sodium-selective ion channels, potassium flows out of the vesicle, establishing an electrochemical gradient. The fluorescent dye ACMA is added to these vesicles. Then, the proton ionophore CCCP is added. In vesicles with functional ion channels, protons pass into the vesicles, down their gradient. This establishes a pH gradient, which quenches ACMA. Thus, reduced fluorescence at the CCCP stage indicates functional ion channels (Figure 3.11). Finally, valinomycin (a K$^+$ ionophore) is added to measure the minimum fluorescence.
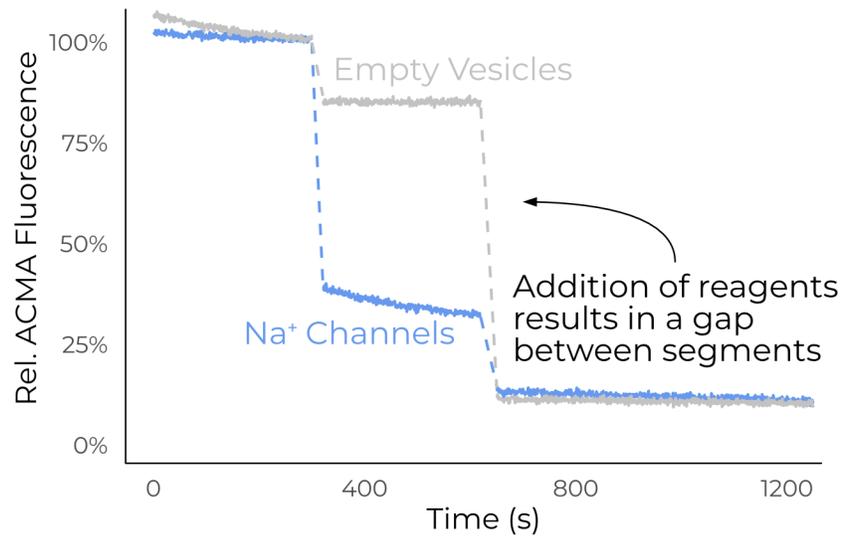
Figure 3.11.: A model example of flux data. ACMA fluorescence relative to the steady-state equilibrated value is plotted on Y, time on X. After the addition of each reagent the vesicles are allowed to equilibrate before addition of the next. In this example, it is clear the blue vesicles have functional ion channels since their fluorescence decreased with the addition of CCCP, while the grey vesicles are intact but do not have ion channels, since their fluorescence decreased with the addition of Na$^+$ ionophore but not CCCP.

To adapt this protocol to Na$^+$ required swapping to internal sodium and external potassium and a sodium-specific ionophore to replace valinomycin. Luckily, several such ionophores are commercially

available. None of them have quite the selectivity or flux of valino-mycin, but they are less important than the CCCP anyway. I selected Sodium Ionophore IV, or 2,3:11,12-Didecalino-16-crown-5[229].

This assay was, in the end, reliably able to produce readings of empty vesicles (Figure 3.12), but ENaC never passed any ions with the addition of CCCP (Figure 3.13). Moreover, addition of ENaC in any amount seemed to disrupt the empty vesicles. It is likely, then, that the ENaC is not properly folded, or that the addition of concentrated digitonin disrupts the vesicles on its own. A good next step in the development of this assay would be a positive control with ASIC or some other sodium channel.
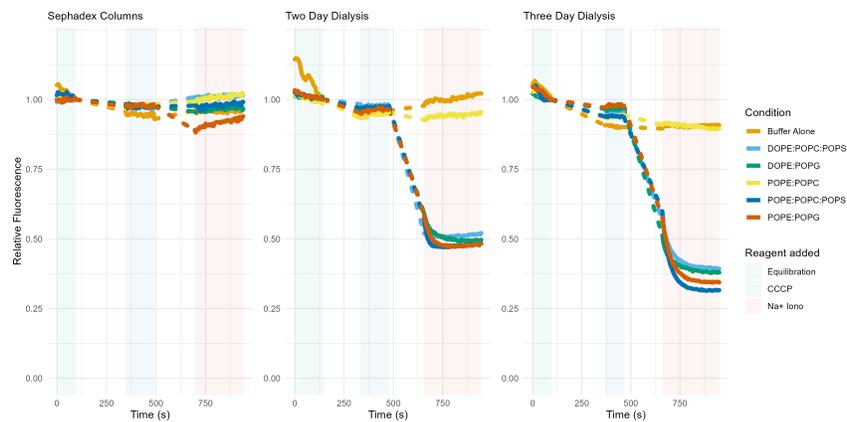
Figure 3.12.: The Na^+ flux assay reliably measures flux through empty vesicles composed of a variety of lipid mixes. Lipid mixes (colors) were tested for the ability to form vesicles as measured by the flux assay. Three different methods of forming vesicles were tested (facets).

3.4. What can be salvaged?

I've tried a great list of experiments to improve the quality of our TMD, none of which really worked. Here's what of my work can be carried forward into future studies.
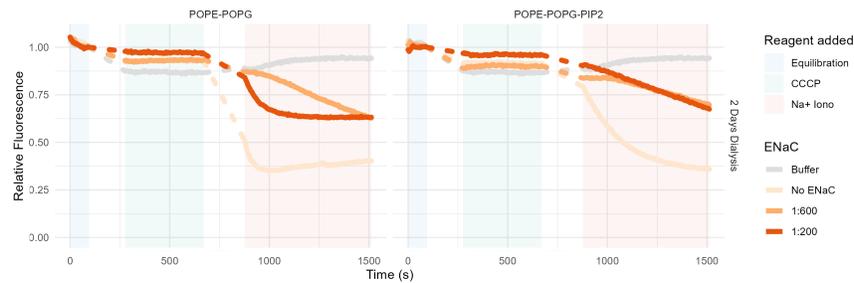
Figure 3.13.: The flux assay was performed with two lipid mixes (facets). In addition to the buffer control (grey), three ENaC:lipid ratios were tested: no ENaC, 1:600, and 1:200 (increasing color saturation). None of these show a decrease in fluorescence with addition of CCCP, indicating that there was no Na^+ flux in any mixture.

3.4.1. Future studies should avoid digitonin

I believe the TMD is misfolded as a result of solubilization with digitonin. Digitonin solubilizes membranes by chelating cholesterol[230]. ENaC is activated by cholesterol-mediated PIP_2 interactions and is found in cholesterol-rich lipid rafts[200,203]. Additionally, the helices in the low-resolution TMD region of truncated ENaC, which was never exposed to digitonin, do have the expected pore-lining TM2 architecture[147].

Of course, all of the TMD maps to date are very low-resolution. Although I am confident in my TM assignments, it is possible that the wrong TM identity has been assigned to some of the densities. Hopefully future, higher-resolution maps of the TMD will settle the matter.

3.4.2. Cysteine knock-out mutations should be abandoned

The CKO mutations do increase ENaC yield, but their theoretical underpinning is not sound at all. Channels with either one of γC33A and/or γC41A exhibit reduced P_O and increased SSI compared with wild type despite no change in surface expression[219]. More worryingly, γC33 and C41 border the HG motif — any disruption here

Recall that CKO channels have the following mutations in addition to protease site knockouts: αC63A, βC30A, and γC33,41A

69

might have serious consequences on the physiological relevance of a resolved TMD structure. Beyond the concerning question of whether the mutant channels would then recapitulate physiological ENaC gating processes, they clearly act in opposition to the goal of creating channels biased to the open state in CKO/DEG.

Conversely, if the goal is to disrupt palmitoylated sites (which, nominally, it was not), why are αC63 and βC30 knocked out when they are known not to be palmitoylated in the cell[217]? Or, if the goal is to knock out *all* potential palmitoylation sites, why are the majority left un-mutated? Fundamentally, the CKO mutations are logically inconsistent and should either be abandoned or consolidated behind a single theory of action.

3.4.3. Acid shock

I briefly tried "acid shocking" ENaC during the purification. My thinking was that poorly folded ENaC would be the first to aggregate under stressful conditions, leaving behind higher quality material. Similar treatments could have been high temperature or salt concentrations — there was nothing theoretically special about pH aside from the fact that ENaC and channels like it are sensitive to pH.

I did not notice a difference in total yield (beyond the losses expected from salt exchange alone), leading me to believe that the procedure did not have any real effect on ENaC, regardless of its folding state. Additionally, maps made with acid-shocked material (CKO digitonin and CKO/DEG difab) are not of substantially higher quality than the other, un-shocked maps.

4. ECD Stability Under Activating Conditions

Despite the fact that the TMD remains elusive, my hope was that investigating conditions thought to open the channel I might observe large-scale ECD rearrangements like those observed in ASIC. In this chapter I cover my efforts on that front, starting with a map of mouse ENaC solved pre- and post-trypsin treatment. Next, I investigate a putative sodium self-inhibition site that had been described previously in the literature (including by our own lab) in the presence of Na^+ and K^+. Finally, I highlight the extensive newly-resolvable surface glycosylation present in all of my ECD maps.

4.1. ECD conformation is unchanged by trypsin cleavage
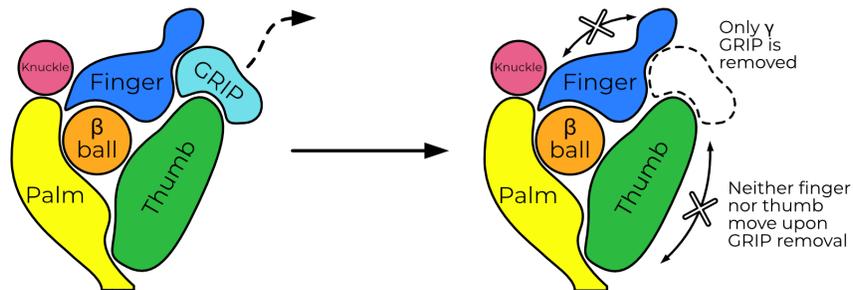
Figure 4.1.: In this section I show that cleavage of mouse ENaC with trypsin does not induce any detectable rearrangement of the ECD

ENaC can reliably be opened by trypsin treatment[180]. Additionally, the inhibitory peptide is easily resolved in all of my ECD maps. I wondered whether treatment with trypsin would result in movement

of the finger and thumb domains as the model of ASIC-like gating movements predicts (Figure 4.1). It's important to note here that I had significant help from Arpita Bharadwaj, who performed the purification and initial characterization of the mouse material for these grids. Both uncleaved and trypsin-treated mouse ENaC were of similar map quality (3.24 and 3.30 Å respectively with whole-protein masks).
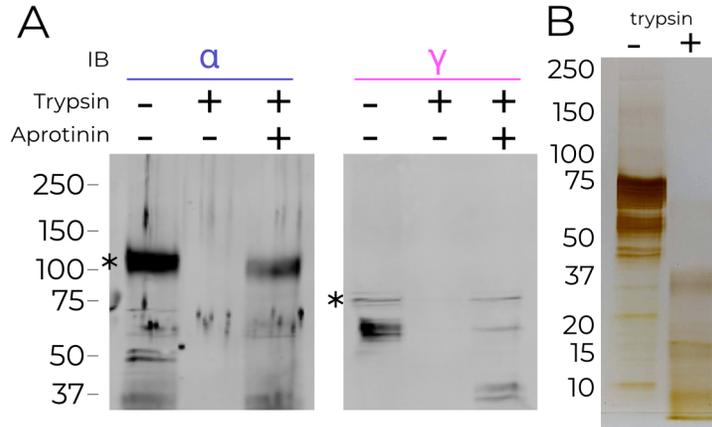
Figure 4.2.: Purified ENaC is cleaved by trypsin. **A**: Western blot for α (left) and γ (right) ENaC. Purified mouse protein was treated with trypsin and aprotinin as indicated. Bands corresponding to full-length subunits are marked with an asterisk. **B**: Silver stain of material with and without trypsin treatment. Material for silver stain and western blot is from different expressions and purifications.

Biochemical analyses show that trypsin treatment cleaves both the α and γ subunits (Figure 4.2). Additionally, trypsin treatment of *X. laevis* oocytes expressing mouse αβγENaC show the expected increase in amiloride sensitive current (Figure 4.3). However, aside from the disappearance of the inhibitory peptide, the ECD is otherwise superimposable (RMSD 0.440 Å; Figure 4.4). The finger and thumb do not shift even a fraction of what the ASIC-like model would predict.

Based on the observed cryoEM map density, only the γ subunit GRIP domain is released from the channel. However, biochemical characterization indicates both are digested by trypsin. I also note that the entire GRIP domain, not just the inhibitory peptide, has reduced
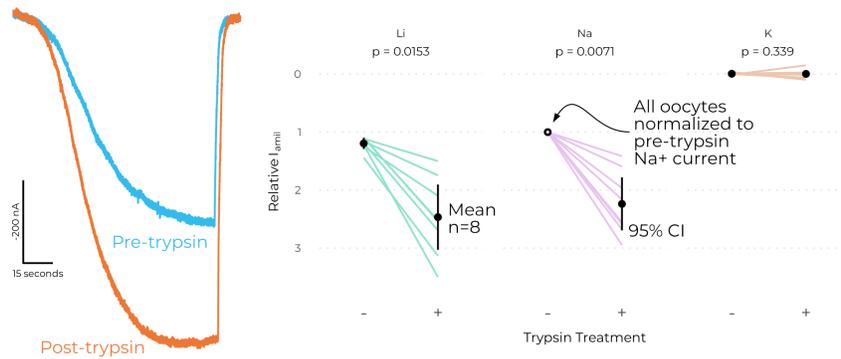
Figure 4.3.: Trypsin treatment increases amiloride-sensitive currents in oocytes. **Left**: representative amiloride-sensitive current before (cyan) and after (orange) trypsin treatment. Only Na$^+$ current is shown. **Right**: Average currents for all eight oocytes measured. All currents are scaled to pre-trypsin Na$^+$ current to account for differential cell size and expression. Error bars represent 95% confidence interval. Values for individual oocytes are plotted as lines. P-values are from a paired t-test on *unnormalized* oocyte currents. Using normalized data does not change the significance decision for any ion.
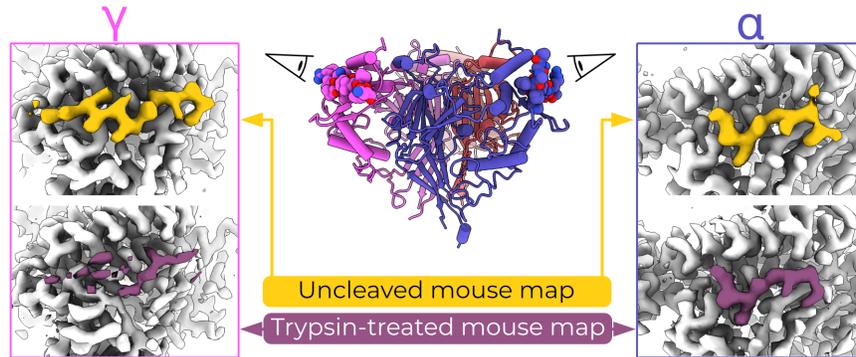
Figure 4.4.: cryoEM maps of mouse ENaC γ (left) and α (right) subunit GRIP domains without (yellow) and with (purple) trypsin treatment. The inhibitory peptide is colored in each map.

map density in the trypsin-treated sample. This suggests that the entire grip domain might be released from the subunit, but of course it's equally possible that release of the inhibitory peptide results in increased GRIP flexibility, which blurs out the map.

These results are incompatible with a large-scale movement of the ECD upon trypsin digestion. The existence of some γ GRIP density indicates that the trypsin-treated map is an ensemble of particles which have and have not released the γ GRIP domain. However, I do not observe any blurring of the γ thumb, which would be expected in a map comprising particles with significantly shifted conformations. I must therefore conclude that the removal of the γ inhibitory peptide is not sufficient, on its own, to induce such changes. Additionally, I note that these maps are the first indication that trypsin processing of the α subunit does not release its GRIP domain. This is surprising but perhaps not wholly unexpected; the γ subunit is known to be essential for activation by trypsin but the same has not yet been shown for αENaC[231].

Biochemical analysis indicates that ENaC is highly cleaved by trypsin, degrading the channel to fragments 37 kDa and smaller. It may be that the material in our map is highly cleaved, but held together by surface contacts throughout the channel which are disrupted by the addition of SDS from the loading buffer. This hypothesis could be tested with a native gel.

4.1.1. A strained tyrosine in the thumb

The high-resolution maps of the γ ECD reveal an interesting rotamer outlier, γY425 (Figure 4.5). The map for this residue is of high quality in five of the six maps, supporting its unlikely (prior probability of 0.035%) conformation (Figure 4.6). The single map with poor quality is the trypsin-treated mouse map, in which the density is blurred and unclear. Human γY425 forms hydrogen bonds with the finger (H233) and inhibitory peptide (Figure 4.5 A). This tyrosine adopts the same pose in all models *except* the trypsin-treated mouse model, in which it may rotate to point toward the outer GRIP domain (Figure 4.5 B). Given the poor quality of γY431 (the equivalent position to human Y425) in the mouse trypsin map, I cannot assign this rotamer with certainty.
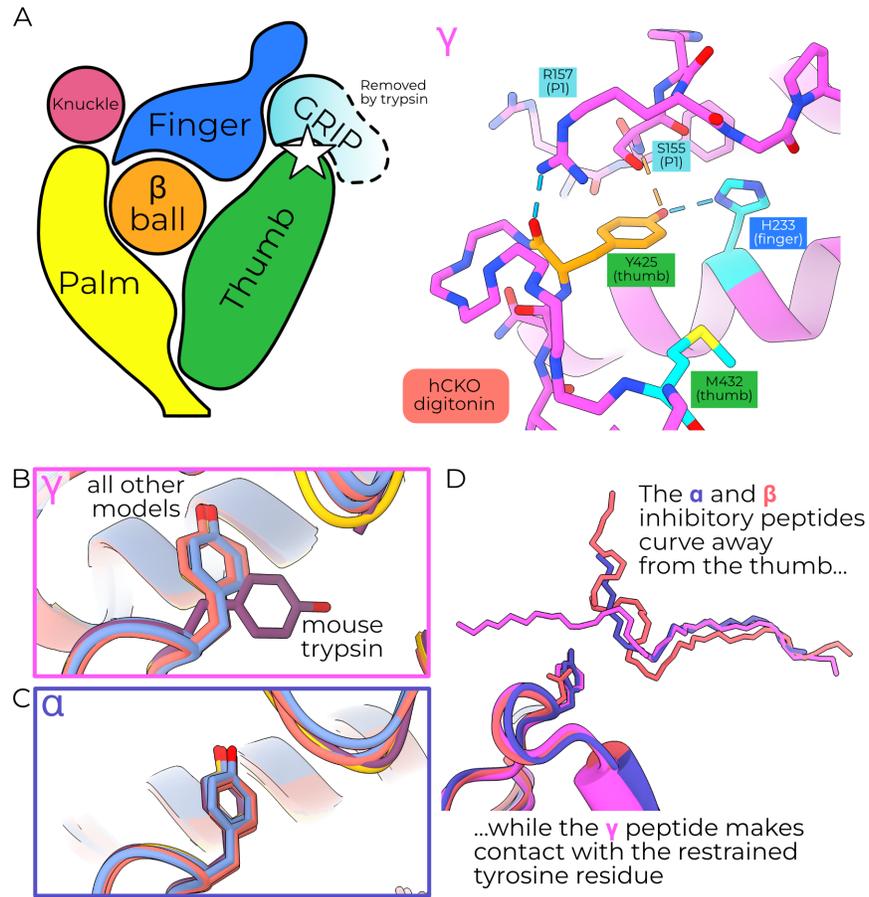
Figure 4.5.: A strained tyrosine rotamer is present in the γ subunit is released by trypsin cleavage. **A**: Human CKO γY425 (right), with approximate position indicated by a star in the cartoon (left). Hydrogen bonds are colored blue for ideal geometry and orange for slightly strained distance. **B**: γY425 (Y431 in mouse) colored by construct: human CKO, human CKO/DEG, mouse uncleaved, and mouse trypsin as red, blue, yellow, and purple respectively. **C**: αY447 (Y474 in mouse) colored by construct. **D**: Comparison of the inhibitory peptides of α (blue), β (red), and γ (magenta). The displayed model is human CKO digitonin, but the peptides are superimposable in all six models.
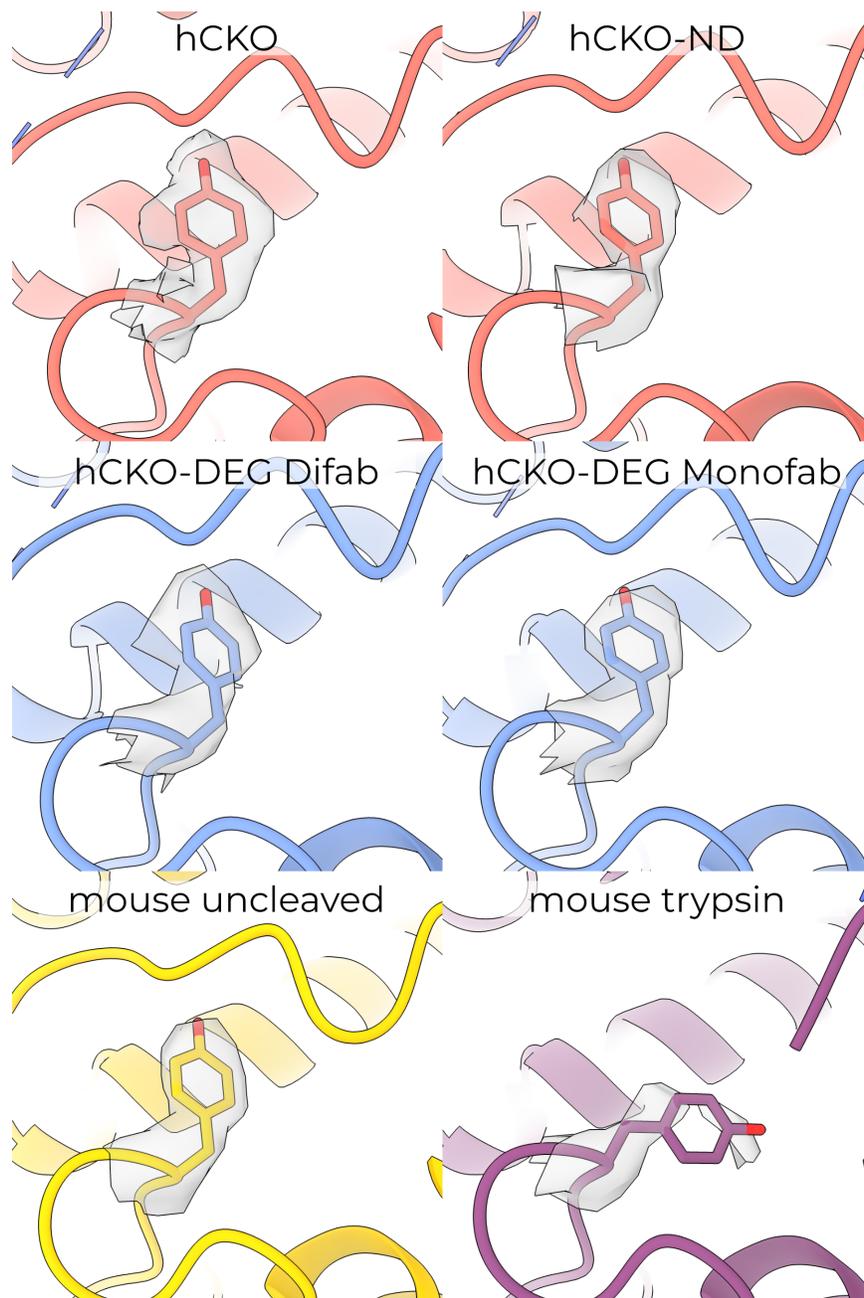
Figure 4.6.: CryoEM map potential for strained γENaC tyrosine for all maps/models. The maps are masked around the residue of interest.

The equivalent residue in α is also a tyrosine (αY447 and 474 in human and mouse respectively), but the inhibitory peptide curves away from the channel center, removing the interactions with the backbone and aromatic oxygen atoms and allowing a more favored rotamer (Figure 4.5 C and D). The same position in β, N417, only forms a hydrogen bond with the finger domain (N225). The lack of any interactions between βN417 and the βENaC GRIP domain, which is not cleaved to open the channel, is further suggestive of this residue's role in proteolytic gating.

I note also that the map quality worsens for the nearby γM438, mutation of which alters channel gating[232]. The reduced quality for this map region upon trypsin treatment may represent increased flexibility, perhaps indicating that conformational strain in the upper thumb is released along with the inhibitory peptide.

4.2. Sodium self-inhibition does not rearrange the ECD

I next investigated differences in ECD conformation among protein purified in external K^+ instead of Na^+. High extracellular K^+ does not prime inhibition in wild-type channels and SSI is rapidly attenuated upon exposure to low (i.e., <10 mM) Na^+[144,232]. Protein purified in K^+ buffer with nominally zero Na^+ should therefore be completely uninhibited.

The linker connecting β6 and β7 is important for SSI, and our lab has previously reported evidence of a putative bound Na^+ ion in this region[144,145]. Moreover, cross-linking of several pairs of amino acids in the ECD affects SSI magnitude, implying that some rearrangement is required for SSI[144,153]. Given this body of research, I solved structures of ENaC in high (200 mM) and low (nominal 0 mM Na^+, 200 mM K^+) sodium. I expected the high-Na^+ model to show rearrangements throughout the ECD, as would be required to transfer Na^+-binding state to the pore.

Our maps of human CKO ENaC in Na^+ and K^+ buffers achieved resolutions of 2.3 and 3.0 Å, respectively. The Na^+ structure was solved in digitonin with both the α- and β-binding Fabs, while the K^+ structure was solved in nanodiscs without any Fabs. Although previously it

has proven difficult to break the pseudo-threefold symmetry without including Fabs, I worried that their inclusion may affect SSI. Fortunately, the high quality of the cryoEM data allowed us to break the symmetry with neither Fabs nor an external reference — I believe the major symmetry breaking features are micelle-proximal glycans (Figure 4.7). Binding of either Fab induces minimal rearrangement of ENaC; the β epitope does not change conformation upon binding, while the α epitope pulls the loop from αP264-T274 approximately 4.5 Å away from the protein core without distorting the structure outside that loop.
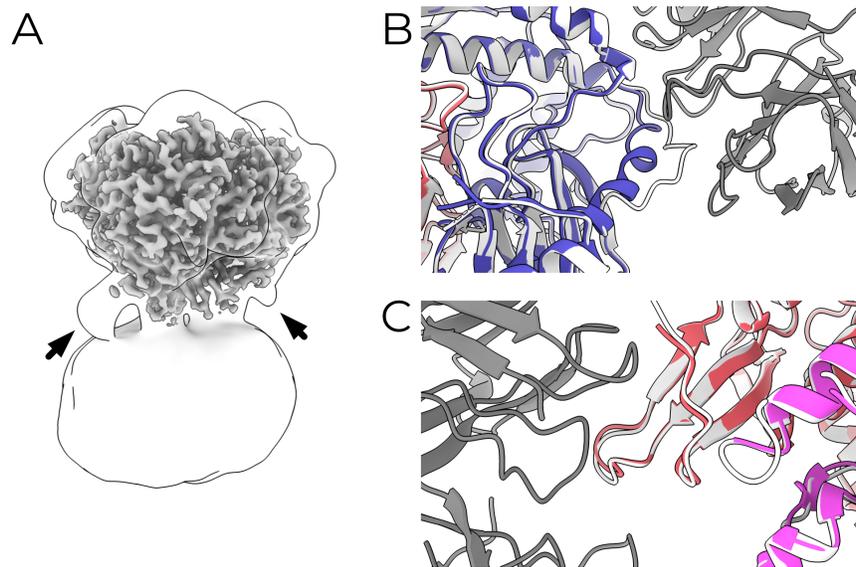
Figure 4.7.: Fab binding induces only minor changes in the extracellular domain of ENaC. A: Human CKO/DEG map. A lowpass filtered map is outlined to show pseudosymmetrybreaking glycosylation sites (arrows). B: the α subunit, C: the β subunit. Human CKO nanodisc model is colored by subunit, the human CKO/DEG ENaC is white, and human CKO/DEG Fabs are grey.

To my surprise, no resolved region of the ECD undergoes any significant structural rearrangement between high- and low-Na$^+$ buffers (RMSD 0.490 Å, Figure 4.8 A). Aside from the changes induced by the α-binding Fab, the only Cα shifts greater than 2 Å are residues terminating the resolved regions of the channel, which are likely a result of poor map quality. An acidic cleft in the αENaC finger, near the β-
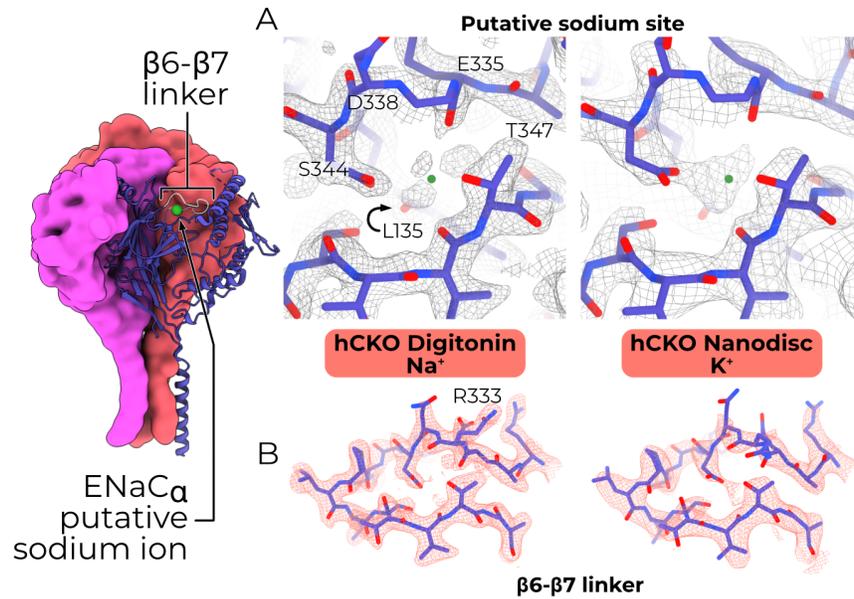
Figure 4.8.: Presence or absence of Na$^+$ does not rearrange the ECD. **A**: A previously identified ion-binding site still shows cryoEM map density with both Na$^+$ (left) and K$^+$ (right). The green dot corresponds to the previously-reported (PDB 6WTH) putative ion position. **B**: The β6-β7 linker in Na$^+$ or K$^+$ buffers.

ball, is implicated in sodium self-inhibition[144]. However, the cryoEM maps have density for a ligand in the acidic cleft in both the Na^+ and K^+ maps (Figure 4.8 A), although the site is slightly expanded in the K^+ map, perhaps to accommodate the larger K^+ ion. The β6-β7 linker has high quality density in both maps, supporting an almost-identical (Cα RMSD 1.076 Å when the whole α subunit is aligned by the palm domain) conformation, aside from the blurring of αR333 across multiple rotamers (Figure 4.8 B).

Although SSI is sensitive to pH, the buffer conditions for the CKO map should be at least 55% inhibited[146]. Attempts at detecting other classes of particle in the CKO ENaC (Na^+) map were not successful, leading us to believe that the particles are homogeneous. The lack of any significant structural difference in the acidic pocket in the presence of Na^+ and K^+ is more compatible with an SSI model in which Na^+-bound ENaC is "locked" in a closed state, rather than some third inhibited state.

4.3. Glycans make important contacts among subunits and with the membrane

Glycosylation of ENaC at conserved asparagine sites is essential for sodium self-inhibition, trypsin activation, and mechanosensitivity[173,225]. The high-quality maps obtained in this study enable modeling of significantly more and longer glycans than in previous work. I find a total of 19 distinct glycosylation sites, with up to nine modellable sugars in a single glycan.

For the most part, the sugars are identical in all six models and make no protein or glycan interactions. These sugars likely play a role in other regulatory roles, such as channel trafficking and maturation or interaction with the extracellular matrix[173,175,225]. However, two classes of glycan are particularly interesting: the micelle-proximal and the intersubunit glycans.

The intersubunit glycans stretch from one subunit to another (Figure 4.9 A). I am able to model long chains for these glycans, with some maps supporting up to nine monosaccharides. Due to the flexibility of these long chains, the terminal side is quite blurred out in the

Figure 4.9.: ENaC's glycosylation sites form important intersubunit interactions. **A**: Cartoon overview of intersubunit glycosylations. Dotted lines represent glycan chains. Hexagons represent sugars, circles represent potentially-interacting residues. Unfiltered maps for the first two sugars are presented to indicate confidence in Asn assignment. **B**: Silver-stained SDS-PAGE gel of protein treated with PNGase F (approx. 36 kDa). **C**: Intersubunit glycan from βN260 to αD235, K495. **D**: Intersubunit interaction between glycans from βN207 (red) and γN271 (magenta). In both C and D, the solid surface is a gaussian-blurred version of the sharp human CKO digitonin map (mesh).

cryoEM maps, and so I cannot be confident about the exact orientation or identity of the constituent sugars. Nonetheless, the maps are of sufficient quality to at least suggest sugar-mediated interactions between subunits, and the first sugars are of sufficient resolution to assign the asparagine residues to which they are coupled.

Treatment with PNGase F induces a size shift in the purified protein, confirming that the protein is glycosylated (Figure 4.9 B). I built typical high-mannose glycans ($Man_5GlcNAc_2$) into the models as expected for GnTI⁻ and Sf9 cells to assess these interactions at a low resolution[233,234]. One glycan reaches from βN260 to the α subunit (Figure 4.9 C), potentially hydrogen bonding with αD235 and αK459. These three residues are absolutely conserved across ENaC genes surveyed. Similarly, glycans attached to conserved sites βN207 and γN271 connect the β GRIP to the γ palm (Figure 4.9 D). Knockout of sugars in similar positions in αENaC increase blood pressure in mice[225]. The relatively high quality of these glycans suggest they are quite conformationally stable and may play a role in channel function.

The micelle-proximal glycans are anchored to hαN397 and hβN364 and the equivalent mouse residues, mαN424 and mβN362 (Figure 4.10 A). The α site is conserved in mammalian ENaCs, while the β site is conserved in all surveyed organisms except lungfish. These glycans extend away from the ECD body and turn down toward the micelle or lipids and are clear in all ENaC maps solved to date. The γ subunit does not have an equivalent asparagine residue, and so does not have a micelle-proximal glycan.

I note that all ENaC maps produced to date also show a consistent tilt of the micelle or nanodisc such that the γ subunit is closer to the surface of the micelle than are the α or β subunits; this tilt does not appear to be an artifact of in-plane rotation (Figure 4.10 B). I propose therefore that this tilt may in part be caused by the presence of the micelle-proximal glycans, which are only missing from γENaC (Figure 4.10 C). Their presence in the nanodisc map may indicate that they perform a similar role in a native cell membrane context.
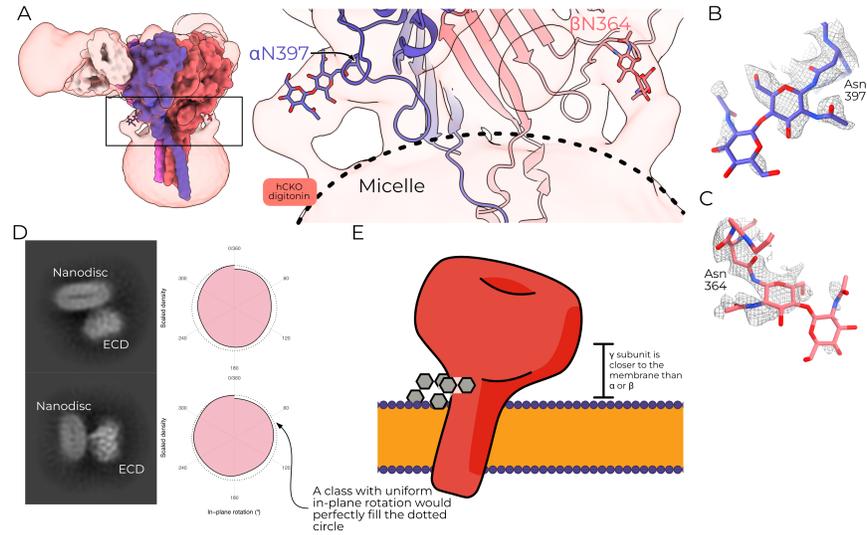
Figure 4.10.: ENaC's glycans contact the micelle. **A**: An overview of the position of the micelle-proximal glycans and the micelle. The image on the right is a zoomed view of the boxed region on the left. **B and C**: The sharpened map of human CKO digitonin for the first sugar attached to αN397 and βN364, respectively. **D**: In-grid rotation distribution for two selected classes of CKO nanodiscs. Note that both classes have even distribution of in-plane angles, indicating that the micelle tilt does not align with some grid force such as fluid flow during blotting. **E**: A cartoon representation of the position of the membrane-proximal glycans relative to the micelle tilt axis.

4.4. How does this change our understanding of the ECD?

4.4.1. A misfolded TMD may uncouple ECD motions

Regardless of the treatment applied, I cannot measure any change in the ECD. This stability stands in stark contrast to the highly dynamic ECD of the gating model widely assumed in the field and based on that of ASIC1[148,150]. I observe trypsin cleavage of both the α and γ GRIP domains, but only reduced cryoEM map density for the γ domain. The maps are otherwise perfectly superimposable, with unchanged ECDs and TMDs. Loss of density for only the γ GRIP domain is surprising but not entirely unexpected — channels lacking the γ subunit or specific lysine residues in the γ ECD are not activated by trypsin[231]. It is therefore possible that while the α GRIP domain is cleaved, it is not directly involved in trypsin-mediated channel activation. Based on biochemical data, I speculate that the α GRIP domain is also cleaved by trypsin, but the GRIP domain is still clearly visible in our cryoEM maps. This could be the result of non-covalent interactions between the α GRIP domain and the α finger and thumb. In any case, a lack of any observable channel rearrangement upon removal of the γ inhibitory peptide (a state in which ENaC's P_O approaches 0.9) must lead us to a deeper consideration of ENaC gating[136].

Although the best-studied mechanism of ENaC opening is GRIP proteolysis, multiple studies have found other stimuli which open the channel, including laminar shear stress and phospholipids (see Section 2.4 for more detail). ENaC P_O is also sensitive to changes in both intracellular and extracellular pH[138]. It is thus possible that the cell possesses multiple mechanisms with which it can open ENaC and uses them in combination to tune Na^+ permeability.

The possibility of a more complex pathway to open ENaC is supported by *in vivo* studies as well. The proportion of cleaved γENaC from mice lacking SGK1 is significantly smaller than that of WT mice, but cells from these kidneys have indistinguishable amiloride-sensitive current[235]. Similarly, ENaC missing the canonical furin cleavage site in the γ subunit is not cleaved when expressed in *X. laevis* oocytes, but currents do not differ between the mutant channels and WT[236].

Indeed, in different tissues and in different studies the cleavage of either α- or γENaC seems to be of greater importance, hinting at an environmental effect on the relationship between GRIP cleavage and channel P_O[136,181,186]. Based on this prior research and the maps I present here, I suspect that ENaC gating is not as simple as the proposed mechanism in which a single, coordinated protein maturation step moves the channel from a low- to high-P_O state[237]. However, I cannot make firm conclusions about ENaC gating due to the unresolved question of the TMD.

As discussed in Chapter 3, the TMDs of all six models are disturbed and likely do not represent a physiological conformation. It is possible that the ECD requires some kind of feedback from the TMD, and that this coupling has been lost during purification and grid preparation.

Mutations in linkers between the TMD and ECD of other channels have dramatic effects on ECD function; for instance, the *lurcher* mutation in the GluR1 ECD/TMD linker dramatically increases ECD affinity for glutamate[238]. I suspect that the ENaC ECD requires a fully-assembled six-TM pore region to respond to GRIP domain excision, but such a conclusion would require deeper investigation. A TMD/ECD decoupling would also explain the lack of ECD shift with the introduction of the DEG mutation, which has been shown to hold the channel in an open state, and for which I see dramatic TMD restructuring but no change in the ECD[161].

I speculate, based on these results, that the structures of both human and mouse ENaC are deeply dependent on some input from the membrane. We know that ENaC requires PIP_2 to open, and is opened when bound by PIP_3 regardless of cleavage state (Section 2.4.2.1). It would not be entirely surprising, then, if other membrane features inform ENaC's folding state. It is possible that finding a more-stable ortholog, or one with a gating mechanism less dependent on membrane lipids, would improve the quality of the TMD, as our mouse maps have significantly better TMD density than our human maps.

4.4.2. A role for the β9-α4 linker in gating

In *Malacoceros fuliginosus* FaNaC, a histidine in the β9-α4 linker forms contacts with both TMs[149]. This interaction blocks channel opening

until ligand is bound. In ENaC and *Helix aspersa* FaNaC the equivalent residue is a tyrosine, while in ASIC it is a tryptophan[239]. It is possible that any bulky or aromatic residue plays a similar ECD-lock role in this β-turn. In my models, only the β-subunit tyrosine is close enough to hydrogen bond with the TMs as I have modeled them, but this could be an artifact of the disordered TMD, or the interaction may be mediated by lipids.

I also note that the proline directly preceding this tyrosine in both the β and γ loops (α does not have a proline in this loop) is in the *cis* conformation. This is true in both human and mouse ENaC, in all treatment conditions. Our previous models missed this conformer, likely because of significantly poorer resolution. ASIC's tryptophan in this position is also preceded by a *cis*-proline[148]. In light of the important role this loop plays in FaNaC gating, and the conserved *cis*-Pro/aromatic pair in ASIC and ENaC, further investigation of this loop may prove fruitful.

4.4.3. The acidic pocket's uncertain role in sodium self-inhibition

Previous reports suggested that rearrangement of an acidic pocket in the α finger plays a key role in SSI[144]. Our K^+ maps are solved in the presence of sodium levels far below those known to release SSI, but the acidic pocket does not rearrange. However, there are species differences in ENaC SSI, and the functional work describing this acidic pocket was all performed on mouse ENaC, while our high- and low-Na^+ models are both of human ENaC[144,146,232].

In human (but not rat) ENaC, pH titration changes the magnitude of SSI but, crucially, not the K_i of Na^+; a surprising result if surface-accessible acidic residues form the SSI Na^+-binding site. Moreover, ENaC cleavage essentially abrogates SSI, and residues in the upper finger which interact with the GRIP domain are implicated in SSI[143,232,240]. Despite this relationship, I also see no conformational shift of the acidic pocket upon trypsin treatment.

It may therefore be that the acidic pocket simply has a higher affinity for Na^+ than K^+ and therefore presents a higher barrier to ECD conformational shift when bound to Na^+. This would effectively trap

the channel in a closed state, rather than some third sodium self-inhibited state. Without observing the complete gating cycle of ENaC and the concomitant conformational changes it is impossible to make any firm conclusions about the precise mechanism of SSI. I therefore hope that our models will serve as a useful guide in future studies on this acidic pocket, as well as a search for other potential sources of SSI.

4.4.4. Glycans may further differentiate ENaC subunits

These maps represent the first structural study of ENaC's extensive glycosylation. I must emphasize that these models all arise from particles which have only high-mannose glycosylation. However, glycosylation is required for ENaC function and trypsin digestion and our channels have the expected electrophysiological properties and respond to trypsin treatment in the expression system (Figure 4.11)[173]. I am therefore confident that the high-mannose glycans are sufficient for mechanistic inference.

Two distinct classes of glycan make observable interactions in our models: membrane-proximal and intersubunit glycans. I propose that the membrane-proximal glycans may help establish the micelle/nanodisc tilt observed in all ENaC maps to date, and that this tilt may have as-yet unknown functional implications.

I am not suggesting that these glycans alone are sufficient to define ENaC's orientation in the membrane For example, in addition to missing a membrane-proximal glycan γENaC has two fewer residues between the palm and TM1 than do the α or β subunits[147].

The β intersubunit glycan interacts with the top of the α thumb, which may serve to rigidify it. Indeed, knock-out of β glycans protects the α subunit from trypsin digestion[173]. Perhaps the β intersubunit glycan holds the α subunit in a pose which primes it for proteolytic cleavage. In contrast, the γ palm, not thumb, is rigidified by the other large intersubunit glycan. I note also that previous observation of channels cleaved by endogenous cellular machinery indicated that removal of the inhibitory peptide reduces the map quality for γ- but not αP3 and P4[145].
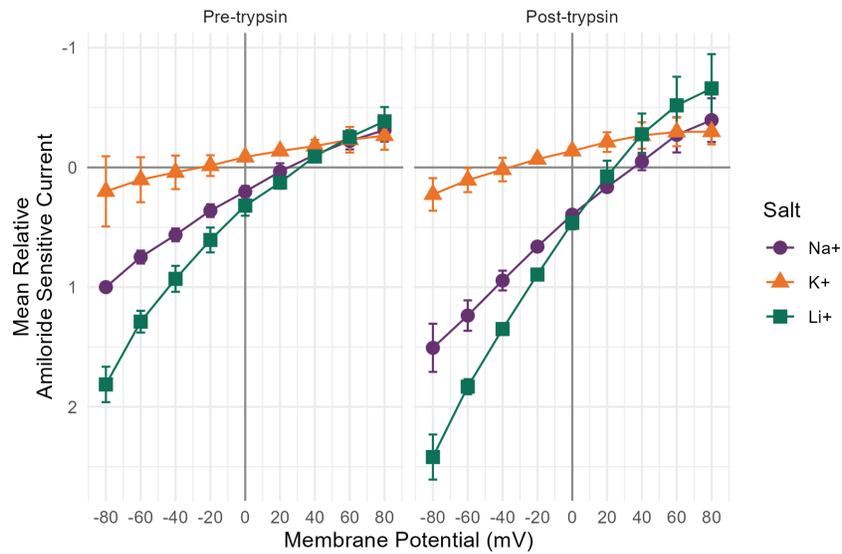
Figure 4.11.: I/V curves for human CKO and CKO/DEG channels. Values are normalized per-cell to the inward current at -80 mV before trypsin treatment. Cells were treated with trypsin for five minutes before being re-recorded. Each point is the average of three cells. Error bars represent +/- one standard deviation.

4.4. How does this change our understanding of the ECD?

This alternate rigidification is interesting in the light of sodium self-inhibition. As yet, there is not a clear explanation for how mutating αH255 and γH233 (occupying the same structural position in their respective subunits) might have opposite effects on SSI (augmenting and eliminating it, respectively)[241]. Considering a rigid macro-domain comprising the uncleavable β subunit, γ palm, and α thumb (connected via glycans) and a flexible macro-domain comprising the α palm and finger and γ thumb, I see that γH233 belongs to the former, while αH255 belongs to the latter. Of course, more functional study is required to firmly establish this link, but I note that the SSI of channels lacking N-linked glycosylation sites is significantly reduced compared to WT[173].

Part III.

Conclusion

5. Conclusion

5.1. Context

ENaC is an essential regulator of sodium permeability in many tissues. It plays an important role in a number of biological processes and diseases, including hypertension and cystic fibrosis. Despite its importance, little is known about the exact molecular mechanism by which the channel opens and closes.

Unlike ENaC, a great deal of structure/function information is available for the close relative ASIC. It is understandable, then, that the field has long assumed the mechanisms of these two channels are similar. In the "ASIC-like" model, the GRIP domain forms a wedge which holds the finger and thumb apart. Proteolytic release of this wedge allows the finger and thumb to collapse. This collapse is transmitted through the palm to open a fenestration near the membrane, allowing ions to pour through the pore. Mutations in the ENaC palm have large effects on current in a pattern similar to that of ASIC[148,172,242].

Proponents of this model (including our own lab) wave away differences between ASIC and ENaC currents. The most obvious is ASIC's desensitization. ASIC closes less than a second after opening[126]. Contrast this with ENaC, which does not desensitize at all — an open channel will remain open essentially indefinitely[140].

Desensitization in ASIC is in large part mediated by the four-residue β11-β12 linker[148]. This β-turn is quite well-conserved among ENaCs and ASIC1, with the important leucine and asparagine residues absolutely conserved, and its conformation in all models solved so far aligns well with ASIC's open state[147]. There is one notable difference between the ASIC and ENaC linkers: an alanine is replaced with an acidic residue in all ENaC subunits and species. In currently-available structures this acidic residue does not form hydrogen bonds with other residues, but it may do so in the open conformation.

ASIC's desensitization kinetics are so fast Nate Yoder, in the Gouaux lab, couldn't capture any open channels even with a hand-built plunge/ligand un-caging system.

ENaC currents do diminish over time in the presence of high external sodium in a process called sodium self-inhibition (SSI). SSI is independent from Na^+ currents and is relieved by proteolytic cleavage[140,143]. SSI seems to induce a large-scale rearrangement of the ECD, unlike ASIC desensitization[153]. Mutagenesis and cross-linking studies suggest that an acidic pocket comprising the finger and β-ball bind Na^+ to close the channel[144,232,240].

The precise relationship between ENaC and ASIC's gating is, if anything, less clear as a result of the work presented in this document. With the highest resolution yet, we detect a clear lack of movement when large-scale rearrangements are expected. In the remaining space afforded to me, I will remind the reader what we've learned and wonder what it might mean for the field moving forward.

5.2. Contrition and Contemplation

5.2.1. What is actually happening with cleavage and self-inhibition?

Two things are true: when I remove the inhibitory peptide from the ECD, I see no large-scale rearrangement of the finger or thumb; and the transmembrane domain of this protein is almost certainly in some non-physiological state. The former finding runs contrary to years of cross linking, mutagenesis, and electrophysiology experiments; the latter should give us pause in throwing out the existing model.

Could it be, then, that ENaC's ECD requires some kind of tension from or coupling to the membrane via the TMD? It's hard for me to come up with a model in which the finger and thumb do move closer together in a physiological environment, but do *not* move together without tension from the membrane, but it is the simplest means by which we might resolve this conflict. It is also possible that gating involves a related, but different motion, as seen in FaNaC[149].

Of course, this is all speculation. ASIC's ECD and TMD are loosely coupled — proton binding and pore opening are related for less than a second. What could we do to probe the relationship between the finger, thumb, GRIP, and pore?

There exist a great number of ECD mutations known to modify ENaC's P_O regardless of open state. Some of these (e.g., the Liddle syndrome mutant αC479R) are in regions of the ECD for which our maps are consistently quite high-quality[244]. ECD-only maps of these mutations would provide valuable insight into the gating mechanism even without a visible TMD.

A better understanding of SSI would further augment our knowledge of protease-mediated channel opening. SSI is unique to ENaC, and so we have little to rely on for mechanistic insight. My finding that ions bind the acidic pocket in Na^+ and K^+ buffers is surprising, as is the lack of any significant rearrangement of the ECD. Cross linking studies indicate that ECD conformational shifts are required for SSI[153]. This leaves us in the same situation as with proteolytic cleavage: is some kind of mis-folding preventing the expected rearrangements, or do they simply not occur?

A number of SSI-abrogating or -augmenting mutations have been described in the literature. At this point, solving ECD structures with resolutions better than 3 Å is routine. Systematic investigation of map densities in channels with and without these mutations could identify promising SSI ion-binding sites which may, in turn, inform further mechanistic studies.

Native material is another obvious answer. Production of a map of high enough quality to analyze gating mechanisms necessitates (at the time of writing) that the material is purified. This brings us to the question of why the transmembrane domain is hard to see in the first place.

5.2.2. A new approach is needed for the transmembrane domain

A single model of the TMD would go a long way toward providing a believable model of ENaC's gating cycle. As discussed in Chapter 3, I believe that solubilization with digitonin presents a significant obstacle to TMD resolution. FaNaC purified in n-dodecyl-β-D-maltoside (DDM) and exchanged into GDN and then 3:1 POPC:POPG nanodiscs yields a high-resolution TMD[149]. Our first maps of ENaC, also purified in DDM, provided the best TMD until the present work with mouse ENaC[147].

Out of consideration for my audience, I have covered only a fraction of these. The interested reader, or my unlucky successor, might check Kleyman and Eaton for more detail[243].

However, the nanodiscs presented in this work have the worst TMD map of any presented. Moreover, my experience has demonstrated that ENaC is particularly difficult to get into nanodiscs in the first place when purified with DDM or digitonin. We know that the TMD is properly folded in the expression system, since it is the same system in which we perform electrophysiology. Purification with styrene-maleic acid may yield the first TMD map, as it yielded the first map of the re-entrant loop in ASIC[169]. Alternately, spiking in required lipids (especially PIPs) during solubilization may stabilize the TMD enough to get it into nanodiscs.

I do not think these minor changes alone will be sufficient. Rather, I believe future work should pursue homologues in parallel to efforts toward improved purification. In what I find difficult to believe is a coincidence, the authors of the FaNaC study published a phylogenetic analysis the year before they published their structure of one of the more distantly related FaNaC genes[245]. ENaCs exist as far back as jawless fishes; there is a wealth of orthologs to pick from[246].

Despite their low macroscopic currents in exogenous expression systems, homomeric channels certainly seem to exist in the body (see Section 1.1, especially the tongue and blood vessels). A homomeric channel does away with the difficulties of using Fabs without introducing the concomitant difficulties of subunit assignment. Their small currents mean that the number of properly folded channels may be even smaller than for αβγ channels, but it's probably worth checking.

5.2.3. Electrophysiology

Not everyone likes structure — that's okay, there's something here for you too. I have identified several glycans which, based on their extended visibility in my maps, may serve a structural role. We also know, as covered in Section 2.4.3, that glycans are necessary for sensation of laminar shear stress. Electrophysiological studies of ENaCs with single asparagine mutations have not been performed by any lab, to my knowledge. Using my maps as a guide, it may be fruitful to investigate the sensitivity of ENaCs lacking the most visible (presumably the most structurally constrained) glycans to LSS.

Additionally, the FaNaC paper raises an interesting question: is the bulky residue in the β9-α4 linker necessary for proper gating? Conservation of the surrounding residues and an adjacent *cis*-proline would suggest so. An investigation of this loop is interesting whether the channels can gate or not — the best kind of experiment.

5.3. Conjecture

What do I think should be done next, if I'm so smart?

5.3.1. We need a functional assay

Why doesn't our channel seem to undergo structural changes when it's sodium self-inhibited? Why can't we see our TMD? Why doesn't the GRIP domain release from the ECD when it's cleaved? All of these questions and more are essentially unanswerable without knowing *whether our channels are functional in the first place*. All of the mysterious observations from my work are fully satisfied by the conjecture that *we're looking at misfolded garbage*.

As such, my first priority moving forward would be the development and implementation of a functional assay. As I discussed in Section B.2, the SPA assay shows no sign of working any time soon, and isn't even truly a functional assay.

The sodium flux assay is, on the other hand, already halfway to usefulness. Using a known-good ion channel (ASIC comes to mind, but any sodium-specific ion channel will do) would help push it to completion by isolating the "protein is good" variable from the "assay works" variable. With more confidence in the fact that our purified material has some bearing on what is present in the cells, we can move back to structural study.

5.3.2. Find a better construct for the TMD

As discussed in Section 3.4.2, the CKO and DEG mutations should both be abandoned. They never made sense in the first place, and they did not accomplish their stated goals of stabilizing the TMD and

holding the TMD and ECD in open states, respectively. Returning to a wild-type-like construct will make our results more interpretable.

To find a satisfactory gene for further study, we should first perform thermo-FSEC assays on a wide range of ENaC orthologs. Thermal stability, like SPA, is not an assay for function. It is, however, high-throughput, and channels which are stable are more likely to remain functional once purified.

In this context, a thermo-FSEC assay is the typical FSEC assessment of particle homogeneity with the added step of heating a sample from 4 through 90 °C. Essentially, measuring peak height degradation with increasing temperature is used as a proxy for temperature stability.

I would then take the most-stable 10% of these constructs and perform whatever functional assay we end up developing on all of them. Any gene with significant flux could be screened using the same cryoEM concentrations and grid parameters I've determined in this work. We thus know we'd be starting with the most functional, most stable material we can find, rather than picking genes at essentially random as was done previously. Any promising maps could have their purification and grid parameters refined while simultaneously performing proper electrophysiological studies to ensure selectivity and currents are within reason.

One potential objection to this method is that we do not know whether our symmetry-breaking Fabs will bind to all forms of ENaC. My response is two-fold. First, it is easy to determine this during the high-throughput thermo-FSEC experiments by adding a condition with Fabs and looking for a shift. Second, my Fab-less nanodisc dataset demonstrates that < 3 Å maps can be achieved without the use of Fabs.

Moreover, solving maps just to solve maps is pointless. Fabs bind tightly and predictably to human and mouse ENaC, and look where that got us.

5.3.3. There are other interesting regions of the channel

I think it was a mistake for me to focus exclusively on the TMD. Instead, there are exciting mutations in the ECD with described functional consequences that we already have map. For instance, mutation of a disulfide in the α subunit palm (αC479) results in Liddle syndrome, and we have high-quality map density for both halves of this disulfide (Figure 5.1).
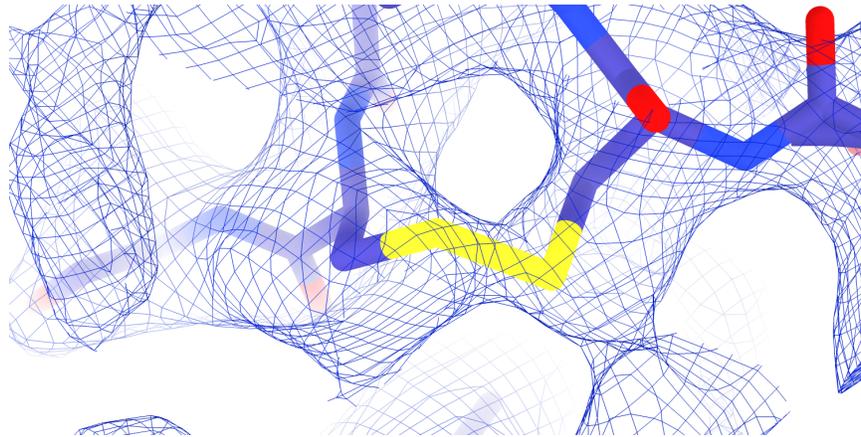
Figure 5.1.: The human CKO/DEG map surrounding the disulfide between αC479 and αC394.

5.4. Conclusion

After six years of work, I'm left with more questions than I had at the start. For decades, the ENaC field has been moving away from the gating model of "ASIC with an internal ligand". Rather, ENaC P_O is fine-tuned by a variety of internal and external signals. I believe that my findings here are consistent with that premise. I hope that this work is eventually a small piece of our understanding of this deceptively complicated channel.

References

1. Hille, B. (2001). Ion Channels of Excitable Membranes 3rd ed. (Sinauer Associates).

2. Ackerman, M.J., and Clapham, D.E. (1997). Ion Channels — Basic Science and Clinical Disease. N Engl J Med *336*, 1575–1586. 10.1056/NEJM199705293362207.

3. Guyton, A.C. (1991). Blood Pressure Control—Special Role of the Kidneys and Body Fluids. Science *252*, 1813–1816. 10.1126/science.2063193.

4. Liddle, G.W., Bledsoe, T., and Coppage, W.S. (1963). A familial renal disorder simulating primary aldosteronism but with negligible aldosterone secretion. Trans. Assoc. Am. Physicians *76*, 199–213.

5. Hanukoglu, I., and Hanukoglu, A. (2016/04/01/). Epithelial sodium channel (ENaC) family: Phylogeny, structure–function, tissue distribution, and associated inherited diseases. Gene *579*, 95–132. 10.1016/j.gene.2015.12.061.

6. Tetti, M., Monticone, S., Burrello, J., Matarazzo, P., Veglio, F., Pasini, B., Jeunemaitre, X., and Mulatero, P. (2018). Liddle Syndrome: Review of the Literature and Description of a New Case. International Journal of Molecular Sciences *19*. 10.3390/ijms19030812.

7. Wang, L.-P., Yang, K.-Q., Jiang, X.-J., Wu, H.-Y., Zhang, H.-M., Zou, Y.-B., Song, L., Bian, J., Hui, R.-T., Liu, Y.-X., et al. (2015). Prevalence of Liddle Syndrome Among Young Hypertension Patients of Undetermined Cause in a Chinese Population. The Journal of Clinical Hypertension *17*, 902–907. 10.1111/jch.12598.

8. Liu, K., Qin, F., Sun, X., Zhang, Y., Wang, J., Wu, Y., Ma, W., Wang, W., Wu, X., Qin, Y., et al. (2018). Analysis of the genes involved in Mendelian forms of low-renin hypertension in Chinese early-onset hypertensive patients. Journal of Hypertension *36*.

9. Yang, K.-Q., Xiao, Y., Tian, T., Gao, L.-G., and Zhou, X.-L. (2014). Molecular genetics of Liddle's syndrome. Clinica Chimica Acta *436*, 202–206. 10.1016/j.cca.2014.05.015.

10. Schild, L., Canessa, C.M., Shimkets, R.A., Gautschi, I., Lifton, R.P., and Rossier, B.C. (1995). A mutation in the epithelial sodium channel causing Liddle disease increases channel activity in the Xenopus laevis oocyte expression system. Proceedings of the National Academy of Sciences *92*, 5699–5703. 10.1073/pnas.92.12.5699.

11. Abriel, H., Loffing, J., Rebhun, J.F., Pratt, J.H., Schild, L., Horisberger, J.-D., Rotin, D., and Staub, O. (1999). Defective regulation of the epithelial Na+ channel by Nedd4 in Liddle's syndrome. J Clin Invest *103*, 667–673. 10.1172/JCI5713.

References

12.   Lu, C., Pribanic, S., Debonneville, A., Jiang, C., and Rotin, D. (2007). The PY Motif of ENaC, Mutated in Liddle Syndrome, Regulates Channel Internalization, Sorting and Mobilization from Subapical Pool. Traffic *8*, 1246–1264. 10.1111/j.1600-0854.2007.00602.x.

13.   PRADERVAND, S., WANG, Q., BURNIER, M., BEERMANN, F., HORISBERGER, J.D., HUMMLER, E., and ROSSIER, B.C. (1999). A Mouse Model for Liddle's Syndrome. Journal of the American Society of Nephrology *10*.

14.   Bertog, M., Cuffe, J.E., Pradervand, S., Hummler, E., Hartner, A., Porst, M., Hilgers, K.F., Rossier, B.C., and Korbmacher, C. (2008). Aldosterone responsiveness of the epithelial sodium channel (ENaC) in colon is increased in a mouse model for Liddle's syndrome. The Journal of Physiology *586*, 459–475. 10.1113/jphysiol.2007.140459.

15.   CHEEK, D.B., and PERRY, J.W. (1958). A salt wasting syndrome in infancy. Arch Dis Child *33*, 252–256. 10.1136/adc.33.169.252.

16.   Geller, D.S., Rodriguez-Soriano, J., Boado, A.V., Schifter, S., Bayer, M., Chang, S.S., and Lifton, R.P. (1998). Mutations in the mineralocorticoid receptor gene cause autosomal dominant pseudohypoaldosteronism type I. Nature Genetics *19*, 279–281. 10.1038/966.

17.   Chang, S.S., Grunder, S., Hanukoglu, A., Rösler, A., Mathew, P.M., Hanukoglu, I., Schild, L., Lu, Y., Shimkets, R.A., Nelson-Williams, C., et al. (1996). Mutations in subunits of the epithelial sodium channel cause salt wasting with hyperkalaemic acidosis, pseudohypoaldosteronism type 1. Nature Genetics *12*, 248–253. 10.1038/ng0396-248.

18.   Edelheit, O., Hanukoglu, I., Gizewska, M., Kandemir, N., Tenenbaum-Rakover, Y., Yurdakök, M., Zajaczek, S., and Hanukoglu, A. (2005). Novel mutations in epithelial sodium channel (ENaC) subunit genes and phenotypic expression of multisystem pseudohypoaldosteronism. Clinical Endocrinology *62*, 547–553. 10.1111/j.1365-2265.2005.02255.x.

19.   Schaedel, C., Marthinsen, L., Kristoffersson, A.-C., Kornfält, R., Nilsson, K.O., Orlenius, B., and Holmberg, L. (1999). Lung symptoms in pseudohypoaldosteronism type 1 are associated with deficiency of the α-subunit of the epithelial sodium channel. The Journal of Pediatrics *135*, 739–745. 10.1016/S0022-3476(99)70094-6.

20.   Riordan, J.R., Rommens, J.M., Kerem, B.-S., Alon, N., Rozmahel, R., Grzelczak, Z., Zielenski, J., Lok, S., Plavsic, N., Chou, J.-L., et al. (1989). Identification of the Cystic Fibrosis Gene: Cloning and Characterization of Complementary DNA. Science *245*, 1066–1073. 10.1126/science.2475911.

21.   Quinton, P.M. (1983). Chloride impermeability in cystic fibrosis. Nature *301*, 421–422. 10.1038/301421a0.

22.   Zabner, J., Smith, J.J., Karp, P.H., Widdicombe, J.H., and Welsh, M.J. (1998). Loss of CFTR Chloride Channels Alters Salt Absorption by Cystic Fibrosis Airway Epithelia In Vitro. Molecular Cell *2*, 397–403. 10.1016/S1097-2765(00)80284-1.

23.   Randell, S.H., and Boucher, R.C. (2006). Effective Mucus Clearance Is Essential for Respiratory Health. Am J Respir Cell Mol Biol *35*, 20–28. 10.1165/rcmb.2006-0082SF.

24. Button, B., Cai, L.-H., Ehre, C., Kesimer, M., Hill, D.B., Sheehan, J.K., Boucher, R.C., and Rubinstein, M. (2012). A Periciliary Brush Promotes the Lung Health by Separating the Mucus Layer from Airway Epithelia. Science *337*, 937–941. 10.1126/science.1223012.

25. Knowles, M.R., Stutts, M.J., Spock, A., Fischer, N., Gatzy, J.T., and Boucher, R.C. (1983). Abnormal Ion Permeation Through Cystic Fibrosis Respiratory Epithelium. Science *221*, 1067–1070. 10.1126/science.6308769.

26. Ji, H.-L., Chalfant, M.L., Jovov, B., Lockhart, J.P., Parker, S.B., Fuller, C.M., Stanton, B.A., and Benos, D.J. (2000). The Cytosolic Termini of the β- and γ-ENaC Subunits Are Involved in the Functional Interactions between Cystic Fibrosis Transmembrane Conductance Regulator and Epithelial Sodium Channel *. Journal of Biological Chemistry *275*, 27947–27956. 10.1074/jbc.M002848200.

27. Mall, M., Grubb, B.R., Harkema, J.R., O'Neal, W.K., and Boucher, R.C. (2004). Increased airway epithelial Na+ absorption produces cystic fibrosis-like lung disease in mice. Nature Medicine *10*, 487–493. 10.1038/nm1028.

28. Fyfe, G.K., and Canessa, C.M. (1998). Subunit Composition Determines the Single Channel Kinetics of the Epithelial Sodium Channel. Journal of General Physiology *112*, 423–432. 10.1085/jgp.112.4.423.

29. Grubb, B.R., O'Neal, W.K., Ostrowski, L.E., Kreda, S.M., Button, B., and Boucher, R.C. (2012). Transgenic hCFTR expression fails to correct β-ENaC mouse lung disease. American Journal of Physiology-Lung Cellular and Molecular Physiology *302*, L238–L247. 10.1152/ajplung.00083.2011.

30. Mall, M.A., Button, B., Johannesson, B., Zhou, Z., Livraghi, A., Caldwell, R.A., Schubert, S.C., Schultz, C., O'Neal, W.K., Pradervand, S., et al. (2010). Airway Surface Liquid Volume Regulation Determines Different Airway Phenotypes in Liddle Compared with βENaC-overexpressing Mice *. Journal of Biological Chemistry *285*, 26945–26955. 10.1074/jbc.M110.151803.

31. Sheridan, M.B., Fong, P., Groman, J.D., Conrad, C., Flume, P., Diaz, R., Harris, C., Knowles, M., and Cutting, G.R. (2005). Mutations in the beta-subunit of the epithelial Na+ channel in patients with a cystic fibrosis-like syndrome. Human Molecular Genetics *14*, 3493–3498. 10.1093/hmg/ddi374.

32. Kerem, E., Bistritzer, T., Hanukoglu, A., Hofmann, T., Zhou, Z., Bennett, W., MacLaughlin, E., Barker, P., Nash, M., Quittell, L., et al. (1999). Pulmonary Epithelial Sodium-Channel Dysfunction and Excess Airway Liquid in Pseudohypoaldosteronism. N Engl J Med *341*, 156–162. 10.1056/NEJM199907153410304.

33. Collawn, J.F., Lazrak, A., Bebok, Z., and Matalon, S. (2012). The CFTR and ENaC debate: How important is ENaC in CF lung disease? Am J Physiol Lung Cell Mol Physiol *302*, L1141–1146. 10.1152/ajplung.00036.2012.

34. GRUBB, B.R., and BOUCHER, R.C. (1999). Pathophysiology of Gene-Targeted Mouse Models for Cystic Fibrosis. Physiological Reviews *79*, S193–S214. 10.1152/physrev.1999.79.1.S193.

References

35. Yarmolinsky, D.A., Zuker, C.S., and Ryba, N.J.P. (2009). Common Sense about Taste: From Mammals to Insects. Cell *139*, 234–244. 10.1016/j.cell.2009.10.001.

36. Zhao, G.Q., Zhang, Y., Hoon, M.A., Chandrashekar, J., Erlenbach, I., Ryba, N.J.P., and Zuker, C.S. (2003). The Receptors for Mammalian Sweet and Umami Taste. Cell *115*, 255–266. 10.1016/S0092-8674(03)00844-4.

37. Chandrashekar, J., Hoon, M.A., Ryba, N.J.P., and Zuker, C.S. (2006). The receptors and cells for mammalian taste. Nature *444*, 288–294. 10.1038/nature05401.

38. Danilova, V., Hellekant, G., Tinti, J.-M., and Nofre, C. (1998). Gustatory Responses of the Hamster Mesocricetus auratus to Various Compounds Considered Sweet by Humans. Journal of Neurophysiology *80*, 2102–2112. 10.1152/jn.1998.80.4.2102.

39. Alan C. Spector, Nick A. Guagliardo, and Steven J. St. John (1996). Amiloride Disrupts NaCl versus KCl Discrimination Performance: Implications for Salt Taste Coding in Rats. J. Neurosci. *16*, 8115. 10.1523/JNEUROSCI.16-24-08115.1996.

40. Gannon, K.S., and Contreras, R.J. (1995). Sodium intake linked to amiloride-sensitive gustatory transduction in C57BL/6J and 129/7 mice. Physiology & Behavior *57*, 231–239. 10.1016/0031-9384(94)00279-E.

41. Jennifer K. Roebber, Stephen D. Roper, and Nirupa Chaudhari (2019). The Role of the Anion in Salt (NaCl) Detection by Mouse Taste Buds. J. Neurosci. *39*, 6224. 10.1523/JNEUROSCI.2367-18.2019.

42. Kretz, O., Barbry, P., Bock, R., and Lindemann, B. (1999). Differential Expression of RNA and Protein of the Three Pore-forming Subunits of the Amiloride-sensitive Epithelial Sodium Channel in Taste Buds of the Rat. J Histochem Cytochem. *47*, 51–64. 10.1177/002215549904700106.

43. Chandrashekar, J., Kuhn, C., Oka, Y., Yarmolinsky, D.A., Hummler, E., Ryba, N.J.P., and Zuker, C.S. (2010). The cells and peripheral representation of sodium taste in mice. Nature *464*, 297–301. 10.1038/nature08783.

44. Lossow, K., Hermans-Borgmeyer, I., Meyerhof, W., and Behrens, M. (2020). Segregated Expression of ENaC Subunits in Taste Cells. Chemical Senses *45*, 235–248. 10.1093/chemse/bjaa004.

45. Canessa, C.M., Schild, L., Buell, G., Thorens, B., Gautschi, I., Horisberger, J.-D., and Rossier, B.C. (1994). Amiloride-sensitive epithelial Na+ channel is made of three homologous subunits. Nature *367*, 463–467. 10.1038/367463a0.

46. Shigemura, N., Ohkuri, T., Sadamitsu, C., Yasumatsu, K., Yoshida, R., Beauchamp, G.K., Bachmanov, A.A., and Ninomiya, Y. (2008). Amiloride-sensitive NaCl taste responses are associated with genetic variation of ENaC α-subunit in mice. American Journal of Physiology-Regulatory, Integrative and Comparative Physiology *294*, R66–R75. 10.1152/ajpregu.00420.2007.

47. Desor, J.A., and Finn, J. (1989). Effects of amiloride on salt taste in humans. Chemical Senses *14*, 793–803. 10.1093/chemse/14.6.793.

48. Stähler, F., Riedel, K., Demgensky, S., Neumann, K., Dunkel, A., Täubert, A., Raab, B., Behrens, M., Raguse, J.-D., Hofmann, T., et al. (2008). A Role of the Epithelial Sodium Channel in Human Salt Taste Transduction? Chemosensory Perception *1*, 78–90. 10.1007/s12078-008-9006-4.

49. Drummond, H.A., Gebremedhin, D., and Harder, D.R. (2004). Degenerin/Epithelial Na+ Channel Proteins Components of a Vascular Mechanosensor. Hypertension *44*, 643–648. 10.1161/01.HYP.0000144465.56360.ad.

50. Althaus, M., Bogdan, R., Clauss, W.G., and Fronius, M. (2007). Mechano-sensitivity of epithelial sodium channels (ENaCs): Laminar shear stress increases ion channel open probability. The FASEB Journal *21*, 2389–2399. 10.1096/fj.06-7694com.

51. Gu, G., Caldwell, G.A., and Chalfie, M. (1996). Genetic interactions affecting touch sensitivity in Caenorhabditis elegans. Proceedings of the National Academy of Sciences *93*, 6577–6582. 10.1073/pnas.93.13.6577.

52. Kougias, P., Weakley, S.M., Yao, Q., Lin, P.H., and Chen, C. (2010). Arterial baroreceptors in the management of systemic hypertension. Med Sci Monit *16*, RA1–8.

53. Drummond, H.A., Price, M.P., Welsh, M.J., and Abboud, F.M. (1998). A Molecular Component of the Arterial Baroreceptor Mechanotransducer. Neuron *21*, 1435–1441. 10.1016/S0896-6273(00)80661-3.

54. Epple, H.J., Amasheh, S., Mankertz, J., Goltz, M., Schulzke, J.D., and Fromm, M. (2000). Early aldosterone effect in distal colon by transcriptional regulation of ENaC subunits. American Journal of Physiology-Gastrointestinal and Liver Physiology *278*, G718–G724. 10.1152/ajpgi.2000.278.5.G718.

55. Sandle, G.I., Higgs, N., Crowe, P., Marsh, M.N., Venkatesan, S., and Peters, T.J. (1990). Cellular basis for defective electrolyte transport in inflamed human colon. Gastroenterology *99*, 97–105. 10.1016/0016-5085(90)91235-X.

56. Zeissig, S., Bergann, T., Fromm, A., Bojarski, C., Heller, F., Guenther, U., Zeitz, M., Fromm, M., and Schulzke, J. (2008). Altered ENaC Expression Leads to Impaired Sodium Absorption in the Noninflamed Intestine in Crohn's Disease. Gastroenterology *134*, 1436–1447. 10.1053/j.gastro.2008.02.030.

57. Amasheh, S., Barmeyer, C., Koch, C.S., Tavalali, S., Mankertz, J., Epple, H.-J., Gehring, M.M., Florian, P., Kroesen, A.-J., Zeitz, M., et al. (2004). Cytokine-dependent transcriptional downregulation of epithelial sodium channel in ulcerative colitis. Gastroenterology *126*, 1711–1720. 10.1053/j.gastro.2004.03.010.

58. Weir, M.R., and Dzau, V.J. (1999). The renin-angiotensin-aldosterone system: A specific target for hypertension management. American Journal of Hypertension *12*, 205S–213S. 10.1016/S0895-7061(99)00103-X.

References

59. Stockand, J.D. (2002). New ideas about aldosterone signaling in epithelia. American Journal of Physiology-Renal Physiology *282*, F559–F576. 10.1152/ajprenal.00320.2001.

60. Garty, H., and Palmer, L.G. (1997). Epithelial sodium channels: Function, structure, and regulation. Physiol. Rev. *77*, 359–396. 10.1152/physrev.1997.77.2.359.

61. Kemendy, A.E., Kleyman, T.R., and Eaton, D.C. (1992). Aldosterone alters the open probability of amiloride-blockable sodium channels in A6 epithelia. American Journal of Physiology-Cell Physiology *263*, C825–C837. 10.1152/ajpcell.1992.263.4.C825.

62. Naray-Fejes-Toth, A., and Fejes-Toth, G. (2000). The sgk, an aldosterone-induced gene in mineralocorticoid target cells, regulates the epithelial sodium channel. Kidney International *57*, 1290–1294. 10.1046/j.1523-1755.2000.00964.x.

63. Kellenberger, S., Gautschi, I., Rossier, B.C., and Schild, L. (06/15/ 1998). Mutations causing Liddle syndrome reduce sodium-dependent downregulation of the epithelial sodium channel in the Xenopus oocyte expression system. The Journal of Clinical Investigation *101*, 2741–2750. 10.1172/JCI2837.

64. Chen, S., Bhargava, A., Mastroberardino, L., Meijer, O.C., Wang, J., Buse, P, Firestone, G.L., Verrey, F., and Pearce, D. (1999). Epithelial sodium channel regulated by aldosterone-induced protein sgk. Proceedings of the National Academy of Sciences *96*, 2514–2519. 10.1073/pnas.96.5.2514.

65. Păunescu, T.G., Blazer-Yost, B.L., Vlahos, C.J., and Helman, S.I. (2000). LY-294002-inhibitable PI 3-kinase and regulation of baseline rates of Na+ transport in A6 epithelia. American Journal of Physiology-Cell Physiology *279*, C236–C247. 10.1152/ajpcell.2000.279.1.C236.

66. Staruschenko, A., Pochynyuk, O.M., Tong, Q., and Stockand, J.D. (2005). Ras couples phosphoinositide 3-OH kinase to the epithelial Na+ channel. Biochimica et Biophysica Acta (BBA) - Biomembranes *1669*, 108–115. 10.1016/j.bbamem.2005.01.005.

67. Frindt, G., and Palmer, L.G. (2015). Acute effects of aldosterone on the epithelial Na channel in rat kidney. American Journal of Physiology-Renal Physiology *308*, F572–F578. 10.1152/ajprenal.00585.2014.

68. Asher, C., Wald, H., Rossier, B.C., and Garty, H. (1996). Aldosterone-induced increase in the abundance of Na+ channel subunits. American Journal of Physiology-Cell Physiology *271*, C605–C611. 10.1152/ajpcell.1996.271.2.C605.

69. Frindt, G., and Palmer, L.G. (2009). Surface expression of sodium channels and transporters in rat kidney: Effects of dietary sodium. Am. J. Physiol. Renal Physiol. *297*, F1249–F1255. 10.1152/ajprenal.00401.2009.

70. Weisz, O.A., Wang, J.-M., Edinger, R.S., and Johnson, J.P. (2000). Non-coordinate Regulation of Endogenous Epithelial Sodium Channel (ENaC) Subunit Expression at the Apical Membrane of A6 Cells in Response to Various Transporting Conditions *. Journal of Biological Chemistry *275*, 39886–39893. 10.1074/jbc.M003822200.

71. Loffing, J., Pietri, L., Aregger, F., Bloch-Faure, M., Ziegler, U., Meneton, P., Rossier, B.C., and Kaissling, B. (2000). Differential subcellular localization of ENaC subunits in mouse kidney in response to high- and low-Na diets. American Journal of Physiology-Renal Physiology *279*, F252–F258. 10.1152/ajprenal.2000.279.2.F252.

72. May, A., Puoti, A., Gaeggeler, H.P., Horisberger, J.D., and Rossier, B.C. (1997). Early effect of aldosterone on the rate of synthesis of the epithelial sodium channel alpha subunit in A6 renal cells. Journal of the American Society of Nephrology *8*.

73. Stockand, J.D., Bao, H.-F., Schenck, J., Malik, B., Middleton, P., Schlanger, L.E., and Eaton, D.C. (2000). Differential Effects of Protein Kinase C on the Levels of Epithelial Na+ Channel Subunit Proteins *. Journal of Biological Chemistry *275*, 25760–25765. 10.1074/jbc.M003615200.

74. Escoubet, B., Coureau, C., Bonvalet, J.P., and Farman, N. (1997). Noncoordinate regulation of epithelial Na channel and Na pump subunit mRNAs in kidney and colon by aldosterone. American Journal of Physiology-Cell Physiology *272*, C1482–C1491. 10.1152/ajpcell.1997.272.5.C1482.

75. Masilamani, S., Kim, G.-H., Mitchell, C., Wade, J.B., and Knepper, M.A. (1999). Aldosterone-mediated regulation of ENaC α, β, and γ subunit proteins in rat kidney. J Clin Invest *104*, R19–R23. 10.1172/JCI7840.

76. Dagenais, A., Denis, C., Vives, M.-F., Girouard, S., Massé, C., Nguyen, T., Yamagata, T., Grygorczyk, C., Kothary, R., and Berthiaume, Y. (2001). Modulation of α-ENaC and A1-Na+-K+-ATPase by cAMP and dexamethasone in alveolar epithelial cells. American Journal of Physiology-Lung Cellular and Molecular Physiology *281*, L217–L230. 10.1152/ajplung.2001.281.1.L217.

77. Mick, V.E., Itani, O.A., Loftus, R.W., Husted, R.F., Schmidt, T.J., and Thomas, C.P. (2001). The α-Subunit of the Epithelial Sodium Channel Is an Aldosterone-Induced Transcript in Mammalian Collecting Ducts, and This Transcriptional Response Is Mediated via Distinct cis-Elements in the 5'-Flanking Region of the Gene. Molecular Endocrinology *15*, 575–588. 10.1210/mend.15.4.0620.

78. Dijkink, L., Hartog, A., Deen, P.M.T., van Os, C.H., and Bindels, R.J.M. (1999). Time-dependent regulation by aldosterone of the amiloride-sensitive Na+ channel in rabbit kidney. Pflügers Archiv *438*, 354–360. 10.1007/s004240050920.

79. Loffing, J., Zecevic, M., Féraille, E., Kaissling, B., Asher, C., Rossier, B.C., Firestone, G.L., Pearce, D., and Verrey, F. (2001). Aldosterone induces rapid apical translocation of ENaC in early portion of renal collecting system: Possible role of SGK. American Journal of Physiology-Renal Physiology *280*, F675–F682. 10.1152/ajprenal.2001.280.4.F675.

80. Renard, S., Voilley, N., Bassilana, F., Lazdunski, M., and Barbry, P. (1995). Localization and regulation by steroids of the α, β and γ subunits of the amiloride-sensitive Na+ channel in colon, lung and kidney. Pflügers Archiv *430*, 299–307. 10.1007/BF00373903.

References

81. Butterworth, M.B., Edinger, R.S., Frizzell, R.A., and Johnson, J.P. (2009). Regulation of the epithelial sodium channel by membrane trafficking. American Journal of Physiology-Renal Physiology *296*, F10–F24. 10.1152/ajprenal.90248.2008.

82. Kamynina, E., Debonneville, C., Bens, M., Vandewalle, A., and Staub, O. (2001). A novel mouse Nedd4 protein suppresses the activity of the epithelial Na+ channel. The FASEB Journal *15*, 204–214. 10.1096/fj.00-0191com.

83. Snyder, P.M., Steines, J.C., and Olson, D.R. (2004). Relative Contribution of Nedd4 and Nedd4-2 to ENaC Regulation in Epithelia Determined by RNA Interference *. Journal of Biological Chemistry *279*, 5042–5046. 10.1074/jbc.M312477200.

84. Rizo, J., and Südhof, T.C. (1998). C2-domains, Structure and Function of a Universal Ca2+-binding Domain. Journal of Biological Chemistry *273*, 15879–15882. 10.1074/jbc.273.26.15879.

85. Plant, P.J., Yeger, H., Staub, O., Howard, P., and Rotin, D. (1997). The C2 Domain of the Ubiquitin Protein Ligase Nedd4 Mediates Ca2+-dependent Plasma Membrane Localization. J. Biol. Chem. *272*, 32329–32336. 10.1074/jbc.272.51.32329.

86. Plant, P.J., Lafont, F., Lecat, S., Verkade, P., Simons, K., and Rotin, D. (2000). Apical Membrane Targeting of Nedd4 Is Mediated by an Association of Its C2 Domain with Annexin Xiiib. The Journal of Cell Biology *149*, 1473. 10.1083/jcb.149.7.1473.

87. Schild, L., Lu, Y., Gautschi, I., Schneeberger, E., Lifton, R.P., and Rossier, B.C. (1996). Identification of a PY motif in the epithelial Na channel subunits as a target sequence for mutations causing channel activation found in Liddle syndrome. The EMBO Journal *15*, 2381–2387. 10.1002/j.1460-2075.1996.tb00594.x.

88. Buetow, L., and Huang, D.T. (2016). Structural insights into the catalysis and regulation of E3 ubiquitin ligases. Nature Reviews Molecular Cell Biology *17*, 626–642. 10.1038/nrm.2016.91.

89. Wiesner, S., Ogunjimi, A.A., Wang, H.-R., Rotin, D., Sicheri, F., Wrana, J.L., and Forman-Kay, J.D. (2007/08/24/). Autoinhibition of the HECT-Type Ubiquitin Ligase Smurf2 through Its C2 Domain. Cell *130*, 651–662. 10.1016/j.cell.2007.06.050.

90. Bruce, M.C., Kanelis, V., Fouladkou, F., Debonneville, A., Staub, O., and Rotin, D. (2008). Regulation of Nedd4-2 self-ubiquitination and stability by a PY motif located within its HECT-domain. Biochem. J. *415*, 155. 10.1042/BJ20071708.

91. Chen, Z., Jiang, H., Xu, W., Li, X., Dempsey, D.R., Zhang, X., Devreotes, P., Wolberger, C., Amzel, L.M., Gabelli, S.B., et al. (2017/05/04/). A Tunable Brake for HECT Ubiquitin Ligases. Mol. Cell *66*, 345–357.e6. 10.1016/j.molcel.2017.03.020.

92. Araki, N., Umemura, M., Miyagi, Y., Yabana, M., Miki, Y., Tamura, K., Uchino, K., Aoki, R., Goshima, Y., Umemura, S., et al. (2008). Expression, Transcription, and Possible Antagonistic Interaction of the Human Nedd4L Gene Variant. Hypertension *51*, 773–777. 10.1161/HYPERTENSIONAHA.107.102061.

93. Goulet, C.C., Volk, K.A., Adams, C.M., Prince, L.S., Stokes, J.B., and Snyder, P.M. (1998). Inhibition of the Epithelial Na+ Channel by Interaction of Nedd4 with a PY Motif Deleted in Liddle's Syndrome *. Journal of Biological Chemistry *273*, 30012–30017. 10.1074/jbc.273.45.30012.

94. Malik, B., Schlanger, L., Al-Khalili, O., Bao, H.-F., Yue, G., Price, S.R., Mitch, W.E., and Eaton, D.C. (2001). ENaC Degradation in A6 Cells by the Ubiquitin-Proteosome Proteolytic Pathway *. Journal of Biological Chemistry *276*, 12903–12910. 10.1074/jbc.M010626200.

95. Staub, O., Gautschi, I., Ishikawa, T., Breitschopf, K., Ciechanover, A., Schild, L., and Rotin, D. (1997). Regulation of stability and function of the epithelial Na+ channel (ENaC) by ubiquitination. The EMBO Journal *16*, 6325. 10.1093/emboj/16.21.6325.

96. Snyder, P.M., Olson, D.R., McDonald, F.J., and Bucher, D.B. (2001). Multiple WW Domains, but Not the C2 Domain, Are Required for Inhibition of the Epithelial Na+ Channel by Human Nedd4. J. Biol. Chem. *276*, 28321–28326. 10.1074/jbc.M011487200.

97. Itani, O.A., Campbell, J.R., Herrero, J., Snyder, P.M., and Thomas, C.P. (2003). Alternate promoters and variable splicing lead to hNedd4–2 isoforms with a C2 domain and varying number of WW domains. American Journal of Physiology-Renal Physiology *285*, F916–F929. 10.1152/ajprenal.00203.2003.

98. Itani, O.A., Stokes, J.B., and Thomas, C.P. (2005). Nedd4–2 isoforms differentially associate with ENaC and regulate its activity. American Journal of Physiology-Renal Physiology *289*, F334–F346. 10.1152/ajprenal.00394.2004.

99. Umemura, M., Ishigami, T., Tamura, K., Sakai, M., Miyagi, Y., Nagahama, K., Aoki, I., Uchino, K., Rohrwasser, A., Lalouel, J.-M., et al. (2006). Transcriptional diversity and expression of NEDD4L gene in distal nephron. Biochemical and Biophysical Research Communications *339*, 1129–1137. 10.1016/j.bbrc.2005.11.120.

100. Kamynina, E., Tauxe, C., and Staub, O. (2001). Distinct characteristics of two human Nedd4 proteins with respect to epithelial Na+ channel regulation. American Journal of Physiology-Renal Physiology *281*, F469–F477. 10.1152/ajprenal.2001.281.3.F469.

101. Minegishi, S., Ishigami, T., Kino, T., Chen, L., Nakashima-Sasaki, R., Araki, N., Yatsu, K., Fujita, M., and Umemura, S. (2016). An isoform of Nedd4-2 is critically involved in the renal adaptation to high salt intake in mice. Sci. Rep. *6*, 27137. 10.1038/srep27137.

102. Fotia, A.B., Dinudom, A., Shearwin, K.E., Koch, J.-P, Korbmacher, C., Cook, D.I., and Kumar, S. (2003). The role of individual Nedd4–2 (KIAA0439) WW domains in binding and regulating epithelial sodium channels. The FASEB Journal *17*, 70–72. 10.1096/fj.02-0497fje.

103. Kanelis, V., Farrow, N.A., Kay, L.E., Rotin, D., and Forman-Kay, J.D. (1998). NMR studies of tandem WW domains of Nedd4 in complex with a PY motif-containing region of the epithelial sodium channel. Biochem. Cell Biol. *76*, 341–350. 10.1139/o98-042.

References

104. Butterworth, M.B., Edinger, R.S., Ovaa, H., Burg, D., Johnson, J.P., and Frizzell, R.A. (2007). The Deubiquitinating Enzyme UCH-L3 Regulates the Apical Membrane Recycling of the Epithelial Sodium Channel *. Journal of Biological Chemistry *282*, 37885–37893. 10.1074/jbc.M707989200.

105. Fakitsas, P., Adam, G., Daidie[Combining Acute Accent], D.A.A., van Bemmelen, M.X., Fouladkou, F., Patrignani, A., Wagner, U., Warth, R., Camargo, S.M.R., Staub, O., et al. (2007). Early Aldosterone-Induced Gene Product Regulates the Epithelial Sodium Channel by Deubiquitylation. Journal of the American Society of Nephrology *18*.

106. Ruffieux-Daidié, D., Poirot, O., Boulkroun, S., Verrey, F., Kellenberger, S., and Staub, O. (2008). Deubiquitylation Regulates Activation and Proteolytic Cleavage of ENaC. J. Am. Soc. Nephrol. *19*, 2170. 10.1681/ASN.2007101130.

107. Kim, H.C., and Huibregtse, J.M. (2009). Polyubiquitination by HECT E3s and the Determinants of Chain Type Specificity. Molecular and Cellular Biology *29*, 3307–3318. 10.1128/MCB.00240-09.

108. Maspero, E., Mari, S., Valentini, E., Musacchio, A., Fish, A., Pasqualato, S., and Polo, S. (03/11 07/23/received 01/04/revised 01/13/accepted 2011). Structure of the HECT:ubiquitin complex and its role in ubiquitin chain elongation. EMBO Reports *12*, 342–349. 10.1038/embor.2011.21.

109. Komander, D., and Rape, M. (2012). The Ubiquitin Code. Annu. Rev. Biochem. *81*, 203–229. 10.1146/annurev-biochem-060310-170328.

110. Wiemuth, D., Ke, Y., Rohlfs, M., and McDonald, F.J. (2007). Epithelial sodium channel (ENaC) is multi-ubiquitinated at the cell surface. Biochem. J. *405*, 147–155. 10.1042/BJ20060747.

111. Waldegger, S., Barth, P., Raber, G., and Lang, F. (1997). Cloning and characterization of a putative human serine/threonine protein kinase transcriptionally modified during anisotonic and isotonic alterations of cell volume. Proceedings of the National Academy of Sciences *94*, 4440–4445. 10.1073/pnas.94.9.4440.

112. Náray-Fejes-Tóth, A., Canessa, C., Cleaveland, E.S., Aldrich, G., and Fejes-Tóth, G. (1999). Sgk Is an Aldosterone-induced Kinase in the Renal Collecting Duct: EFFECTS ON EPITHELIAL Na+ CHANNELS *. Journal of Biological Chemistry *274*, 16973–16978. 10.1074/jbc.274.24.16973.

113. Wulff, P., Vallon, V., Huang, D.Y., Völkl, H., Yu, F., Richter, K., Jansen, M., Schlünz, M., Klingel, K., Loffing, J., et al. (11/01/ 2002). Impaired renal Na+ retention in the Sgk1-knockout mouse. The Journal of Clinical Investigation *110*, 1263–1268. 10.1172/JCI15696.

114. Debonneville, C., Flores, S.Y., Kamynina, E., Plant, P.J., Tauxe, C., Thomas, M.A., Münster, C., Chraïbi, A., Pratt, J.H., Horisberger, J.-D., et al. (2001). Phosphorylation of Nedd4-2 by Sgk1 regulates epithelial Na+ channel cell surface expression. The EMBO Journal *20*, 7052–7059. 10.1093/emboj/20.24.7052.

115. Snyder, P.M., Olson, D.R., and Thomas, B.C. (2002). Serum and Glucocorticoid-regulated Kinase Modulates Nedd4-2-mediated Inhibition of the Epithelial Na+Channel *. Journal of Biological Chemistry *277*, 5–8. 10.1074/jbc.C100623200.

116. Zhou, R., and Snyder, P.M. (2005). Nedd4-2 Phosphorylation Induces Serum and Glucocorticoid-regulated Kinase (SGK) Ubiquitination and Degradation. J. Biol. Chem. *280*, 4518–4523. 10.1074/jbc.M411053200.

117. Diakov, A., and Korbmacher, C. (2004). A Novel Pathway of Epithelial Sodium Channel Activation Involves a Serum- and Glucocorticoid-inducible Kinase Consensus Motif in the C Terminus of the Channel's α-Subunit *. Journal of Biological Chemistry *279*, 38134–38142. 10.1074/jbc.M403260200.

118. Thomas, S.V., Kathpalia, P.P., Rajagopal, M., Charlton, C., Zhang, J., Eaton, D.C., Helms, M.N., and Pao, A.C. (2011). Epithelial Sodium Channel Regulation by Cell Surface-associated Serum- and Glucocorticoid-regulated Kinase 1. J. Biol. Chem. *286*, 32074–32085. 10.1074/jbc.M111.278283.

119. de la Rosa, D.A., Zhang, P., Náray-Fejes-Tóth, A., Fejes-Tóth, G., and Canessa, C.M. (1999). The Serum and Glucocorticoid Kinase sgk Increases the Abundance of Epithelial Sodium Channels in the Plasma Membrane of Xenopus Oocytes *. Journal of Biological Chemistry *274*, 37834–37839. 10.1074/jbc.274.53.37834.

120. Muslin, A.J., Tanner, J.W., Allen, P.M., and Shaw, A.S. (1996). Interaction of 14-3-3 with Signaling Proteins Is Mediated by the Recognition of Phosphoserine. Cell *84*, 889–897. 10.1016/S0092-8674(00)81067-3.

121. Ichimura, T., Yamamura, H., Sasamoto, K., Tominaga, Y., Taoka, M., Kakiuchi, K., Shinkawa, T., Takahashi, N., Shimada, S., and Isobe, T. (2005). 14-3-3 Proteins Modulate the Expression of Epithelial Na+ Channels by Phosphorylation-dependent Interaction with Nedd4-2 Ubiquitin Ligase *. Journal of Biological Chemistry *280*, 13187–13194. 10.1074/jbc.M412884200.

122. Liang, X., Butterworth, M.B., Peters, K.W., Walker, W.H., and Frizzell, R.A. (2008). An Obligatory Heterodimer of 14-3-3β and 14-3-3ε Is Required for Aldosterone Regulation of the Epithelial Sodium Channel *. Journal of Biological Chemistry *283*, 27418–27425. 10.1074/jbc.M803687200.

123. Pohl, P., Joshi, R., Petrvalska, O., Obsil, T., and Obsilova, V. (2021). 14-3-3-protein regulates Nedd4-2 by modulating interactions between HECT and WW domains. Communications Biology *4*, 899. 10.1038/s42003-021-02419-0.

124. Joshi, R., Pohl, P., Strachotova, D., Herman, P., Obsil, T., and Obsilova, V. (2022). Nedd4-2 binding to 14-3-3 modulates the accessibility of its catalytic site and WW domains. Biophysical Journal *121*, 1299–1311. 10.1016/j.bpj.2022.02.025.

References

125. Aguilar-Camacho, J.M., Foreman, K., Jaimes-Becerra, A., Aharoni, R., Gründer, S., and Moran, Y. (2023). Functional analysis in a model sea anemone reveals phylogenetic complexity and a role in cnidocyte discharge of DEG/ENaC ion channels. Communications Biology *6*, 17. 10.1038/s42003-022-04399-1.

126. Hesselager, M., Timmermann, D.B., and Ahring, P.K. (2004). pH Dependency and Desensitization Kinetics of Heterologously Expressed Combinations of Acid-sensing Ion Channel Subunits*. Journal of Biological Chemistry *279*, 11006–11015. 10.1074/jbc.M313507200.

127. Palmer, L.G., and Frindt, G. (1986). Amiloride-sensitive Na channels from the apical membrane of the rat cortical collecting tubule. Proceedings of the National Academy of Sciences *83*, 2767–2770. 10.1073/pnas.83.8.2767.

128. Kellenberger, S., Hoffmann-Pochon, N., Gautschi, I., Schneeberger, E., and Schild, L. (1999). On the Molecular Basis of Ion Permeation in the Epithelial Na+ Channel. Journal of General Physiology *114*, 13–30. 10.1085/jgp.114.1.13.

129. Palmer, L.G. (1984). Voltage-dependent block by amiloride and other monovalent cations of apical Na channels in the toad urinary bladder. The Journal of Membrane Biology *80*, 153–165. 10.1007/BF01868771.

130. Li, J., Sheng, S., Perry, C.J., and Kleyman, T.R. (2003). Asymmetric Organization of the Pore Region of the Epithelial Sodium Channel *. Journal of Biological Chemistry *278*, 13867–13874. 10.1074/jbc.M300149200.

131. Baconguis, I., Bohlen, C.J., Goehring, A., Julius, D., and Gouaux, E. (2014). X-Ray Structure of Acid-Sensing Ion Channel 1–Snake Toxin Complex Reveals Open State of a Na+-Selective Channel. Cell *156*, 717–729. 10.1016/j.cell.2014.01.011.

132. Kellenberger, S., Auberson, M., Gautschi, I., Schneeberger, E., and Schild, L. (2001). Permeability Properties of Enac Selectivity Filter Mutants. Journal of General Physiology *118*, 679–692. 10.1085/jgp.118.6.679.

133. Kleyman, T.R., and Cragoe, E.J. (1988). Amiloride and its analogs as tools in the study of ion transport. The Journal of Membrane Biology *105*, 1–21. 10.1007/BF01871102.

134. Palmer, L.G. (1985). Interactions of amiloride and other blocking cations with the apical Na channel in the toad urinary bladder. The Journal of Membrane Biology *87*, 191–199. 10.1007/BF01871218.

135. Schild, L., Schneeberger, E., Gautschi, I., and Firsov, D. (1997). Identification of Amino Acid Residues in the α, β, and γ Subunits of the Epithelial Sodium Channel (ENaC) Involved in Amiloride Block and Ion Permeation. Journal of General Physiology *109*, 15–26. 10.1085/jgp.109.1.15.

136. Bruns, J.B., Carattino, M.D., Sheng, S., Maarouf, A.B., Weisz, O.A., Pilewski, J.M., Hughey, R.P., and Kleyman, T.R. (2007). Epithelial Na+ Channels Are Fully Activated by Furin- and Prostasin-dependent Release of an Inhibitory Peptide from the γ-Subunit. J. Biol. Chem. *282*, 6153–6160. 10.1074/jbc.M610636200.

137. Palmer, L.G., and Frindt, G. (1987). Effects of cell Ca and pH on Na channels from rat cortical collecting tubule. American Journal of Physiology-Renal Physiology *253*, F333–F339. 10.1152/ajprenal.1987.253.2.F333.

138. Chalfant, M.L., Denton, J.S., Berdiev, B.K., Ismailov, I.I., Benos, D.J., and Stanton, B.A. (1999). Intracellular H+ regulates the α-subunit of ENaC, the epithelial Na+ channel. American Journal of Physiology-Cell Physiology *276*, C477–C486. 10.1152/ajpcell.1999.276.2.C477.

139. Fuchs, W., Larsen, E.H., and Lindemann, B. (1977). Current—voltage curve of sodium channels and concentration dependence of sodium permeability in frog skin. The Journal of Physiology *267*, 137–166. 10.1113/jphysiol.1977.sp011805.

140. Chraïbi, A., and Horisberger, J.-D. (2002). Na Self Inhibition of Human Epithelial Na Channel. The Journal of General Physiology *120*, 133. 10.1085/jgp.20028612.

141. Askwith, C.C., Benson, C.J., Welsh, M.J., and Snyder, P.M. (2001). DEG/ENaC ion channels involved in sensory transduction are modulated by cold temperature. Proceedings of the National Academy of Sciences *98*, 6459–6463. 10.1073/pnas.111155398.

142. Eaton, D.C., and Marunaka, Y. (1990). Chapter 3 Ion Channel Fluctuations: "Noise" and Single-Channel Measurements. In Current Topics in Membranes and Transport, F. Bronner, ed. (Academic Press), pp. 61–114. 10.1016/S0070-2161(08)60229-4.

143. Sheng, S., Carattino, M.D., Bruns, J.B., Hughey, R.P., and Kleyman, T.R. (2006). Furin cleavage activates the epithelial Na+ channel by relieving Na+ self-inhibition. American Journal of Physiology-Renal Physiology *290*, F1488–F1496. 10.1152/ajprenal.00439.2005.

144. Kashlan, O.B., Blobner, B.M., Zuzek, Z., Tolino, M., and Kleyman, T.R. (2015). Na+ Inhibits the Epithelial Na+ Channel by Binding to a Site in an Extracellular Acidic Cleft *. Journal of Biological Chemistry *290*, 568–576. 10.1074/jbc.M114.606152.

145. Noreng, S., Posert, R., Bharadwaj, A., Houser, A., and Baconguis, I. (2020). Molecular principles of assembly, activation, and inhibition in epithelial sodium channel. eLife *9*, e59038. 10.7554/eLife.59038.

146. Collier, D.M., and Snyder, P.M. (2009). Extracellular Protons Regulate Human ENaC by Modulating Na+ Self-inhibition *. Journal of Biological Chemistry *284*, 792–798. 10.1074/jbc.M806954200.

147. Noreng, S., Bharadwaj, A., Posert, R., Yoshioka, C., and Baconguis, I. (2018). Structure of the human epithelial sodium channel by cryo-electron microscopy. eLife *7*, e39340. 10.7554/eLife.39340.

148. Yoder, N., Yoshioka, C., and Gouaux, E. (2018). Gating mechanisms of acid-sensing ion channels. Nature *555*, 397–401. 10.1038/nature25782.

149. Valeria Kalienkova, Mowgli Dandamudi, Cristina Paulino, and Timothy Lynagh (2023). Structural basis for excitatory neuropeptide signaling. bioRxiv, 2023.04.29.538817. 10.1101/2023.04.29.538817.

References

150. Kashlan, O.B., and Kleyman, T.R. (2011). ENaC structure and function in the wake of a resolved structure of a family member. American Journal of Physiology-Renal Physiology *301*, F684–F696. 10.1152/ajprenal.00259.2011.

151. Kim, C.S., Ahmad, S., Wu, T., Walton, W.G., Redinbo, M.R., and Tarran, R. (2018). SPLUNC1 is an allosteric modulator of the epithelial sodium channel. The FASEB Journal *32*, 2478–2491. 10.1096/fj.201701126R.

152. Baconguis, I., and Gouaux, E. (2012). Structural plasticity and dynamic selectivity of acid-sensing ion channel–spider toxin complexes. Nature *489*, 400–405. 10.1038/nature11375.

153. Zhang, L., Wang, X., Chen, J., Sheng, S., and Kleyman, T.R. (2023). Extracellular intersubunit interactions modulate epithelial Na+ channel gating. Journal of Biological Chemistry *299*, 102914. 10.1016/j.jbc.2023.102914.

154. Kashlan, O.B., Adelman, J.L., Okumura, S., Blobner, B.M., Zuzek, Z., Hughey, R.P., Kleyman, T.R., and Grabe, M. (2011). Constraint-based, Homology Model of the Extracellular Domain of the Epithelial Na+ Channel α Subunit Reveals a Mechanism of Channel Activation by Proteases. J. Biol. Chem. *286*, 649–660. 10.1074/jbc.M110.167098.

155. Kashlan, O.B., Blobner, B.M., Zuzek, Z., Carattino, M.D., and Kleyman, T.R. (2012). Inhibitory Tract Traps the Epithelial Na+ Channel in a Low Activity Conformation *. Journal of Biological Chemistry *287*, 20720–20726. 10.1074/jbc.M112.358218.

156. Balchak, D.M., Thompson, R.N., and Kashlan, O.B. (2018). The epithelial Na+ channel γ subunit autoinhibitory tract suppresses channel activity by binding the γ subunit's finger–thumb domain interface. Journal of Biological Chemistry *293*, 16217–16225. 10.1074/jbc.RA118.004362.

157. Carattino, M.D., Passero, C.J., Steren, C.A., Maarouf, A.B., Pilewski, J.M., Myerburg, M.M., Hughey, R.P., and Kleyman, T.R. (2008). Defining an inhibitory domain in the α-subunit of the epithelial sodium channel. American Journal of Physiology-Renal Physiology *294*, F47–F52. 10.1152/ajprenal.00399.2007.

158. Kashlan, O.B., Boyd, C.R., Argyropoulos, C., Okumura, S., Hughey, R.P., Grabe, M., and Kleyman, T.R. (2010). Allosteric inhibition of the epithelial Na+ channel through peptide binding at peripheral finger and thumb domains. J Biol Chem *285*, 35216–35223. 10.1074/jbc.M110.167064.

159. Passero, C.J., Carattino, M.D., Kashlan, O.B., Myerburg, M.M., Hughey, R.P., and Kleyman, T.R. (2010). Defining an inhibitory domain in the gamma subunit of the epithelial sodium channel. American Journal of Physiology-Renal Physiology *299*, F854–F861. 10.1152/ajprenal.00316.2010.

160. Jasti, J., Furukawa, H., Gonzales, E.B., and Gouaux, E. (2007). Structure of acid-sensing ion channel 1 at 1.9 Å resolution and low pH. Nature *449*, 316–323. 10.1038/nature06163.

114

161. Snyder, P.M., Bucher, D.B., and Olson, D.R. (2000). Gating Induces a Conformational Change in the Outer Vestibule of Enac. Journal of General Physiology *116*, 781–790. 10.1085/jgp.116.6.781.

162. Kasimova, M.A., Lynagh, T., Sheikh, Z.P., Granata, D., Borg, C.B., Carnevale, V., and Pless, S.A. (2020). Evolutionarily Conserved Interactions within the Pore Domain of Acid-Sensing Ion Channels. Biophysical Journal *118*, 861–872. 10.1016/j.bpj.2019.09.001.

163. Carattino, M.D., and Della Vecchia, M.C. (2012). Contribution of Residues in Second Transmembrane Domain of ASIC1a Protein to Ion Selectivity *. Journal of Biological Chemistry *287*, 12927–12934. 10.1074/jbc.M111.329284.

164. Kellenberger, S., Gautschi, I., and Schild, L. (1999). A single point mutation in the pore region of the epithelial Na+ channel changes ion selectivity by modifying molecular sieving. Proceedings of the National Academy of Sciences *96*, 4170–4175. 10.1073/pnas.96.7.4170.

165. Snyder, P.M., Olson, D.R., and Bucher, D.B. (1999). A Pore Segment in DEG/ENaC Na+ Channels *. Journal of Biological Chemistry *274*, 28484–28490. 10.1074/jbc.274.40.28484.

166. Sheng, S., Li, J., McNulty, K.A., Avery, D., and Kleyman, T.R. (2000). Characterization of the Selectivity Filter of the Epithelial Sodium Channel *. Journal of Biological Chemistry *275*, 8572–8581. 10.1074/jbc.275.12.8572.

167. Palmer, L.G. (1982). Ion selectivity of the apical membrane Na channel in the toad urinary bladder. The Journal of Membrane Biology *67*, 91–98. 10.1007/BF01868651.

168. Mähler, J., and Persson, I. (2012). A Study of the Hydration of the Alkali Metal Ions in Aqueous Solution. Inorg. Chem. *51*, 425–438. 10.1021/ic2018693.

169. Yoder, N., and Gouaux, E. (2020). The His-Gly motif of acid-sensing ion channels resides in a reentrant "loop" implicated in gating and ion selectivity. eLife *9*, e56527. 10.7554/eLife.56527.

170. Gründer, S., Firsov, D., Chang, S.S., Jaeger, N.F., Gautschi, I., Schild, L., Lifton, R.P., and Rossier, B.C. (1997). A mutation causing pseudohypoaldosteronism type 1 identifies a conserved glycine that is involved in the gating of the epithelial sodium channel. The EMBO Journal *16*, 899–907. 10.1093/emboj/16.5.899.

171. Gründer, S., Fowler Jaeger, N., Gautschi, I., Schild, L., and Rossier, B.C. (1999). Identification of a highly conserved sequence at the N-terminus of the epithelial Na+ channel α subunit involved in gating. Pflügers Archiv *438*, 709–715. 10.1007/s004249900119.

172. Chen, J., Kleyman, T.R., and Sheng, S. (2013). Gain-of-function variant of the human epithelial sodium channel. American Journal of Physiology-Renal Physiology *304*, F207–F213. 10.1152/ajprenal.00563.2012.

173. Kashlan, O.B., Kinlough, C.L., Myerburg, M.M., Shi, S., Chen, J., Blobner, B.M., Buck, T.M., Brodsky, J.L., Hughey, R.P., and Kleyman, T.R. (2018). N-linked glycans are required on epithelial Na(+) channel subunits for maturation and surface expression. Am. J. Physiol. Renal Physiol. *314*, F483–f492. 10.1152/ajprenal.00195.2017.

References

174. Kadurin, I., Golubovic, A., Leisle, L., Schindelin, H., and Gründer, S. (2008). Differential effects of N-glycans on surface expression suggest structural differences between the acid-sensing ion channel (ASIC) 1a and ASIC1b. Biochemical Journal *412*, 469–475. 10.1042/BJ20071614.

175. Hughey, R.P., Bruns, J.B., Kinlough, C.L., and Kleyman, T.R. (2004). Distinct Pools of Epithelial Sodium Channels Are Expressed at the Plasma Membrane. J. Biol. Chem. *279*, 48491–48494. 10.1074/jbc.C400460200.

176. Orce, G.G., Castillo, G.A., and Margolius, H.S. (1980). Inhibition of short-circuit current in toad urinary bladder by inhibitors of glandular kallikrein. American Journal of Physiology-Renal Physiology *239*, F459–F465. 10.1152/ajprenal.1980.239.5.F459.

177. Vallet, V., Chraibi, A., Gaeggeler, H.-P., Horisberger, J.-D., and Rossier, B.C. (1997). An epithelial serine protease activates the amiloride-sensitive sodium channel. Nature *389*, 607–610. 10.1038/39329.

178. Firsov, D., Schild, L., Gautschi, I., Mérillat, A.-M., Schneeberger, E., and Rossier, B.C. (1996). Cell surface expression of the epithelial Na channel and a mutant causing Liddle syndrome: A quantitative approach. Proceedings of the National Academy of Sciences *93*, 15370–15375. 10.1073/pnas.93.26.15370.

179. Palmer, L.G., and Frindt, G. (1996). Gating of Na channels in the rat cortical collecting tubule: Effects of voltage and membrane stretch. Journal of General Physiology *107*, 35–45. 10.1085/jgp.107.1.35.

180. Caldwell, R.A., Boucher, R.C., and Stutts, M.J. (2004). Serine protease activation of near-silent epithelial Na+ channels. American Journal of Physiology-Cell Physiology *286*, C190–C194. 10.1152/ajpcell.00342.2003.

181. Hughey, R.P., Bruns, J.B., Kinlough, C.L., Harkleroad, K.L., Tong, Q., Carattino, M.D., Johnson, J.P., Stockand, J.D., and Kleyman, T.R. (2004). Epithelial Sodium Channels Are Activated by Furin-dependent Proteolysis *. Journal of Biological Chemistry *279*, 18111–18114. 10.1074/jbc.C400080200.

182. Zachar, R.M., Skjødt, K., Marcussen, N., Walter, S., Toft, A., Nielsen, M.R., Jensen, B.L., and Svenningsen, P. (2015). The Epithelial Sodium Channel γ-Subunit Is Processed Proteolytically in Human Kidney. Journal of the American Society of Nephrology *26*.

183. Zachar, R., Mikkelsen, M.K., Skjødt, K., Marcussen, N., Zamani, R., Jensen, B.L., and Svenningsen, P. (2019). The epithelial Na+ channel α-and γ-subunits are cleaved at predicted furin-cleavage sites, glycosylated andmembrane associated in human kidney. Pflügers Archiv - European Journal of Physiology *471*, 1383–1396. 10.1007/s00424-019-02321-z.

184. Yu, J.X., Chao, L., and Chao, J. (1994). Prostasin is a novel human serine proteinase from seminal fluid. Purification, tissue distribution, and localization in prostate gland. Journal of Biological Chemistry *269*, 18843–18848. 10.1016/S0021-9258(17)32244-5.

185. Thomas, G. (2002). Furin at the cutting edge: From protein traffic to embryogenesis and disease. Nature Reviews Molecular Cell Biology *3*, 753–766. 10.1038/nrm934.

186. Caldwell, R.A., Boucher, R.C., and Stutts, M.J. (2005). Neutrophil elastase activates near-silent epithelial Na+ channels and increases airway epithelial Na+ transport. American Journal of Physiology-Lung Cellular and Molecular Physiology *288*, L813–L819. 10.1152/ajplung.00435.2004.

187. Adebamiro, A., Cheng, Y., Rao, U.S., Danahay, H., and Bridges, R.J. (2007). A Segment of γ ENaC Mediates Elastase Activation of Na+ Transport. Journal of General Physiology *130*, 611–629. 10.1085/jgp.200709781.

188. García-Caballero, A., Dang, Y., He, H., and Stutts, M.J. (2008). ENaC Proteolytic Regulation by Channel-activating Protease 2. Journal of General Physiology *132*, 521–535. 10.1085/jgp.200810030.

189. Garcia-Caballero, A., Ishmael, S.S., Dang, Y., Gillie, D., Bond, J.S., Milgram, S.L., and Stutts, M.J. (2011). Activation of the epithelial sodium channel by the metalloprotease meprin β subunit. Channels *5*, 14–22. 10.4161/chan.5.1.13759.

190. Haerteis, S., Krappitz, M., Bertog, M., Krappitz, A., Baraznenok, V., Henderson, I., Lindström, E., Murphy, J.E., Bunnett, N.W., and Korbmacher, C. (2012). Proteolytic activation of the epithelial sodium channel (ENaC) by the cysteine protease cathepsin-S. Pflügers Archiv - European Journal of Physiology *464*, 353–365. 10.1007/s00424-012-1138-3.

191. Ji, H.-L., Zhao, R., Komissarov, A.A., Chang, Y., Liu, Y., and Matthay, M.A. (2015). Proteolytic Regulation of Epithelial Sodium Channels by Urokinase Plasminogen Activator. Journal of Biological Chemistry *290*, 5241–5255. 10.1074/jbc.M114.623496.

192. Passero, C.J., Mueller, G.M., Myerburg, M.M., Carattino, M.D., Hughey, R.P., and Kleyman, T.R. (2012). TMPRSS4-dependent activation of the epithelial sodium channel requires cleavage of the γ-subunit distal to the furin cleavage site. American Journal of Physiology-Renal Physiology *302*, F1–F8. 10.1152/ajprenal.00330.2011.

193. Passero, C.J., Mueller, G.M., Rondon-Berrios, H., Tofovic, S.P., Hughey, R.P., and Kleyman, T.R. (2008). Plasmin Activates Epithelial Na+ Channels by Cleaving the γ Subunit *. Journal of Biological Chemistry *283*, 36586–36591. 10.1074/jbc.M805676200.

194. Patel, A.B., Chao, J., and Palmer, L.G. (2012). Tissue kallikrein activation of the epithelial Na channel. American Journal of Physiology-Renal Physiology *303*, F540–F550. 10.1152/ajprenal.00133.2012.

195. Svenningsen, P., Bistrup, C., Friis, U.G., Bertog, M., Haerteis, S., Krueger, B., Stubbe, J., Jensen, O.N., Thiesson, H.C., Uhrenholt, T.R., et al. (2009). Plasmin in Nephrotic Urine Activates the Epithelial Sodium Channel. Journal of the American Society of Nephrology *20*.

196. Tan, C.D., Hobbs, C., Sameni, M., Sloane, B.F., Stutts, M.J., and Tarran, R. (2014). Cathepsin B contributes to Na+ hyperabsorption in cystic fibrosis airway epithelial cultures. The Journal of Physiology *592*, 5251–5268. 10.1113/jphysiol.2013.267286.

References

197. Bohnert, B.N., Menacher, M., Janessa, A., Wörn, M., Schork, A., Daiminger, S., Kalbacher, H., Häring, H.-U., Daniel, C., Amann, K., et al. (2018). Aprotinin prevents proteolytic epithelial sodium channel (ENaC) activation and volume retention in nephrotic syndrome. Kidney International *93*, 159–172. 10.1016/j.kint.2017.07.023.

198. Frindt, G., Yang, L., Bamberg, K., and Palmer, L.G. (2018). Na restriction activates epithelial Na channels in rat kidney through two mechanisms and decreases distal Na+ delivery. The Journal of Physiology *596*, 3585–3602. 10.1113/JP275988.

199. Hill, W.G., An, B., and Johnson, J.P. (2002). Endogenously Expressed Epithelial Sodium Channel Is Present in Lipid Rafts in A6 Cells. J. Biol. Chem. *277*, 33541–33544. 10.1074/jbc.C200309200.

200. Hill, W.G., Butterworth, M.B., Wang, H., Edinger, R.S., Lebowitz, J., Peters, K.W., Frizzell, R.A., and Johnson, J.P. (2007). The Epithelial Sodium Channel (ENaC) Traffics to Apical Membrane in Lipid Rafts in Mouse Cortical Collecting Duct Cells. J. Biol. Chem. *282*, 37402–37411. 10.1074/jbc.M704084200.

201. Shaw, A.S. (2006). Lipid rafts: Now you see them, now you don't. Nature Immunology *7*, 1139–1142. 10.1038/ni1405.

202. Archer, C.R., Enslow, B.T., Carver, C.M., and Stockand, J.D. (2020). Phosphatidylinositol 4,5-bisphosphate directly interacts with the β and γ subunits of the sodium channel ENaC. Journal of Biological Chemistry *295*, 7958–7969. 10.1074/jbc.RA120.012606.

203. Zhai, Y.-J., Wu, M.-M., Linck, V.A., Zou, L., Yue, Q., Wei, S.-P., Song, C., Zhang, S., Williams, C.R., Song, B.-L., et al. (2019/07/01/). Intracellular cholesterol stimulates ENaC by interacting with phosphatidylinositol-4,5-bisphosphate and mediates cyclosporine A-induced hypertension. Biochimica et Biophysica Acta (BBA) - Molecular Basis of Disease *1865*, 1915–1924. 10.1016/j.bbadis.2018.08.027.

204. Ma, H.-P., Saxena, S., and Warnock, D.G. (2002). Anionic Phospholipids Regulate Native and Expressed Epithelial Sodium Channel (ENaC) *. Journal of Biological Chemistry *277*, 7641–7644. 10.1074/jbc.C100737200.

205. Pochynyuk, O., Tong, Q., Staruschenko, A., Ma, H.-P., and Stockand, J.D. (2006). Regulation of the epithelial Na+ channel (ENaC) by phosphatidylinositides. American Journal of Physiology-Renal Physiology *290*, F949–F957. 10.1152/ajprenal.00386.2005.

206. Kunzelmann, K., Bachhuber, T., Regeer, R., Markovich, D., Sun, J., and Schreiber, R. (2005). Purinergic inhibition of the epithelial Na+ transport via hydrolysis of PIP2. The FASEB Journal *19*, 142–143. 10.1096/fj.04-2314fje.

207. Markadieu, N., Blero, D., Boom, A., Erneux, C., and Beauwens, R. (2004). Phosphatidylinositol 3,4,5-trisphosphate: An early mediator of insulin-stimulated sodium transport in A6 cells. American Journal of Physiology-Renal Physiology *287*, F319–F328. 10.1152/ajprenal.00314.2003.

118

208. Tong, Q., Gamper, N., Medina, J.L., Shapiro, M.S., and Stockand, J.D. (2004). Direct Activation of the Epithelial Na+ Channel by Phosphatidylinositol 3,4,5-Trisphosphate and Phosphatidylinositol 3,4-Bisphosphate Produced by Phosphoinositide 3-OH Kinase *. Journal of Biological Chemistry *279*, 22654–22663. 10.1074/jbc.M401004200.

209. Pochynyuk, O., Staruschenko, A., Tong, Q., Medina, J., and Stockand, J.D. (2005). Identification of a Functional Phosphatidylinositol 3,4,5-Trisphosphate Binding Site in the Epithelial Na+ Channel *. Journal of Biological Chemistry *280*, 37565–37571. 10.1074/jbc.M509071200.

210. Tong, Q., Booth, R.E., Worrell, R.T., and Stockand, J.D. (2004). Regulation of Na+ transport by aldosterone: Signaling convergence and cross talk between the PI3-K and MAPK1/2 cascades. American Journal of Physiology-Renal Physiology *286*, F1232–F1238. 10.1152/ajprenal.00345.2003.

211. Ingólfsson, H.I., Melo, M.N., van Eerden, F.J., Arnarez, C., Lopez, C.A., Wassenaar, T.A., Periole, X., de Vries, A.H., Tieleman, D.P., and Marrink, S.J. (2014). Lipid Organization of the Plasma Membrane. J. Am. Chem. Soc. *136*, 14554–14559. 10.1021/ja507832e.

212. Bao, H.-F., Thai, T.L., Yue, Q., Ma, H.-P., Eaton, A.F., Cai, H., Klein, J.D., Sands, J.M., and Eaton, D.C. (2014). ENaC activity is increased in isolated, split-open cortical collecting ducts from protein kinase Cα knockout mice. American Journal of Physiology-Renal Physiology *306*, F309–F320. 10.1152/ajprenal.00519.2013.

213. Wang, J., Gambhir, A., Hangyás-Mihályneá, G., Murray, D., Golebiewska, U., and McLaughlin, S. (2002). Lateral Sequestration of Phosphatidylinositol 4,5-Bisphosphate by the Basic Effector Domain of Myristoylated Alanine-rich C Kinase Substrate Is Due to Nonspecific Electrostatic Interactions *. Journal of Biological Chemistry *277*, 34401–34412. 10.1074/jbc.M203954200.

214. Alli, A.A., Bao, H.-F., Alli, A.A., Aldrugh, Y., Song, J.Z., Ma, H.-P., Yu, L., Al-Khalili, O., and Eaton, D.C. (2012). Phosphatidylinositol phosphate-dependent regulation of Xenopus ENaC by MARCKS protein. American Journal of Physiology-Renal Physiology *303*, F800–F811. 10.1152/ajprenal.00703.2011.

215. Alli, A.A., Bao, H.-F., Liu, B.-C., Yu, L., Aldrugh, S., Montgomery, D.S., Ma, H.-P., and Eaton, D.C. (2015). Calmodulin and CaMKII modulate ENaC activity by regulating the association of MARCKS and the cytoskeleton with the apical membrane. American Journal of Physiology-Renal Physiology *309*, F456–F463. 10.1152/ajprenal.00631.2014.

216. Montgomery, D.S., Yu, L., Ghazi, Z.M., Thai, T.L., Al-Khalili, O., Ma, H.-P., Eaton, D.C., and Alli, A.A. (2017). ENaC activity is regulated by calpain-2 proteolysis of MARCKS proteins. American Journal of Physiology-Cell Physiology *313*, C42–C53. 10.1152/ajpcell.00244.2016.

References

217. Mueller, G.M., Maarouf, A.B., Kinlough, C.L., Sheng, N., Kashlan, O.B., Okumura, S., Luthy, S., Kleyman, T.R., and Hughey, R.P. (2010). Cys Palmitoylation of the Beta Subunit Modulates Gating of the Epithelial Sodium Channel. J. Biol. Chem. *285*, 30453–30462. 10.1074/jbc.M110.151845.

218. Mueller, G.M., Yan, W., Copelovitch, L., Jarman, S., Wang, Z., Kinlough, C.L., Tolino, M.A., Hughey, R.P., Kleyman, T.R., and Rubenstein, R.C. (2012). Multiple residues in the distal C terminus of the α-subunit have roles in modulating human epithelial sodium channel activity. American Journal of Physiology-Renal Physiology *303*, F220–F228. 10.1152/ajprenal.00493.2011.

219. Mukherjee, A., Mueller, G.M., Kinlough, C.L., Sheng, N., Wang, Z., Mustafa, S.A., Kashlan, O.B., Kleyman, T.R., and Hughey, R.P. (2014/05/16/). Cysteine Palmitoylation of the γ Subunit Has a Dominant Role in Modulating Activity of the Epithelial Sodium Channel*. J. Biol. Chem. *289*, 14351–14359. 10.1074/jbc.M113.526020.

220. Satlin, L.M., Sheng, S., Woda, C.B., and Kleyman, T.R. (2001). Epithelial Na+ channels are regulated by flow. American Journal of Physiology-Renal Physiology *280*, F1010–F1018. 10.1152/ajprenal.2001.280.6.F1010.

221. Karpushev, A.V., Ilatovskaya, D.V., and Staruschenko, A. (2010). The actin cytoskeleton and small G protein RhoA are not involved in flow-dependent activation of ENaC. BMC Research Notes *3*, 210. 10.1186/1756-0500-3-210.

222. Fronius, M., Bogdan, R., Althaus, M., Morty, R.E., and Clauss, W.G. (2010). Epithelial Na+ channels derived from human lung are activated by shear force. Respiratory Physiology & Neurobiology *170*, 113–119. 10.1016/j.resp.2009.11.004.

223. Carattino, M.D., Sheng, S., and Kleyman, T.R. (2004). Epithelial Na+ Channels Are Activated by Laminar Shear Stress *. Journal of Biological Chemistry *279*, 4120–4126. 10.1074/jbc.M311783200.

224. Shi, S., Blobner, B.M., Kashlan, O.B., and Kleyman, T.R. (2012). Extracellular Finger Domain Modulates the Response of the Epithelial Sodium Channel to Shear Stress *. Journal of Biological Chemistry *287*, 15439–15444. 10.1074/jbc.M112.346551.

225. Knoepp, F., Ashley, Z., Barth, D., Baldin, J.-P., Jennings, M., Kazantseva, M., Saw, E.L., Katare, R., Alvarez de la Rosa, D., Weissmann, N., et al. (2020). Shear force sensing of epithelial Na+ channel (ENaC) relies on N-glycosylated asparagines in the palm and knuckle domains of αENaC. Proceedings of the National Academy of Sciences *117*, 717–726. 10.1073/pnas.1911243117.

226. Pochynyuk, O., Tong, Q., Staruschenko, A., and Stockand, J.D. (2007). Binding and direct activation of the epithelial Na+ channel (ENaC) by phosphatidylinositides. The Journal of Physiology *580*, 365–372. 10.1113/jphysiol.2006.127449.

227. Quick, M., and Javitch, J.A. (2007). Monitoring the function of membrane transport proteins in detergent-solubilized form. Proceedings of the National Academy of Sciences *104*, 3603–3608. 10.1073/pnas.0609573104.

228. Whorton, M.R., and MacKinnon, R. (2013). X-ray structure of the mammalian GIRK2–βγ G-protein complex. Nature *498*, 190–197. 10.1038/nature12241.

229. Suzuki, K., Sato, K., Hisamoto, H., Siswanta, D., Hayashi, K., Kasahara, N., Watanabe, K., Yamamoto, N., and Sasakura, H. (1996). Design and Synthesis of Sodium Ion-Selective Ionophores Based on 16-Crown-5 Derivatives for an Ion-Selective Electrode. Anal. Chem. *68*, 208–215. 10.1021/ac950773j.

230. Sudji, I.R., Subburaj, Y., Frenkel, N., García-Sáez, A.J., and Wink, M. (2015). Membrane Disintegration Caused by the Steroid Saponin Digitonin Is Related to the Presence of Cholesterol. Molecules *20*, 20146–20160. 10.3390/molecules201119682.

231. Diakov, A., Bera, K., Mokrushina, M., Krueger, B., and Korbmacher, C. (2008). Cleavage in the γ-subunit of the epithelial sodium channel (ENaC) plays an important role in the proteolytic activation of near-silent channels. J Physiol *586*, 4587–4608. 10.1113/jphysiol.2008.154435.

232. Maarouf, A.B., Sheng, N., Chen, J., Winarski, K.L., Okumura, S., Carattino, M.D., Boyd, C.R., Kleyman, T.R., and Sheng, S. (2009). Novel Determinants of Epithelial Sodium Channel Gating within Extracellular Thumb Domains *. Journal of Biological Chemistry *284*, 7756–7765. 10.1074/jbc.M807060200.

233. Reeves, P.J., Callewaert, N., Contreras, R., and Khorana, H.G. (2002). Structure and function in rhodopsin: High-level expression of rhodopsin with restricted and homogeneous N-glycosylation by a tetracycline-inducible N-acetylglucosaminyltransferase I-negative HEK293S stable mammalian cell line. Proceedings of the National Academy of Sciences *99*, 13419–13424. 10.1073/pnas.212519299.

234. Shi, X., and Jarvis, D.L. (2007). Protein N-glycosylation in the baculovirus-insect cell system. Curr Drug Targets *8*, 1116–1125. 10.2174/138945007782151360.

235. Fejes-Tóth, G., Frindt, G., Náray-Fejes-Tóth, A., and Palmer, L.G. (2008). Epithelial Na+ channel activation and processing in mice lacking SGK1. American Journal of Physiology-Renal Physiology *294*, F1298–F1305. 10.1152/ajprenal.00579.2007.

236. Harris, M., Garcia-Caballero, A., Stutts, M.J., Firsov, D., and Rossier, B.C. (2008). Preferential Assembly of Epithelial Sodium Channel (ENaC) Subunits in Xenopus Oocytes: ROLE OF FURIN-MEDIATED ENDOGENOUS PROTEOLYSIS *. Journal of Biological Chemistry *283*, 7455–7463. 10.1074/jbc.M707399200.

237. Hughey, R.P., Mueller, G.M., Bruns, J.B., Kinlough, C.L., Poland, P.A., Harkleroad, K.L., Carattino, M.D., and Kleyman, T.R. (2003). Maturation of the Epithelial Na+ Channel Involves Proteolytic Processing of the α- and γ-Subunits. J. Biol. Chem. *278*, 37073–37082. 10.1074/jbc.M307003200.

References

238. Taverna, F., Xiong, Z., Brandes, L., Roder, J.C., Salter, M.W., and MacDonald, J.F. (2000). The Lurcher Mutation of an α-Amino-3-hydroxy-5-methyl- 4-isoxazolepropionic Acid Receptor Subunit Enhances Potency of Glutamate and Converts an Antagonist to an Agonist *. Journal of Biological Chemistry *275*, 8475–8479. 10.1074/jbc.275.12.8475.

239. Lingueglia, E., Champigny, G., Lazdunski, M., and Barbry, P. (1995). Cloning of the amiloride-sensitive FMRFamide peptide-gated sodium channel. Nature *378*, 730–733. 10.1038/378730a0.

240. Bize, V., and Horisberger, J.-D. (2007). Sodium self-inhibition of human epithelial sodium channel: Selectivity and affinity of the extracellular sodium sensing site. American Journal of Physiology-Renal Physiology *293*, F1137–F1146. 10.1152/ajprenal.00100.2007.

241. Sheng, S., Bruns, J.B., and Kleyman, T.R. (2004). Extracellular Histidine Residues Crucial for Na+ Self-inhibition of Epithelial Na+ Channels *. Journal of Biological Chemistry *279*, 9743–9749. 10.1074/jbc.M311952200.

242. Zhang, L., Wang, X., Chen, J., Kleyman, T.R., and Sheng, S. (2022). Accessibility of ENaC extracellular domain central core residues. Journal of Biological Chemistry *298*. 10.1016/j.jbc.2022.101860.

243. Kleyman, T.R., and Eaton, D.C. (2020). Regulating ENaC's gate. American Journal of Physiology-Cell Physiology *318*, C150–C162. 10.1152/ajpcell.00418.2019.

244. Salih, M., Gautschi, I., van Bemmelen, M.X., Di Benedetto, M., Brooks, A.S., Lugtenberg, D., Schild, L., and Hoorn, E.J. (2017). A Missense Mutation in the Extracellular Domain of αENaC Causes Liddle Syndrome. J. Am. Soc. Nephrol. *28*, 3291–3299. 10.1681/ASN.2016111163.

245. Dandamudi, M., Hausen, H., and Lynagh, T. (2022). Comparative analysis defines a broader FMRFamide-gated sodium channel family and determinants of neuropeptide sensitivity. Journal of Biological Chemistry *298*. 10.1016/j.jbc.2022.102086.

246. Wichmann, L., and Althaus, M. (2020). Evolution of epithelial sodium channels: Current concepts and hypotheses. American Journal of Physiology-Regulatory, Integrative and Comparative Physiology *319*, R387–R400. 10.1152/ajpregu.00144.2020.

247. Kawate, T., and Gouaux, E. (2006/04/01/). Fluorescence-Detection Size-Exclusion Chromatography for Precrystallization Screening of Integral Membrane Proteins. Structure *14*, 673–681. 10.1016/j.str.2006.01.013.

248. Mastronarde, D.N. (2003). SerialEM: A Program for Automated Tilt Series Acquisition on Tecnai Microscopes Using Prediction of Specimen Position. Microscopy and Microanalysis *9*, 1182–1183. 10.1017/S1431927603445911.

249. Jumper, J., Evans, R., Pritzel, A., Green, T., Figurnov, M., Ronneberger, O., Tunyasuvunakool, K., Bates, R., Žídek, A., Potapenko, A., et al. (2021). Highly accurate protein structure prediction with AlphaFold. Nature *596*, 583–589. 10.1038/s41586-021-03819-2.

250. Croll, T. (2018). ISOLDE: A physically realistic environment for model building into low-resolution electron-density maps. Acta Crystallographica Section D *74*, 519–530.

251. Pettersen, E.F., Goddard, T.D., Huang, C.C., Meng, E.C., Couch, G.S., Croll, T.I., Morris, J.H., and Ferrin, T.E. (2021). UCSF ChimeraX: Structure visualization for researchers, educators, and developers. Protein Sci *30*, 70–82. 10.1002/pro.3943.

252. Emsley, P., Lohkamp, B., Scott, W.G., and Cowtan, K. (2010). Features and development of Coot. Acta Crystallographica Section D *66*, 486–501.

253. Liebschner, D., Afonine, P.V., Baker, M.L., Bunkoczi, G., Chen, V.B., Croll, T.I., Hintze, B., Hung, L.-W., Jain, S., McCoy, A.J., et al. (2019). Macromolecular structure determination using X-rays, neutrons and electrons: Recent developments in Phenix. Acta Crystallographica Section D *75*, 861–877.

254. Williams, C.J., Headd, J.J., Moriarty, N.W., Prisant, M.G., Videau, L.L., Deis, L.N., Verma, V., Keedy, D.A., Hintze, B.J., Chen, V.B., et al. (2018). MolProbity: More and better reference data for improved all-atom structure validation. Protein Science *27*, 293–315. 10.1002/pro.3330.

255. Pintilie, G., Zhang, K., Su, Z., Li, S., Schmid, M.F., and Chiu, W. (2020). Measurement of atom resolvability in cryo-EM maps with Q-scores. Nature Methods *17*, 328–334. 10.1038/s41592-020-0731-1.

256. Aiyer, S., Zhang, C., Baldwin, P.R., and Lyumkis, D. (2021). Evaluating Local and Directional Resolution of Cryo-EMCryo-electron microscopy (Cryo-EM) Density Maps. In cryoEM: Methods and Protocols, T. Gonen and B. L. Nannenga, eds. (Springer US), pp. 161–187. 10.1007/978-1-0716-0966-8_8.

257. Harder, D., and Fotiadis, D. (2012). Measuring substrate binding and affinity of purified membrane transport proteins using the scintillation proximity assay. Nature Protocols *7*, 1569–1578. 10.1038/nprot.2012.090.

258. Posert, R., and Baconguis, I. (2023). Appia: Simpler chromatography analysis and visualization. PLOS ONE *18*, e0280255. 10.1371/journal.pone.0280255.

Glossary

14-3-3 a protein which binds and inhibits phosphorylated proteins, including *Nedd4*.

ACMA a fluorescent dye. When ACMA intercalates into a lipid bilayer, it is quenched by a pH gradient across that bilayer.

ASIC the Acid Sensing Ion Channel family. A well-studied member of the ENaC/DEG superfamily opened by low extracellular pH. In this document, I use ASIC to refer to ASIC1 unless specified.

ASL airway surface liquid, a layer of mucous which protects the lung.

Acidic Pocket unfortunately, this name is used to refer to two separate things in the literature. In ASIC, the acidic pocket is between the finger and thumb; the channel opens when the acidic pocket is protonated. In ENaC, the acidic pocket comprises residues from the finger and β-ball and is thought to be involved in *sodium self-inhibition*.

Aldosterone a mineralocorticoid hormone essential for regulation of blood pressure and plasma sodium and potassium levels.

Amiloride a small molecule which blocks ENaC/DEG superfamily ion channels. ENaC binds amiloride several orders of magnitude tighter than other members of the ENaC/DEG superfamily.

Benzamil a derivative of *amiloride* with a higher affinity for ENaC.

C2 domain a lipid- and protein-binding domain.

CCCP a proton ionophore

CF cystic fibrosis.

CKO an ENaC construct with intracellular cysteines knocked out. See Table A.1 for more information.

CKO/DEG *CKO* ENaC with additional mutations to bias the channel toward the open state. See Table A.1 for more information.

DDM n-dodecyl-β-D-maltoside, a detergent commonly used to solubilize membrane proteins.

DM n-decyl-β-D-maltoside, a detergent commonly used to solubilize membrane proteins.

ECD the extracellular domain, comprising the palm, knuckle, finger, GRIP, β-ball, and thumb domains.

ENaC the Epithelial Sodium Channel.

FaNaC the FMRFamide peptide–activated sodium channel family. A member of the ENaC/DEG superfamily found only in mollusks and gated by a small peptide.

Fab the antigen-binding portion of an antibody.

GAS belt a domain swapping loop of TM2 observed in most ASIC structures to date. In ASIC, the GAS belt comprises a Gly-Ala-Ser triad which forms the selectivity filter.

GRIP domain the Gating Relief of Inhibition by Proteolysis domain. Wedged between the finger and the thumb, when this domain is cleaved by proteases in the α and γ subunits, the channel opens.

HECT domain the domain of a *HECT ligase* responsible for transferring a ubiquitin molecule from an E2 ligase to the substrate.

HECT ligase a family of E3 ligases. Most HECT ligases discussed in this work comprise a *C2 domain*, a number of *WW domains*, and a *HECT domain*.

HG motif a highly-conserved His-Gly pair which is essential for proper function of ENaC. In ASIC, the HG motif is found in a re-entrant loop which buttresses the GAS belt

I current. Often used to refer to currents of a specific ion, e.g., I_{Na^+} for sodium current.

IC$_{50}$ concentration of an inhibitor at which the inhibited process is at 50% of its uninhibited value.

Macroscopic current the current recorded from an entire expression system, e.g., a whole-cell current; cf. *unitary current*.

N the number of ion channels at the surface of a cell

NP$_O$ N times P_O (the number of channels times their open probability). Essentially the *macroscopic current* divided by the *unitary current*.

Nedd4 a family of HECT ligases, including the eponymous Nedd4 and Nedd4-2 (also referred to as Nedd4L)

Open probability The proportion of time that a given channel spends in the open state.

PHA pseudohypoaldosteronism. In this text, I discuss only type 1 PHA (PHA1), in which the patient has high plasma potassium and low plasma sodium but normal circulating aldosterone levels.

PIP phosphatidyl inositol, a phospholipid. Most often found in as a triphosphate (PIP_3 or PI3P) or bisphosphate (PIP_2 or PI2P).

PY motif a motif following the form PPXY which is bound by WW domains.

Phenamil a derivative of *amiloride* with a higher affinity for ENaC.

P$_O$ see *open probability*.

SGK Serum- and glucocorticoid-induced kinase, a serine/threonine kinase with a multitude of roles in cell signaling.

SSI see *sodium self-inhibition*.

Sodium self-inhibition The process by which high extracellular sodium concentrations decrease ENaC currents.

Styrene-Maleic Acid a copolymer used to directly solubilize a membrane into nanodiscs of native lipids

TM a transmembrane helix, usually followed by a number (e.g., TM1)

TMD the transmembrane domain, comprising both TMs from all three subunits (six helices total).

TRC taste receptor cells. These cells express channels which respond to a single one of the five basic tastes: salty, sweet, sour, bitter, or umami.

Unitary current currents observed through a single channel; cf. *macroscopic current*.

Valinomycin a potassium ionophore

WT wild-type; a construct which is identical to (or as close as is feasible) to the sequence one would find in the organism.

WW domain a protein-protein interaction domain. WW domains bind *PY motifs*.

A. Materials and Methods

A.1. ENaC Expression

A.1.1. Human ENaC

Human embryonic kidney cells (HEK293T/17) were grown in suspension in Freestyle medium with 2% FBS at a density of $2 - 4 \times 10^6$ cells/mL. BacMam virus carrying the genes for the appropriate ENaC subunits were added to the flasks at an MOI of 1 and incubated at 37 °C for 8 hours, after which 1 µM amiloride was added and the flasks were moved to 30 °C. After a total incubation time of 72 hours, cultures were centrifuged at 4,790 xg for 20 minutes to collect pellets. The pellets were washed with **TBS** (20 mM Tris pH 8.0, 200 mM NaCl) and centrifuged again before snap-freezing in liquid nitrogen. Cell pellets were stored at -80 °C until use.

A.1.2. Mouse ENaC

Sf9 cells were grown in suspension in Sf900-II serum-free media at 27 °C. Cells were infected at log phase with virus encoding full-length mouse $ENaC_\alpha$, $ENaC_\beta$, and $ENaC_\gamma$. After 5–6 hours of growth, 1 µM amiloride was added to the culture. Cells were harvested 24 hours later, washed with TBS, flash frozen in liquid nitrogen, and stored at -80 °C until used.

A.2. ENaC Purification

A.2.1. Human ENaC

Throughout this protocol, quantities of resin and buffer are given "per flask". I grow cell culture in quantities of 800 mL culture per flask,

meaning that, e.g., pelleted cells from 1.6 L of cells require twice the quoted quantities of buffer and resin. In datasets with NaCl listed as the salt, solubilization buffer, wash buffers, elution buffer, and SEC buffer used NaCl in place of KCl.

To purify ENaC, frozen whole-cell pellets were removed from the -80 °C freezer and thawed in a 37 °C water bath. While the pellets were thawing, 50 mL **Solubilization Buffer** was prepared per flask:

- 20 mM Tris pH 7.5, 200 mM KCl
- 1 tablet per 100 mL Pierce EDTA-free protease inhibitor tablets
- 25 U/mL ThermoFisher universal nuclease
- 2.5 mM ATP, 5 mM $MgCl_2$
- 10 mg/mL digitonin
- 10 µM amiloride

The solubilization buffer was prepared fresh at 2x concentration (i.e., half the final volume). Once pellets were fully thawed, they were added to the solubilization buffer and the mixture was brought to the final volume with DI water and poured into a screw-cap bottle. The solubilization mixture was left at 8 °C for 1.5 hours.

After solubilization was complete, the crude lysate was decanted into ultracentrifuge tubes and centrifuged at 100,000 xg for 45 minutes at 4 °C. Meanwhile, in-house-made GFP-nanobody CNBr resin (0.8 mL per flask) was loaded into an XK 16 column and washed with 2 CV of TBK

- 20 mM Tris pH 7.5
- 200 mM KCl

and the following buffers were prepared in the listed quantities:

wash A (10 column volumes [CV]):

- 20 mM Tris pH 7.5, 200 mM KCl
- 0.7 mg/mL digitonin
- 2 mM $MgCl_2$
- 2 mM ATP
- 2 nM phenamil

wash B (10 CV):

- 20 mM Tris pH 7.5
- 200 mM KCl
- 0.7 mg/mL digitonin
- 5 mM CaCl$_2$
- 2 nM phenamil;

elution buffer (5 CV): wash B with 33 μg/mL thrombin

The column was washed with 2 CV of wash A, then clarified lysate was bound to the column under 4 mL/min flow. A small aliquot of pre-column and post-column clarified lysate was reserved to assess binding efficiency by GFP FSEC[247]. If binding efficiency fell below 90% of the initial efficiency the resin was discarded. Otherwise, it was regenerated with pulsed pH cleaning. The GFP-nanobody column was washed with 5 CV wash A and B.

To elute ENaC from the GFP nanobody resin, the column was washed 3 times with 1.5 CV elution buffer and once with TBK with 0.7 mg/mL digitonin. As each wash was flowed on, the eluant was collected in 1 mL or 0.25 CV fractions, whichever was smaller. This results in four sets of fractions: the first comprises largely wash B with little protein (from the initial flow-on of elution buffer), and the remaining three elution buffer. All fractions were run on an SDS-PAGE gel, and fractions with bands at the expected molecular weight for ENaC were pooled and concentrated to a final volume of 0.5 mL. If the preparation was acid-shocked, the protein was desalted into **acid shock** buffer at this stage:

- 20 mM Tris pH 6
- 200 mM KCl
- 0.7 mg/mL digitonin
- 2 nM phenamil

If the preparation required Fabs, they were added in two-fold excess of protein concentration (as determined by nanodrop A$_{280}$) at this stage. A final concentration of 1 mM C8 PIP$_2$ was added to the CKO/DEG monofab samples just before grid preparation.

The concentrated eluant was loaded onto a Superose 6 Increase 10/300 column (Cytiva) equilibrated in **SEC buffer** for further purification via SEC.

- 20 mM Tris pH 7.5

- 200 mM KCl
- 0.7 mg/mL digitonin
- 2 nM phenamil

SEC was typically run overnight, meaning fractions remained at 4 °C until the next morning. Fractions from the SEC peak were collected and assayed for purity and monodispersity by SDS-PAGE and tryptophan FSEC. Monodisperse peaks were pooled and used the same day. Thus, total time between cell pellet thaw and protein use was typically less than 36 hours.

A.2.2. Mouse ENaC

Frozen cell pellet was thawed on ice. Membranes were prepared by sonication and centrifugation, then re-frozen until purification. For each gram of membranes, 15 mL of **solubilization buffer** was added

- 4 mM GDN
- 20 mM HEPES pH 7.6
- 150 mM NaCl
- 2 mM ATP
- 2 mM $MgSO_4$
- 1 mM TCEP
- 100 µM amiloride
- 1 tablet per 100 mL Pierce EDTA-free protease inhibitor tablets

Membrane pellet was mixed thoroughly and homogenized with a Dounce homogenizer. Cell pellet was stirred for 1 hour at 4 °C. Solubilized membranes were centrifuged at 100,000 xg for 45 minutes at 4 °C.

Next, 300 µL GFP nanobody CNBr resin per gram of membrane was loaded into a gravity column and washed with 10 CV **HBS**

- 20 mM HEPES pH 7.6
- 150 mM NaCl)

and 3 CV **wash A**

- 0.1 mg/mL GDN
- 20 mM HEPES pH 7.6

- 150 mM NaCl
- 1 mM TCEP
- 100 nM phenamil

Clarified lysate was flowed over this column under gravity. The column was washed with 6 CV each of wash A, **wash B** (wash A with 2 mM ATP, 2 mM MgSO$_4$), **wash C** (wash A with 25 U/mL ThermoFisher Universal Nuclease), and **elution buffer** (wash A with 5 mM CaCl$_2$). ENaC was eluted by flowing 1 CV of elution buffer with 30 μg/mL thrombin onto the column and collecting the supernatant. After an hour, this process was repeated. These elution steps were repeated for a total of four elutions of 1 CV each.

The first three elutions were pooled and concentrated to 0.5 mL. Fab was added at a one-to-one ratio with nominal protein concentration by nanodrop. Sample was incubated for 10 minutes at room temperature, then centrifuged at 100,000 xg for 20 minutes at 4 °C. The clarified sample was loaded onto a Superose 6 Increase 10/300 column (Cytiva) equilibrated in fresh wash A buffer. Fractions were assessed for purity via SDS-PAGE and FSEC before proceeding to grid preparation or other uses.

A.3. ENaC nanodisc preparation

To prepare nanodiscs, 15 mg of a chloroform stock of POPC (Avanti) was dried down under an argon stream. The lipid film was left overnight in a vacuum desiccator to remove all chloroform. The lipids were then resuspended in 350 μL **reconstitution buffer**

- 20 mM HEPES pH 7.4
- 100 mM KCl
- 1 mM EDTA

and sonicated until the solution was milky in appearance and no lipids remained adhered to the sides of the tube, typically 5–10 minutes. To this solution, 150 μL of 350 μM DM in reconstitution buffer was added. The resulting 500 μL suspension was sonicated in 5 minute bursts until completely clear. To this suspension, 1 mL TBS was added to prepare a final lipid concentration of 10 mg/mL.

Lipids, ENaC, and MSP2N2 were mixed at a final MSP:POPC:ENaC molar ratio of 1:31:0.04. The final concentration of MSP2N2 was kept at 100 µM by further concentrating ENaC or adding lipid reconstitution buffer with 35 mM DM as necessary. This reconstitution mixture was incubated at room temperature for 1 hour. During this incubation, biobeads were washed once in 100% methanol, three times in water, and once in TBS. After 90 minutes, 215 mg washed biobeads per 1 mL reconstitution mixture were added. After 1 hour, the reconstitution mixture was moved to a fresh aliquot of equilibrated biobeads and left nutating overnight at room temperature, approximately 16 hours. The reconstitution mixture was pipetted off the biobeads, filtered with a 0.2 µm filter, and purified via SEC using a Superose 6 Increase 10/300 column in TBS. Typical yields were extremely low, between 5–10% of input ENaC. The protein assembly was stable with minimal aggregation at 4 °C (assessed by cryoEM and SEC) for at least two weeks.

A.4. Western Blots

SDS-PAGE gels were blotted onto nitrocellulose membranes. Membranes were blocked in 50 mg/mL milk in TBST for 1 hour at room temperature. Primary antibody (**ENaC$_\alpha$**: Santa Cruz Biotechnology αENaC (H-95) sc-21012 lot no. L2812; **ENaC$_\gamma$**: abcam Anti-epithelial Sodium Channel gamma ab133430) was added to this same blocking buffer at 10 µg/blot and incubated overnight at 4 °C. Membranes were washed 3 times with TBST for 5 minutes before addition of secondary antibody (LI-COR IRDye 800 CW Goat anti-Mouse 925-32210 lot no. D21115-21) in TBST. Membranes were incubated at room temperature with secondary for 1 hour, washed 3 times with TBST and once with TBS, then imaged (LI-COR Odyssey DLx).

A.5. cryoEM Grid Preparation

Grid preparation different slightly for each dataset, but followed the same general procedure (Table A.2). Purified GFP-cleaved ENaC was concentrated for grid preparation just before blotting and freezing. All grids were glow discharged at 15 mA for 60 seconds on a Pelco easiGlow before blotting. Grids were frozen using a Vitrobot Mark

III (Thermo Fisher). Vitrobot parameters were set as follows: blot time 2, wait time 0, drain time 0, blot force 1, humidity 100%, temperature 12 °C. "Double-blotted" grids had a protein droplet loaded, manually blotted with torn Whatman filter paper, and a fresh droplet loaded onto the grid before Vitrobot blotting (with Vitrobot filter paper rings) and freezing. This double-blotting process typically took approximately five seconds from first drop to plunge-freeze. In all cases, each protein droplet was 3 μL.

A.6. cryoEM Data Collection

Datasets were collected using SerialEM by microscopy core staff at the facilities used (Table A.3)[248]. In all cases, multi-shot multi-hole regimes were used to maximize the number of movies recorded. Number of shots per hole and maximum beam shift were a function of ice quality and grid type, but typically a 3x3 pattern of holes was imaged 2–4 times per hole.

A.7. cryoEM Image Processing

Each dataset was processed slightly differently, but following the same general pipeline. First, movies were imported into cryoSPARC for pre-processing. Default parameters were used for both motion correction and CTF estimation. Next, particles were picked using the blob picker in cryoSPARC. Adjustments were made to the minimum and maximum radii to account for the number of Fabs present in each sample. Blob picks for several micrographs were manually inspected and adjusted. First, the NCC parameter was adjusted until few contaminant and carbon-edge picks remained. Next, in a low-defocus micrograph, the low power threshold was adjusted to remove empty ice picks. Finally, in a high-defocus micrograph, the high power threshold was adjusted to remove all carbon-edge and contaminant picks. These initial blob picks were cleaned by 2D classification, and the resulting particle sets used to generate templates for template picking. Template picked thresholds were adjusted as for blob picked particles.

A. Materials and Methods

The template picked particles were repeatedly 3D classified using heterogeneous refinement in cryoSPARC, providing one "good" class and a number of "junk" classes (typically noisy or bad *ab initio* models of the blob picked particles) until all particles produced reasonable ENaC classes. The final particle set was never 2D classified, since I find that 2D classification reduces the frequency of rare particle views. From this point, processing proceeded *ad hoc* to produce the final maps (Image Processing).
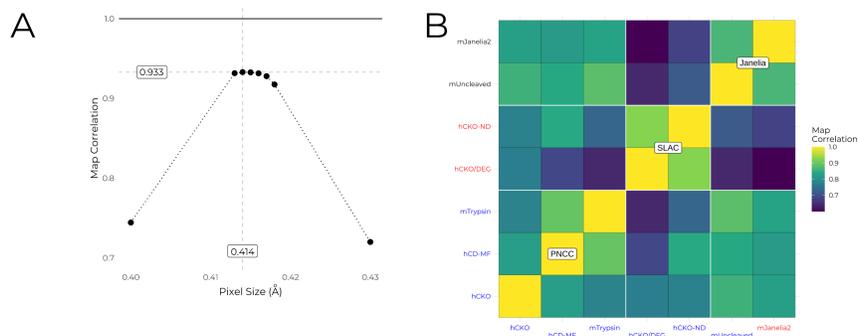

Figure A.1.: S^2C^2 pixel sizes seem miscalibrated. **A**: Scaling the nominal pixel size for human CKO/DEG dramatically increases the correlation with human CKO digitonin. **B**: Correlation coefficients for all maps. Maps were aligned prior to taking correlation coefficients. Abbreviated as follows: hCKO: human CKO; hCD-MF: human CKO/DEG monofab; mTrypsin: trypsin-cleaved mouse; hCKO/DEG: human CKO/DEG difab; hCKO-ND: human CKO nanodisc; mUncleaved: mouse uncleaved; mJanelia2: a second uncleaved mouse dataset collected at Janelia, but not presented here.

During image processing, I began to suspect that the pixel sizes provided by S^2C^2 are likely miscalibrated. First, other users reported pixel size calibration issues with S^2C^2 microscopes around the time these datasets were collected (Patrick Mitchell, S^2C^2 Director of Operations, personal communication). Second, scaling the CKO/DEG difab pixel size from the nominally-correct 0.43 to 0.414 (a change of approximately 3.6%) changes the map correlation value from 0.72 to 0.93 (Figure A.1 A). Finally, a comparison of the correlation between seven recently-collected ENaC maps shows that S^2C^2 is an outlier, with unscaled maps generated from data collected at PNCC and

Janelia Farm correlating better with themselves and each other than with those collected at S^2C^2 regardless of construct (Figure A.1 B). I therefore decided to scale both S^2C^2 maps to correlate best with the same condition and construct recorded at PNCC after processing was complete. I present the models built into the scaled maps in this work.

A.8. Model Building

The starting model for mouse ENaC was generated using a local installation of AlphaFold[249]. The amino acid sequences for mENaC α (Uniprot ID Q61180), β (Uniprot ID Q9WU38), and γ (Uniprot ID Q9WU39) were joined using 10xGS linkers between α and β, and β and γ. This meta-sequence was then entered as the AlphaFold target. The linkers and large, unstructured, low-confidence loops were removed from the model before proceeding.

Before docking into experimental maps, starting models had Fabs and waters deleted to ease early model building steps. Initial models were rigid-body fitted into the experimental maps. Any loops in poor or missing regions of the map were deleted. The whole models were simulated with distance restraints using ISOLDE and ChimeraX[250,251]. Once models were roughly fit into the potential, strained distance restraints were released. Once the backbone appeared to fit reasonably well into the map, all distance restraints were released. Simulating one chain at a time, a pass over every residue in ENaC was performed, focusing on Ramachandran values and rotamers. Once all chains had been optimized in this manner, glycans were added using Coot's carbohydrate module[252]. Fabs were rigid-body fitted and simulated similarly to the initial models once these steps were complete.

Models were refined using Phenix real-space refinement[253]. In some cases, the TMD map was used as-is for refinement. In other cases, the ECD and TMD map were combined using Phenix's "Combine Focused Maps" job and the resulting map was used for refinement. In these cases, the lowest GSFSC resolution was provided to Phenix. Parameters were left as default, except rotamers were only refined when they had both poor map quality *and* were outliers (rather than *or*). I changed this setting because rotamer and clash statistics were significantly worse if it was left as the default. Model quality

was assessed using MolProbity within Phenix, Q-scores calculated in ChimeraX, and 3DFSC as implemented in cryoSPARC (Table A.4 and Appendix D)[254–256].

A.9. Constructs

The four constructs I present here can broadly be split into those I expect to be open (CKO/DEG and mouse trypsin) and those I expect to be closed (CKO, mouse) (Table A.1). All human channels in this work have mutant furin sites (αR178A R204A and γR138A). Additionally, all human channels are "cysteine knock-out" (CKO) mutants, with the following mutations: αC63A, βC30A, and γC33A C41A. Some (but not all) cysteines in the ENaC TMD are known to be palmitoylated[217–219]. CKO channels express at approximately eight times the yield of wild-type-like channels, with similar electrophysiological traits. Mouse channels presented in this work have no mutations from the consensus gene. I expect mouse and CKO channels to be closed.

DEG channels have two mutations: βS520K and αT240W. The former mutation at what has been named the "DEG site" holds the channel in an open state regardless of proteolytic cleavage state[161]. The DEG site sits in the TMD just above the predicted amiloride-binding site. The latter mutation in α lies in the GRIP domain and also increases the P_O of uncleaved ENaC[158].

A.10. Whole cell patch clamp

Human embryonic kidney cells (HEK293S/17) were grown in suspension in Freestyle medium with 10% FBS to a density of 1×10^6 cells/mL, at which point they were infected with virus carrying the appropriate ENaC genes. Cells were incubated at 37 °C overnight with 1 μM amiloride. Cells were then pipetted over a dish of DMEM with 10% FBS with several small coverslips and allowed to adhere at 37 °C while the electrophysiology rig was prepared, approximately 2 hours. Pipettes were pulled to 2–3 MΩ resistance and filled with filtered **internal solution**

- 150 mM KCl
- 2 mM MgCl$_2$
- 5 mM EGTA
- 10 mM HEPES pH 7.4

Working one coverslip at a time, cells were moved from DMEM at 37 °C to a dish on the rig (at room temperature) containing **K$^+$ external solution**

- 150 mM KCl
- 2 mM MgCl$_2$
- 2 mM CaCl$_2$
- and 10 mM HEPES pH 7.4

Also prepared were solutions of Na$^+$ and Li$^+$, the same as the K$^+$ solution but with NaCl or LiCl replacing the KCl, respectively. Each salt solution also had a counterpart with 100 μM amiloride added. Finally, a **trypsin solution** (KCl external solution with 5 μg/mL trypsin) was prepared.

Amiloride sensitive current was determined by placing a cell in the amiloride external solution for 1 second, the amiloride-free solution for 2 seconds, and returning to the amiloride solution for 1 second. Average current during no-amiloride traces was subtracted to set the baseline to 0 A, and the maximum current during the 2 second no-amiloride duration taken as the amiloride-sensitive current. The K$^+$ recordings show a current spike when returning to the amiloride-containing solution, which I exclude from the calculations. This process was performed once for each holding potential between -80 and +80 mV, stepping by 20 mV. Then, this entire voltage sweep was repeated for each of the two remaining salts. The cell was then exposed to the trypsin solution for 5 minutes, and the entire set of voltage and salt sweeps repeated for the post-trypsin measurements. Thus, the full combination of voltage, salt, and proteolytic cleavage states was recorded on each cell. Once a dish had been exposed to the trypsin solution, the dish was replaced with a fresh dish and coverslip to prevent early cleavage of unmeasured cells.

A.11. Tables

Table A.1.: Mutations in human ENaC constructs. Mouse constructs do not have any mutations.

	CKO	CKO/DEG
α mutations	C63A, R178A, R204A	C63A, R178A, R204A, T240W
β mutations	C30A	C30A, S520K
γ mutations	C33A, C41A, R138A	C33A, C41A, R138A

Table A.2.: Grid preparation parameters

	hCKO		hCKO/DEG		mouse	
	Digitonin	Nanodisc	Difab	Monofab	Uncleaved	Trypsin
ENaC (μM)	19.8	2	21.3	24	9.6	9.6
Salt	NaCl	KCl	KCl	KCl	NaCl	NaCl
Acid Shock	Yes	No	Yes	No	No	No
Fabs	α and β	—	α and β	α	α	α
Grid Type[1]	2/1 200	2/2 200 + 2 nm carbon	2/1 200	2/1 200	2/2 200	2/1 200
FOM (μM)	2	10	10	2	100	2

[1] All grids are Quantifoil grids with gold mesh

Table A.3.: Data collection and image processing parameters

	hCKO		hCKO/DEG		mouse	
	Digitonin	Nanodisc	Difab	Monofab	Uncleaved	Trypsin
Facility	PNCC	S2C2	S2C2	PNCC	Janelia Farm	Janelia Farm
No. Movies	13,689	9,882	5,126	5,832	11,334	6,960
Frames[1]	50	65	50	50	65	65
Pixel Size (Å/pix)[2,3,4]	0.8015	0.86	0.86	0.83	0.844	0.788
No. particles	612,591	237,730	257,341	373,495	499,081	264,228
ECD resolution (Å)[5,6]	2.34	3.06	2.94	—	—	3.03
Whole protein resolution (Å)[5,6]	2.89	—	3.26	3.04	3.24	3.3
ECD sharpening factor[5]	-56.6	-77.1	-88.9	—	—	-66.7
Whole protein sharpening factor[5]	-66	—	-110.4	-104.4	-96.4	-67.4

[1] Electron flux is 1 e-/Å²/frame
[2] All datsets collected in super-resolution mode and Fourier-cropped back to this physical size.
[3] Nominal pixel sizes given by the microscopy facility.
[4] These values were used for processing and are listed to the precision given by the microscopy facility at the time of collection.
[5] A dash indicates that a focused map for this region was not used in model building
[6] GSFSC resolution

Table A.4.: Model building, refinement, and validation parameters

	hCKO/DEG			mouse		hCKO	
	Difab	Monofab	Uncleaved		Trypsin	Digitonin	Nanodisc
Starting Model	CKO digitonin	6WTH	AlphaFold	mouse uncleaved		6WTH	CKO/DEG difab
No. non-H atoms	12,807	11,588	11,466	11,617		12,416	9,971
No. residues	1,714	1,476	1,506	1,540		1,628	1,174
No. ligands	35	43	26	29		49	38
Bond length RMSD	0.003	0.004	0.003	0.003		0.006	0.003
Bond angle RMSD	0.519	0.499	0.438	0.446		0.709	0.505
Molprobity score	1.10	1.27	1.48	1.44		1.49	1.11
Clash score	3.06	5.03	6.44	5.70		4.61	3.14
Rama. outliers (%)	0.00	0.00	0.00	0.00		0.00	0.00
Rama. allowed (%)	1.26	1.82	2.65	2.67		2.00	1.57
Rama. favored (%)	98.74	98.18	97.35	97.33		98.00	98.43
Rotamer outliers	0.72	0.28	0.09	0.00		2.15	0.09
Cβ outliers	0.00	0.00	0.00	0.00		0.00	0.00
CaBLAM outliers	0.40	1.15	1.52	0.86		0.81	0.44
Resolution (0.143 FSC)	2.8	3.1	3.2	3.0		2.3	2.9
CC (mask)	0.83	0.82	0.83	0.84		0.85	0.84
Q-score	0.71	0.71	0.68	0.72		0.80	0.71

B. The Graveyard

In this appendix, I will go into more detail on experiments that did not work, or that did not produce interpretable results. I will also discuss dead ends on the protein purification pathway to guide future efforts. This section is isolated from the main body of the text since it is only interesting to those who may follow after me. As such, a basic familiarity with lab protocols is assumed.

B.1. Nedd4-2

Early on, my work included purification of Nedd4-2 with an eye toward both a functional assay for Nedd4-2/ENaC interaction and a structure of the bound complex. Nedd4-2 comprises structured domains connected by disordered linkers, and so it should come as no surprise that this proved too difficult and time consuming and was dropped[123,124]. However, it may be that adding Nedd4-2 helps to resolve ENaC's TMD and even regions of the intracellular loops, so future research into the topic may yet prove fruitful.

B.1.1. Expression and purification

B.1.1.1. Insect cells and TALON

Nedd4-2 was initially expressed in Sf9 cells as a C-terminal GFP fusion. Cells were infected at an MOI of 5 and left to express protein at 21 °C for 48 hours. Cells were collected via centrifugation (100k xg for 45 minutes) and frozen in liquid nitrogen until use.

Cells were thawed and resuspended in 100 mL TBS per flask, then sonicated for a total of 5 minutes of 10 seconds on, 30 seconds off, power level 7. Crude lysate was centrifuged for 45 minutes at 100,000 xg and clarified lysate collected.

Clarified lysate was bound to 10 mL TALON resin per flask and washed with 5 CV TBS followed by 2 CV TBS plus 10 mM imidazole. Finally, 1 mL fractions are collected from a 4 CV elution with 250 mM imidazole. These fractions are concentrated and sized on a Superose 6 Increase 10/300 column (Figure B.1). The SEC protocol for Nedd4-2 is essentially unchanged from that for ENaC (Section A.2.1), with the exception that TBS alone (i.e., without detergent) is used as a running buffer.
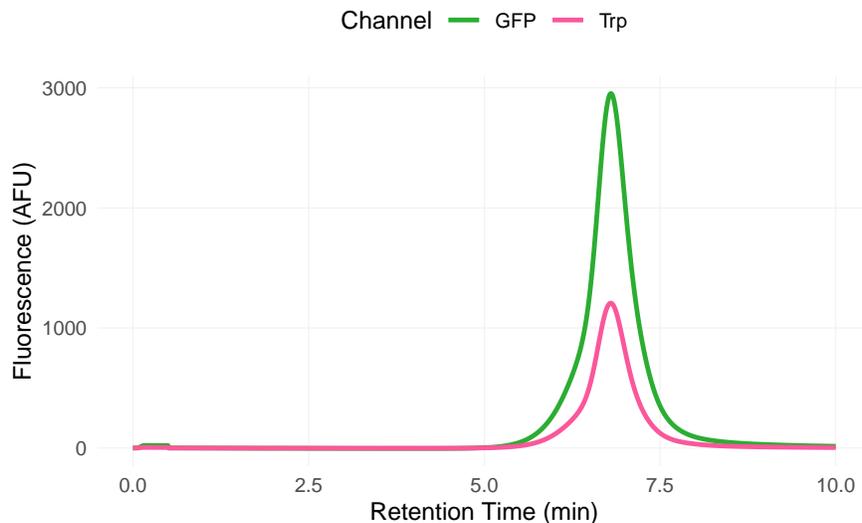

Figure B.1.: FSEC analysis of a fraction of Nedd4-2 expressed in Sf9 cells. This sample has been purified by both TALON and SEC.

There are several problems with this protocol. First, tagging a Nedd4-family ligase on its C-terminus renders it completely non-functional. This is probably why yield is so high and pure — the protein is incapable of affecting itself or the cell in any way. Second, most of the field uses material prepared from *E. coli*, and it's generally best to follow convention. Finally, Nedd4-2 harbors a cryptic thrombin site, so GFP cleavage also cleaves the protein.

B.1.1.2. *E. coli* **and strep tags**

I thus moved to expression of strep-tagged material in *E. coli*. The Nedd4-2 gene was cloned into pJAC148 and transformed into

BL21(DE3) cells. At OD_{600} 0.75, expression was induced with 250 μM IPTG and transferred to a 16°C incubator and allowed to express overnight. Cells were pelleted and frozen with liquid nitrogen.

Following a standard strep purification protocol, the material looks significantly worse than that purified by IMAC (Figure B.2). I believe this is most likely due to the fact that this material is actually functional, which means it is capable of self-degradation. It also likely puts the *E. coli* cells under significantly more stress than non-functional material.

This material, obviously, contains a large leading peak centered around 11 mL. Since there seems to be no protein at all in this peak, but it is after the void volume, I suspect it is nucleotide contamination. In any case, this protocol seemed the most reliable means by which I could purify large amounts of (potentially) active Nedd4-2.

I do not have A_{260}/A_{280} measurements for this material, unfortunately

B.1.2. ENaC Binding

The Nedd4-2 purified from both Sf9 cells and *E. coli* binds ENaC. A simple, single-replicate experiment shows increased movement of GFP-tagged Nedd4-2 from its unbound peak to a peak eluting before ENaC (Figure B.3). This is, of course, not an entirely rigorous experiment. Most concerning is the fact that increased ENaC does not always translate to an increase in the presumptive Nedd4-2 bound ENaC species.

B.1.3. Ubiquitination assay

If this project had progressed, we would have needed a way to assess whether our purified Nedd4-2 was functional or not. My idea for this was an *in vitro* ubiquitination assay. Ideally, we'd take tagged ubiquitin (Ub), an E1, an E2, and our purified Nedd4-2 and incubate them together. Next we'd detect ubiquitination of ENaC via western blot. Only the mixture with all of these components should have ubiquitinated ENaC.
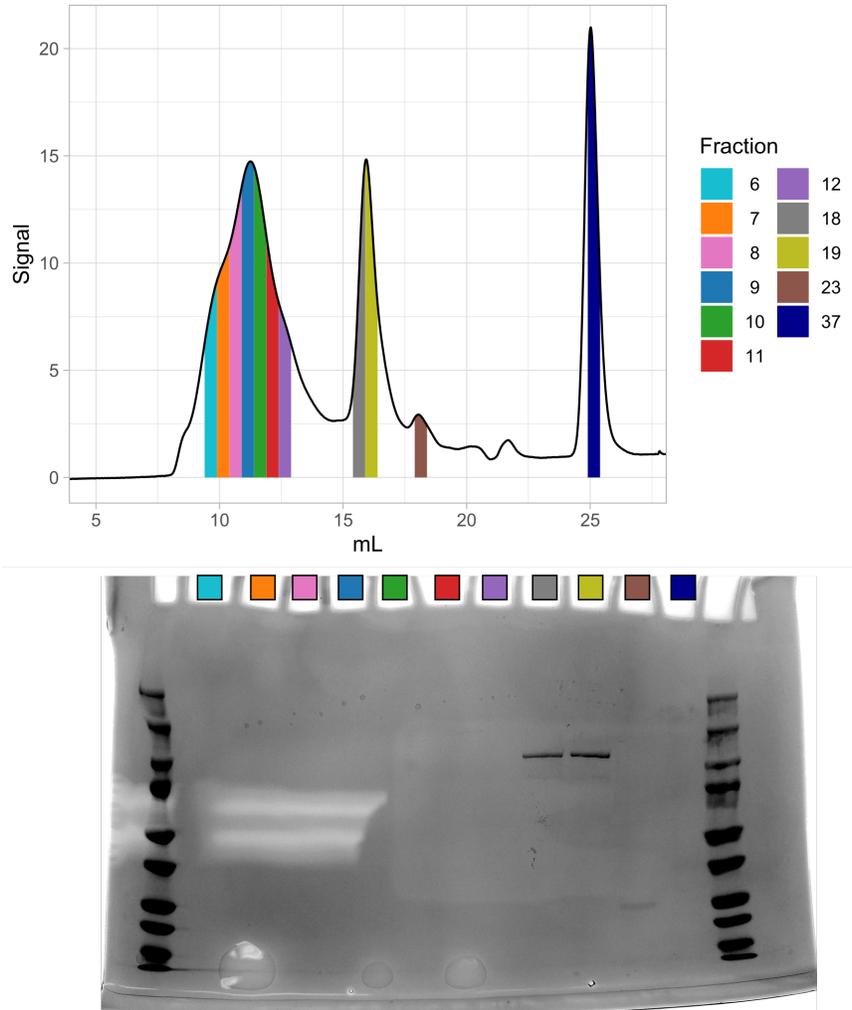
Figure B.2.: Twin-strep purification of Nedd4-2 expressed in *E. coli*. **Top**: SEC trace of twin-strep purified material. Indicated fractions are further analyzed by SDS-PAGE. **Bottom**: SDS-PAGE analysis of the indicated fractions. Note that only fractions 18 and 19 contain Nedd4-2.
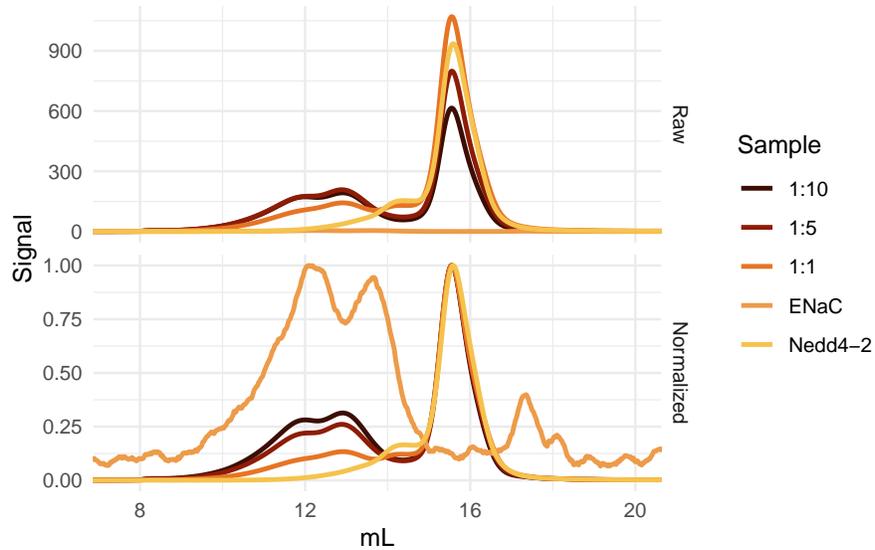
Figure B.3.: Binding experiment. 170 nM of GFP-tagged Nedd4-2 was bound to 1, 5, or 10 times as much untagged ENaC. Increasing ENaC concentrations results in increasing amounts of the species eluting around 12 mL, but not monotonically. **Top**: raw, unnormalized GFP fluorescence. **Bottom**: fluorescence normalized to the maximum peak height in the trace. ENaC is visible in this normalized trace due to a small amount of remaining material which did not have its GFP tag cleaved during purification.

I made a few attempts at this, and none of them really worked. It's not worth reproducing the exact protocols here — for the truly interested reader, they are in Lab Meetings 2, 3, and 4. The two major categories I tried were what I'd call a "minimal" or "supplementary" ubiquitination assays.

The minimal assay involved purchasing an *in vitro* ubiquitination kit and replacing the company's E3 enzyme with the same molar amount of my purified Nedd4-2 (as assayed by nanodrop). Using this assay I was potentially able to detect a moderate amount of ubiquitination of ENaC (Figure B.4). However, overall signal is low, and there appears to be some ENaC-Ub signal in lanes without purified Nedd4-2. Additionally, longer incubation times do not result in stronger ENaC-Ub signal. I take it from this assay that our purified material was not functional.

However, my western blots are never great, and it may be that refinement of the detection technique is required. For instance, another of my blots for the minimal assay did seem to show some ubiquitination by our purified Nedd4-2 (Figure B.5). Regardless, this inconsistency means the assay needs work in addition to whatever work needs doing on Nedd4-2 and ENaC themselves.

For a supplementary assay, I add purified Nedd4-2 to rabbit reticulocyte lysate. The idea was to check for increased ubiquitination when more E3 enzyme is added. I never ended up running this assay because it made less sense than the minimal assay, and I abandoned Nedd4-2 before I could get to it.

B.1.4. What should be done?

If I were starting over, I'd find a good positive control to make sure we could test the function of our Nedd4-2. That the purified Nedd4-2 is much more important than that it binds ENaC. Next, an assessment of the necessary ratios and concentrations for stable complex formation would be useful. I expect that some form of cross-linking would be required to guarantee complex formation on the grid without overcrowding.

Ultimately, though, I think I was right to abandon this facet of my project. The domains of Nedd4-2 have already been resolved, and it seems to be largely unstructured aside from those domains. Rather
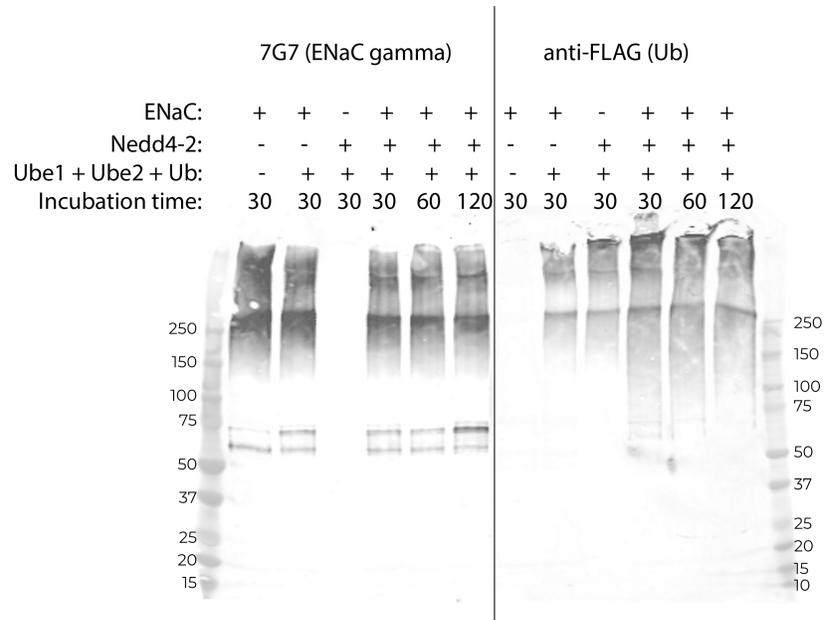
Figure B.4.: A western blot of the minimal *in vitro* ubiquitination assay. The **left blot** is against γ ENaC; the **right blot** is against a FLAG tag present on the ubiquitin used during the assay. Purified ENaC and Nedd4-2 are used in combination with commercial Ube1 and Ube2 along with the FLAG Ub as indicated in each lane. Note that minimal movement of ENaC out of the expected bands is observed on the left, and little accumulation of signal is seen on the right.
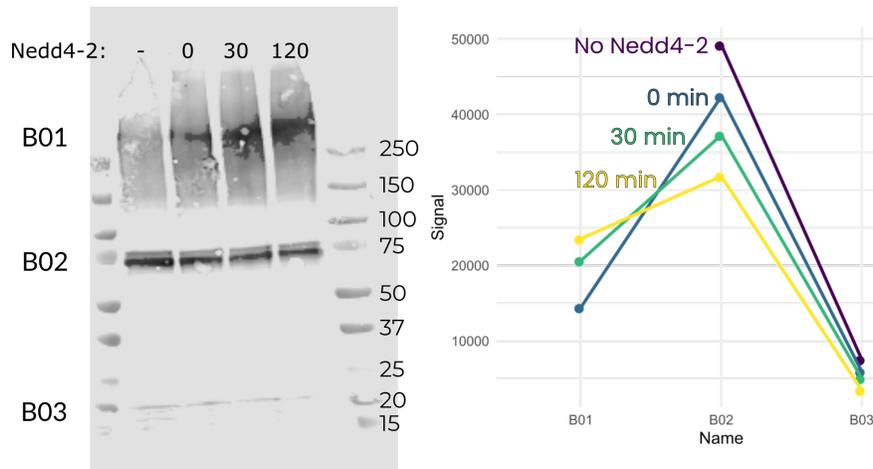
Figure B.5.: **Left**: A western blot against ENaC γ. The high molecular weight band is ENaC in the stacking gel. **Right**: quantification of the upper, middle, and lower bands (B01, 02, and 03 respectively). Note that as B01 increases, B02 decreases.

than rely on it to help align the intracellular and transmembrane domains, I would try a megabody or other scaffolding system.

B.2. Scintillation Proximity Assay

As discussed in Section 3.3.1, SPA never worked for anybody in our entire lab, working across three proteins. As a reminder, our main problem was that specific and non-specific counts were essentially indistinguishable.

Ideally, non-specific counts increase linearly and specific counts increase logarithmically with increasing substrate, and signal-to-background ratios should be around 1.5[257]. Our background and "specific" counts both increased linearly with more substrate, leading me to believe that our "specific" counts are merely unaccounted-for background. Additionally, our signal-to-background ratio typically falls between 0.2 and 0.01 (one to two orders of magnitude too low). Finally, our "specific" counts are often negative.

If you're saying to yourself, "Well then it just seems like your protein isn't binding the ligand at all" I'd agree with you. I don't think playing around the edges here will fix anything. It is worth noting that the same exact trends occur in ASIC, which we know has a properly-folded TMD by cryoEM. This indicates that there is likely something fundamentally wrong with our process, rather than (or, more likely, in addition to) something wrong with our purified ENaC.

B.2.1. BSA

It's fairly common practice to include additives to reduce non-specific binding in SPA assays. We tried BSA, which is typically added at around 5%. Surveying a number of percentages around there yields no improvement in background or specific counts (Figure B.6).
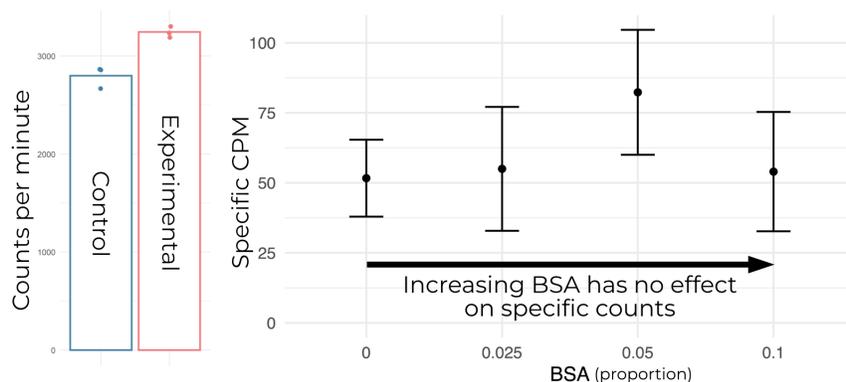

Figure B.6.: Addition of BSA does not improve SPA results. **Left**: ENaC held at a constant concentration with increasing proportion of BSA added shows no improvement in specific counts.

Changing the acidity of the mixture, alongside the pH, does not improve background or specific counts (Figure B.7). I also include this plot to show that specific counts are, more often than not, negative.

B.2.2. Data collection time

The time at which data are collected changes the result (Figure B.8). Counts are recorded from a plate, and the amount of incubation re-
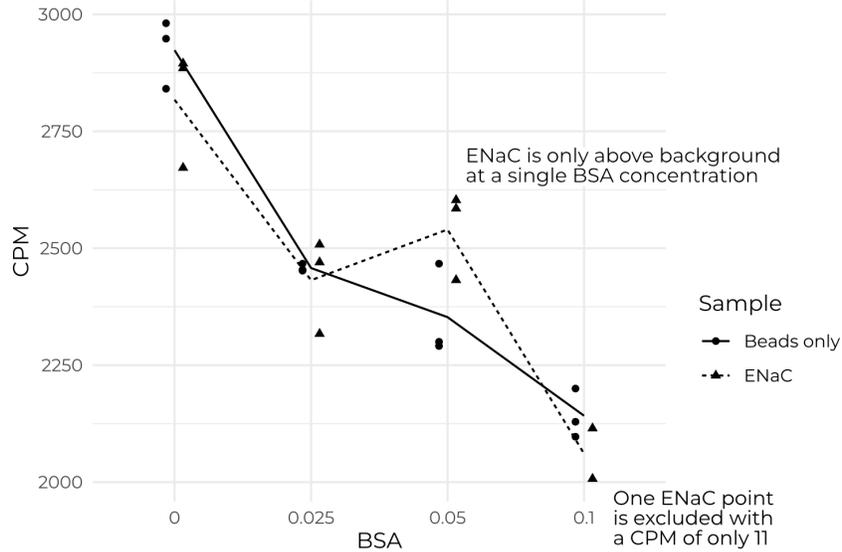
Figure B.7.: Changing the pH of the mixture from 7.4 to 6.0 does not improve counts, and specific counts are often negative. Lines follow the mean for each condition.

quired to reach a steady signal must be determined empirically. However, with low specific counts, the selection of recording time can dramatically change the interpretation of results.

B.2.3. Membrane memetic

Switching from digitonin to nanodiscs yields a marginal improvement in that specific counts are generally positive (Figure B.9). However, specific counts still increase linearly with ligand concentration well beyond the reported K_d of ENaC for benzamil (approximately 10 nM), calling into question whether they are truly specific. Additionally, the signal-to-background ratio remains below 1.0.

B.2.4. Bead type

Use of nanoSPA's smaller, lower-background beads does improve total counts, i.e., reduces the background counts (Figure B.10). It is,
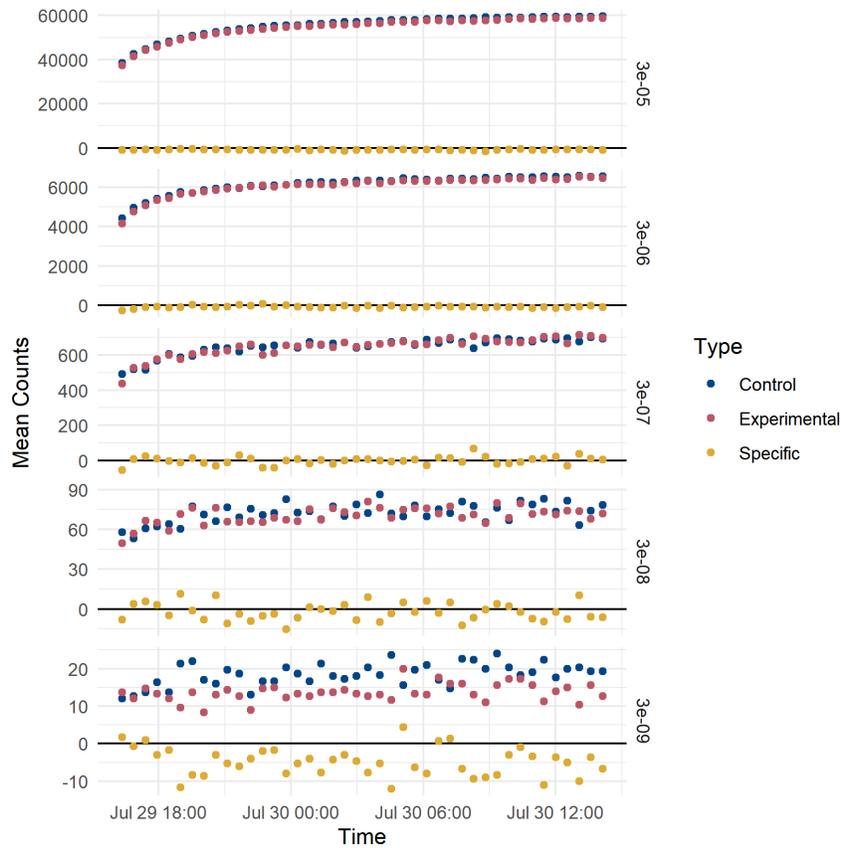
Figure B.8.: The plate is re-recorded approximately every 10 minutes. Note that high ligand concentrations (upper facets) maintain a steady signal, while low ligand concentrations (lower facets) are too noisy to reliably determine. Thus, datasets recorded only 10 minutes apart might show dramatically different Specific (Experimental - Control) counts for low concentrations, which would significantly affect fitted K_d values. Note, also, that despite their stability, specific counts at high ligand concentrations are almost entirely negative.
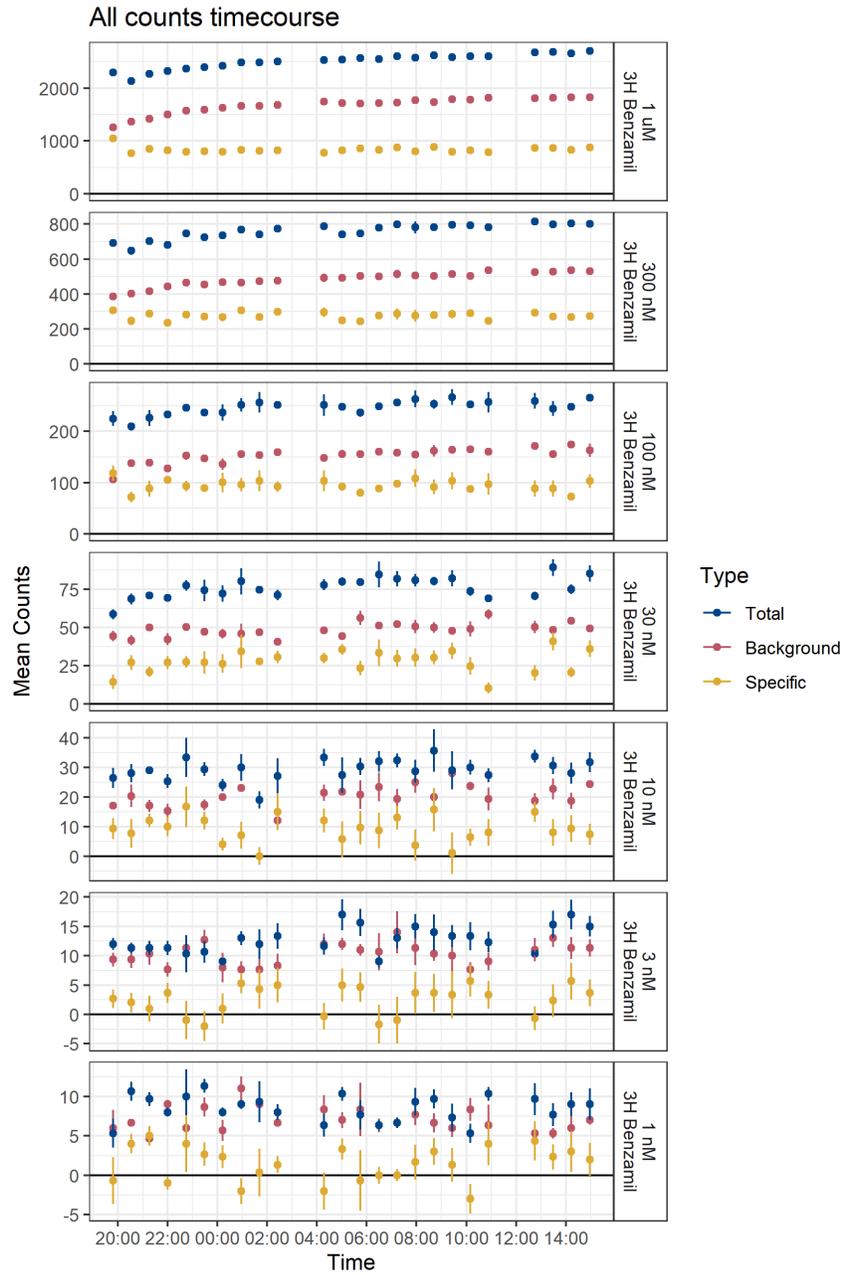
Figure B.9.: SPA data collected from nanodiscs does not result in better specific counts or lower total counts. Bars represent the standard error of the mean for three replicates, but are too small to see in the higher-concentration plots.

however, extremely important to note here that **none of the samples in this experiment had any ENaC**. There thus **cannot be** any specific counts — there is no protein for benzamil to bind! It is thus very concerning to me that the counts in this experiment follow the same trend as our proper, ENaC-containing experiments, with low but present "specific" signal.

Along this line, addition of ENaC nanodiscs to the nanoSPA bead mixture does not elicit any increase in counts, or even any noticeable difference from the ENaC-less experiment (Figure B.11).

B.2.5. What should be done?

In my opinion, nothing. This assay is a dead end, or at least requires much more work than the more promising flux assay.

I personally also would like to note that, despite how it is used in several labs at OHSU, SPA is fundamentally a *binding assay*. It *does not* provide any information about whether an ion channel is capable of passing currents, let alone the specificity of those currents. As such, it is not truly a functional assay. Spending more time working on an assay that doesn't even tell us what we need to know seems like a lose-lose to me.
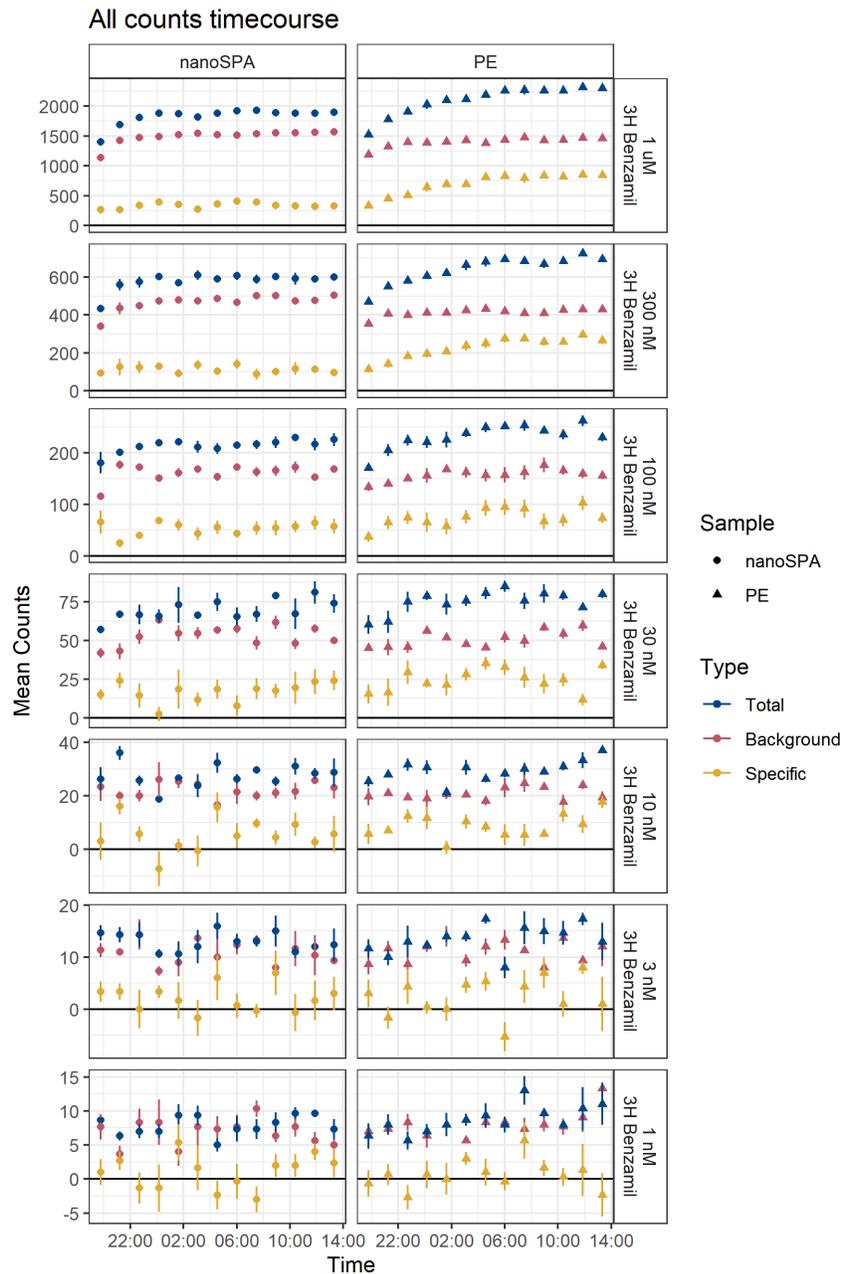
Figure B.10.: Comparison of nanoSPA and Perkin Elmer (PE) beads. In this context, "background" and "total" differ only in that "background" does not have any detergent added and "total" does. Note that nanoSPA beads quickly level off to a steady signal while PE beads increase for several hours. Note also that "specific" counts, which should be zero in all cases, are lower in nanoSPA beads than PE. Bars represent the standard error of the mean for three replicates, but are too small to see in the higher-concentration plots.
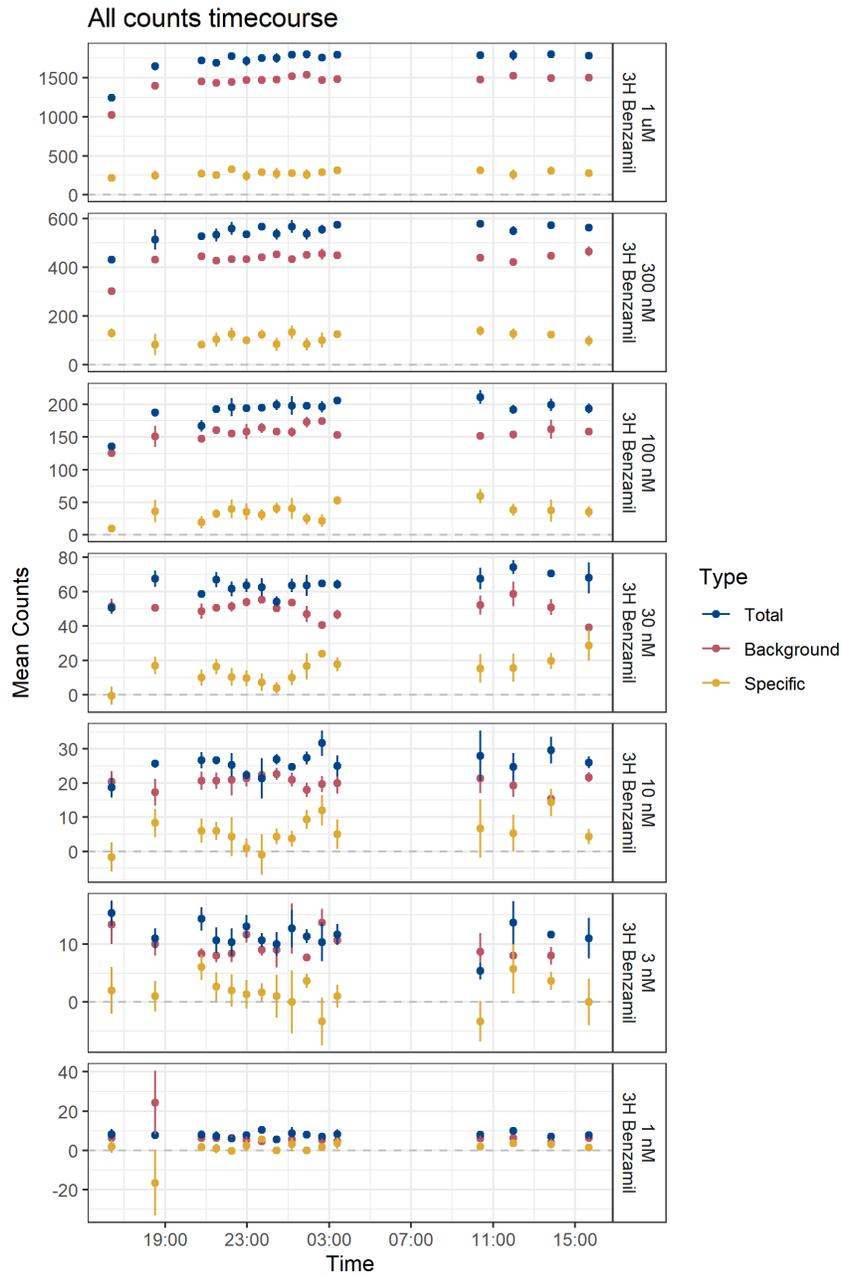
Figure B.11.: nanoSPA beads with ENaC added. Bars represent the standard error of the mean for three replicates, but are too small to see in the higher-concentration plots.

C. Image Processing

Below are the image processing workflows for each map. The human CKO digitonin map workflow includes more detail for the initial steps — these steps are the same for each map, and so are elided in the others. In each case, masks are contoured to 0.5. Additionally, particle and movie numbers are rounded for ease of comparison. See Table A.3 for precise numbers.

Human CKO

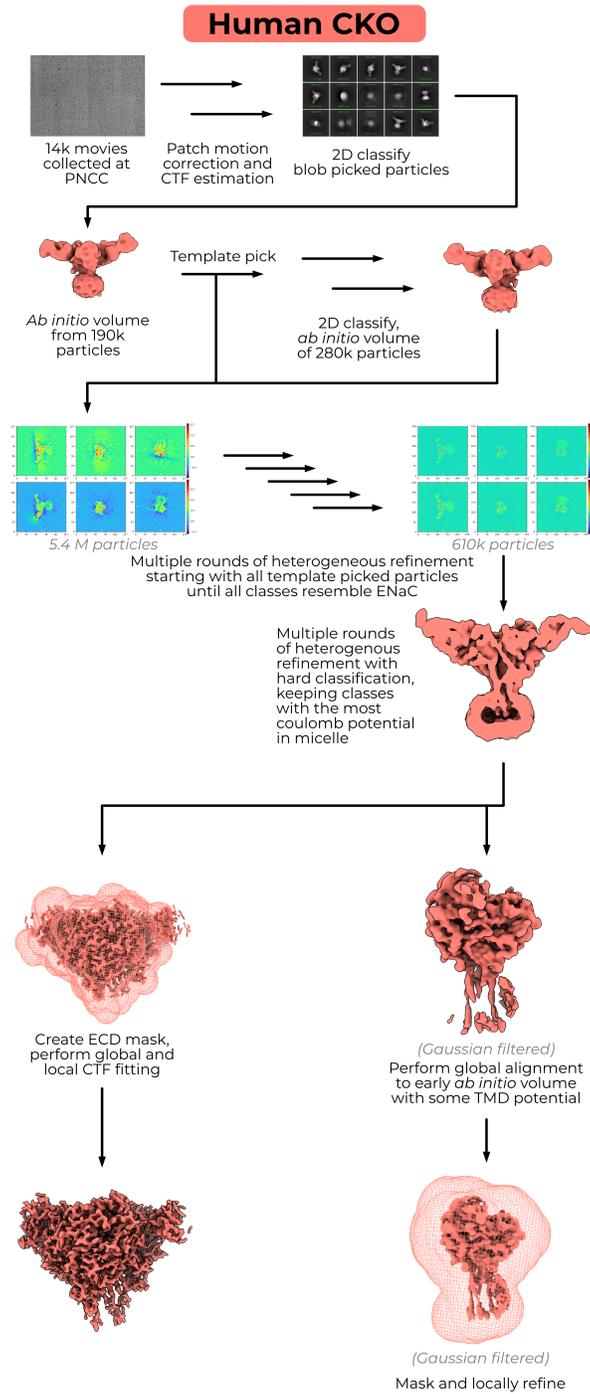14k movies collected at PNCC → Patch motion correction and CTF estimation → 2D classify blob picked particles

Ab initio volume from 190k particles → Template pick → 2D classify, *ab initio* volume of 280k particles

5.4 M particles → *610k particles*
Multiple rounds of heterogeneous refinement starting with all template picked particles until all classes resemble ENaC

Multiple rounds of heterogenous refinement with hard classification, keeping classes with the most coulomb potential in micelle

Create ECD mask, perform global and local CTF fitting

(Gaussian filtered)
Perform global alignment to early *ab initio* volume with some TMD potential

(Gaussian filtered)
Mask and locally refine

Figure C.1.: Human CKO processing pipeline. The TMD volumes are gaussian filtered to reduce noise.

CKO Nanodisc (No Fabs)

10k movies collected at S²C² Farm

Templates generated from CKO/DEG difab model with Fabs erased

Ab initio map from 2M particles

Het. refine into four classes, keep classes resembling ENaC

Het. refine into three classes, keep classes resembling ENaC

Non-uniform refine 730k particles

Het. refine into three classes, keep least symmetric class

Non-uniform refinement yields first asymmetric map without Fabs

330k particles

3D classification without alignment. Keep best classes, masked non-uniform refinement.

240k particles

Figure C.2.: Human CKO nanodisc pipeline. Masks are contoured to 0.5. Note that the CKO/DEG map was provided in the form of low-pass filtered templates for particle picking, but never to an alignment.
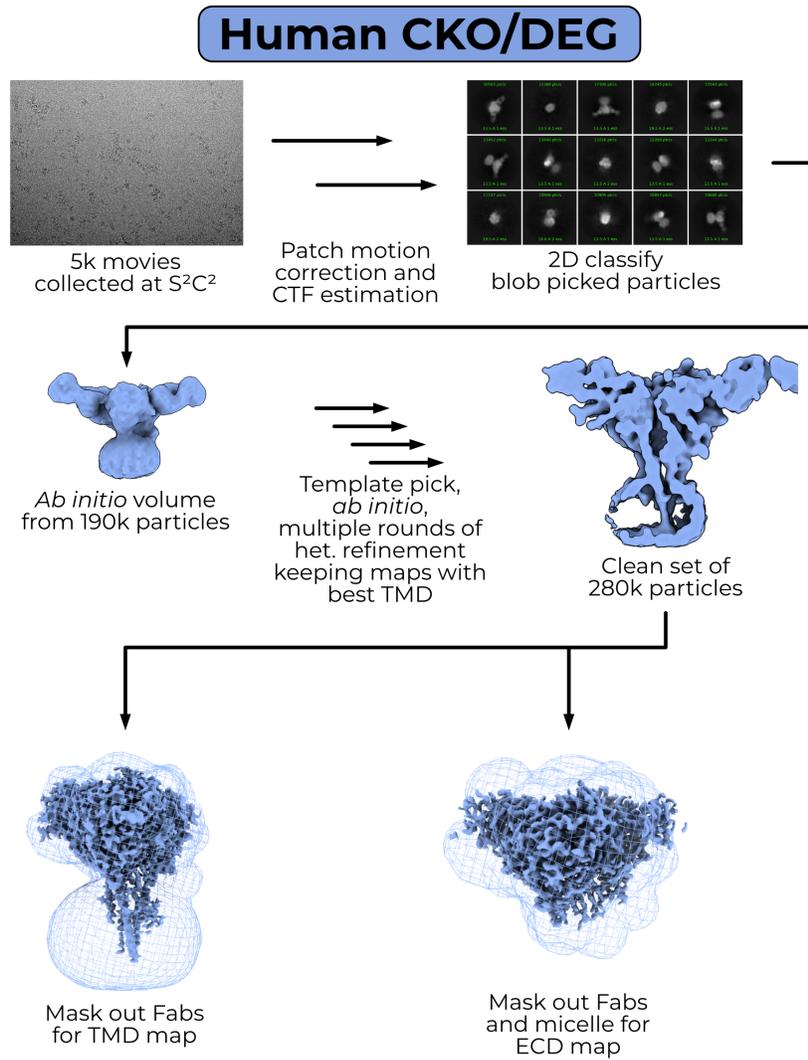
Human CKO/DEG

5k movies
collected at S²C²

Patch motion
correction and
CTF estimation

2D classify
blob picked particles

Ab initio volume
from 190k particles

Template pick,
ab initio,
multiple rounds of
het. refinement
keeping maps with
best TMD

Clean set of
280k particles

Mask out Fabs
for TMD map

Mask out Fabs
and micelle for
ECD map

Figure C.3.: Human CKO/DEG Difab pipeline.

Human CKO/DEG Monofab

6k movies collected at PNCC

Patch motion correction and CTF estimation

2D classify blob picked particles

Ab initio volume from 180k particles

Template pick, *ab initio*, multiple rounds of het. refinement until all classes are clean

Clean set of 420k particles

(Gaussian filtered) Mask out Fab for TMD map

Mask out Fab and micelle for ECD map
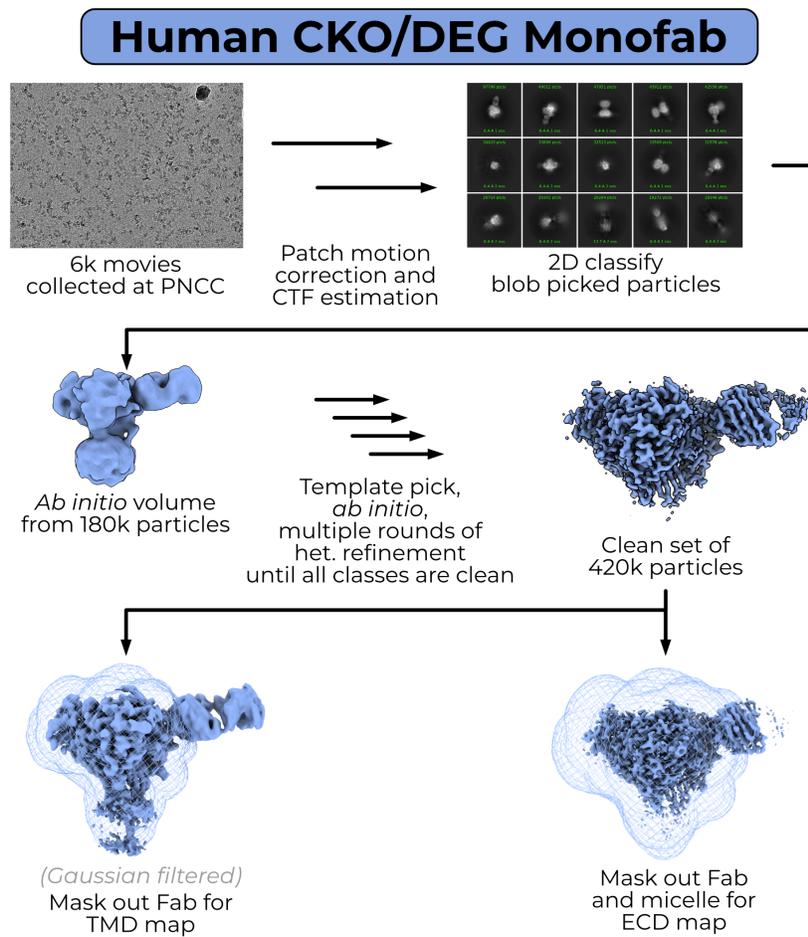
Figure C.4.: Human CKO/DEG Monofab pipeline.

Uncleaved Mouse

11k movies collected at Janelia Farm

Patch motion correction, CTF estimation, blob pick 920k particles

Generate three *ab initio* volumes, keep the best

Het. refine against three copies of good volume, keep cleanest result

Template pick, *ab initio*, multiple rounds of het. refinement until all classes are clean

Clean set of 500k particles

Mask out Fab for final map

Figure C.5.: Mouse uncleaved pipeline.

Figure C.6.: Mouse trypsin pipeline. ECD mask is contoured to 0.5. The chimeric mask used to refine the TMD is contoured at 0.5 (orange) and 0.125 (blue). Note that the ECD is not contained within the mask beyond 0.25.

D. Map Validation

These figures present validation of my 3D models. In each, panel A is a local resolution estimation for the α, β, and γ subunits moving from left to right. The color scales for this panel vary slightly in an attempt to capture the resolution range of each map. Panel B is a particle orientation distribution plot. Note that in this panel the color scheme is logarithmic. Panel C is a global and 3DFSC plot. The global FSC is plotted in black, while the histogram of directional FSCs are plotted as a grey histogram. The exact values of the histogram are presented below the histogram as black marks, jittered slightly to give a sense of overlap. Finally, panel D is the model-map FSC.
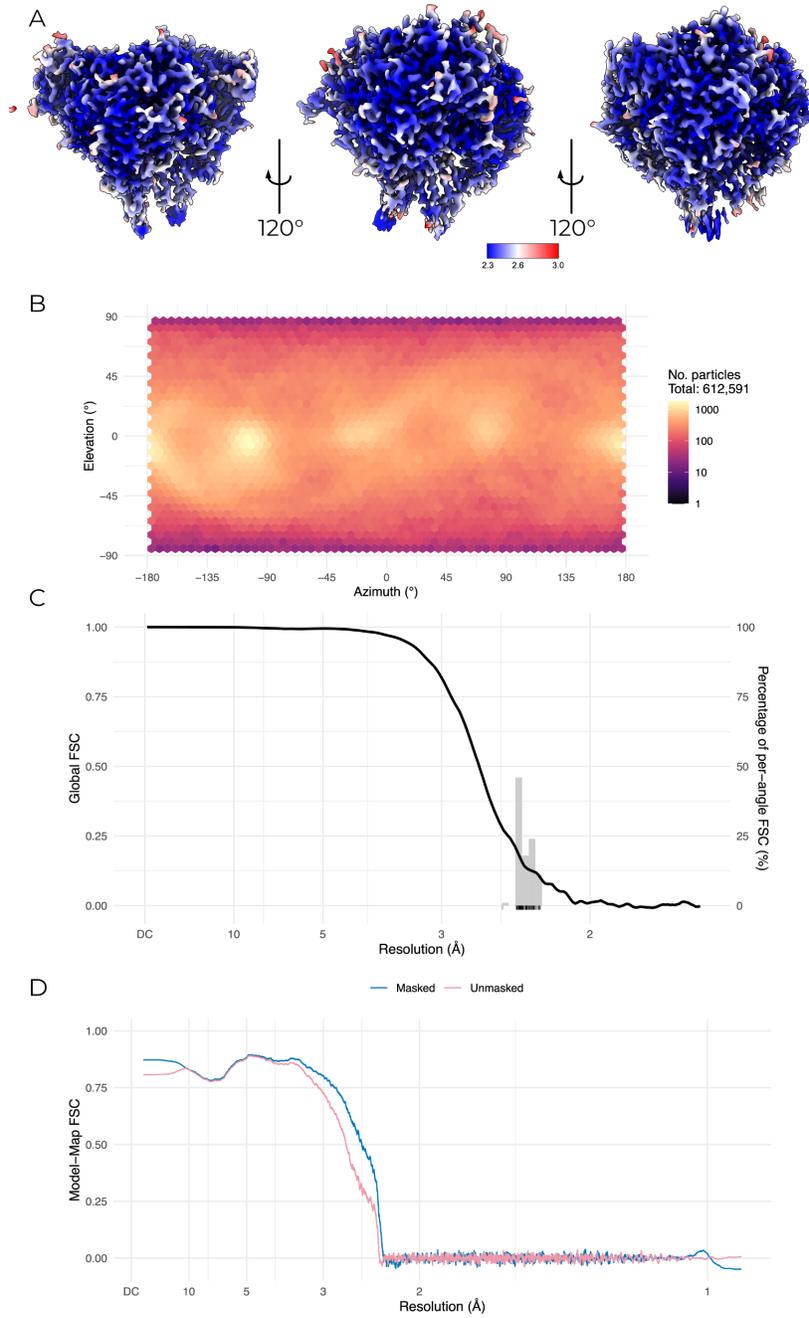
Figure D.1.: Validation of human CKO map and model.
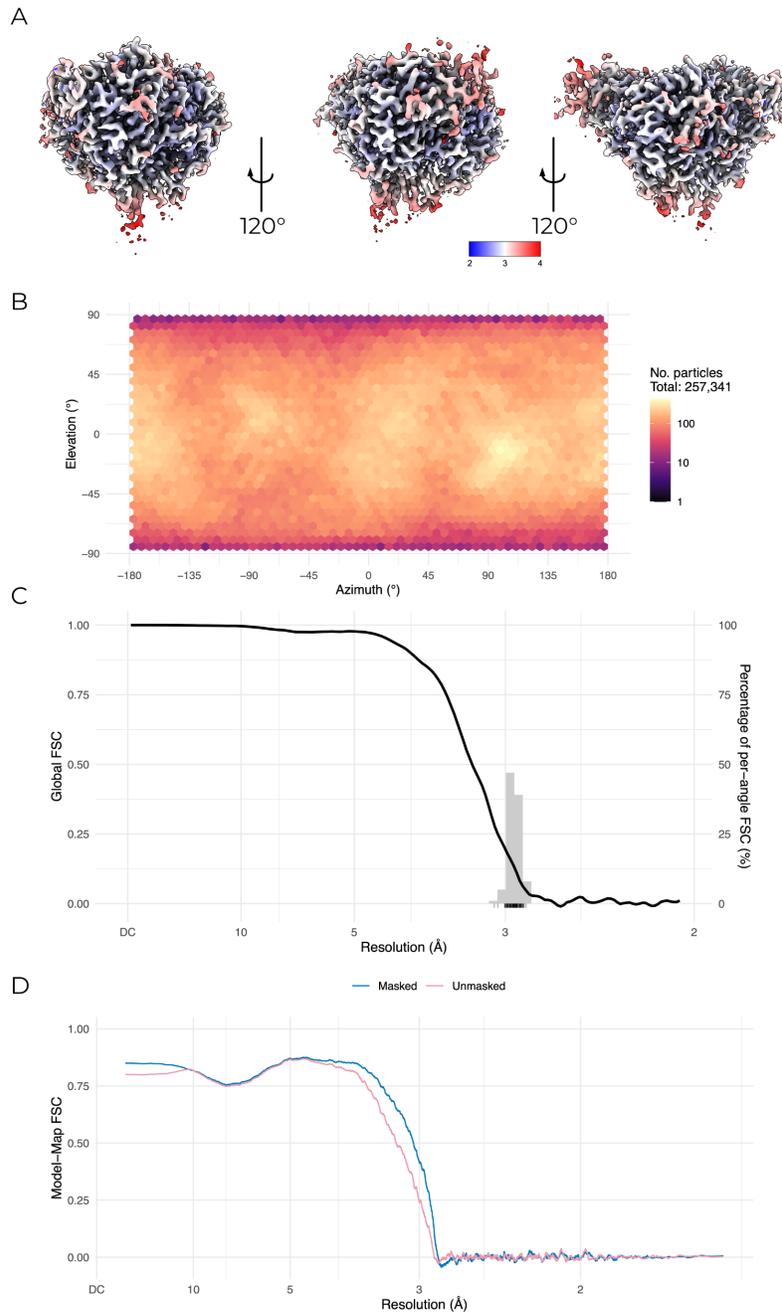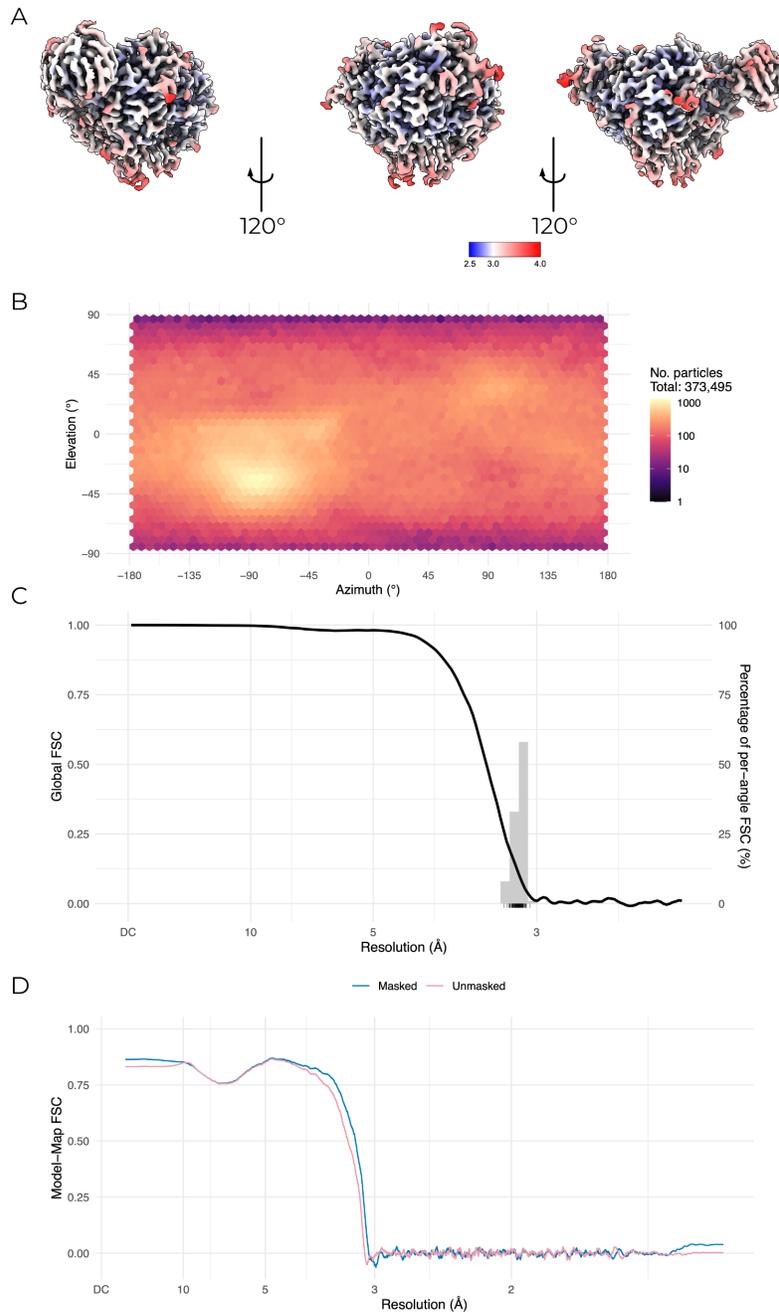
Figure D.2.: Validation of human CKO-DEG map and model.

Figure D.3.: Validation of human CKO-DEG monofab map and model.

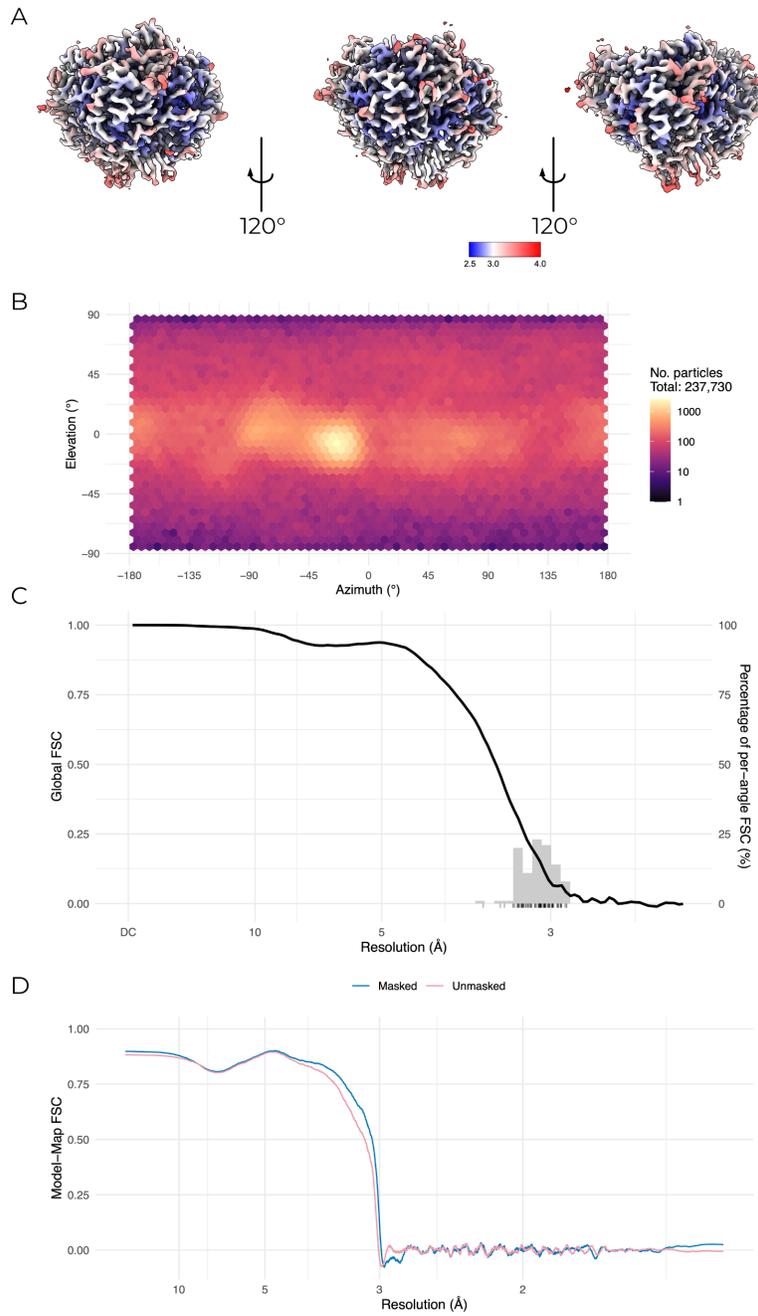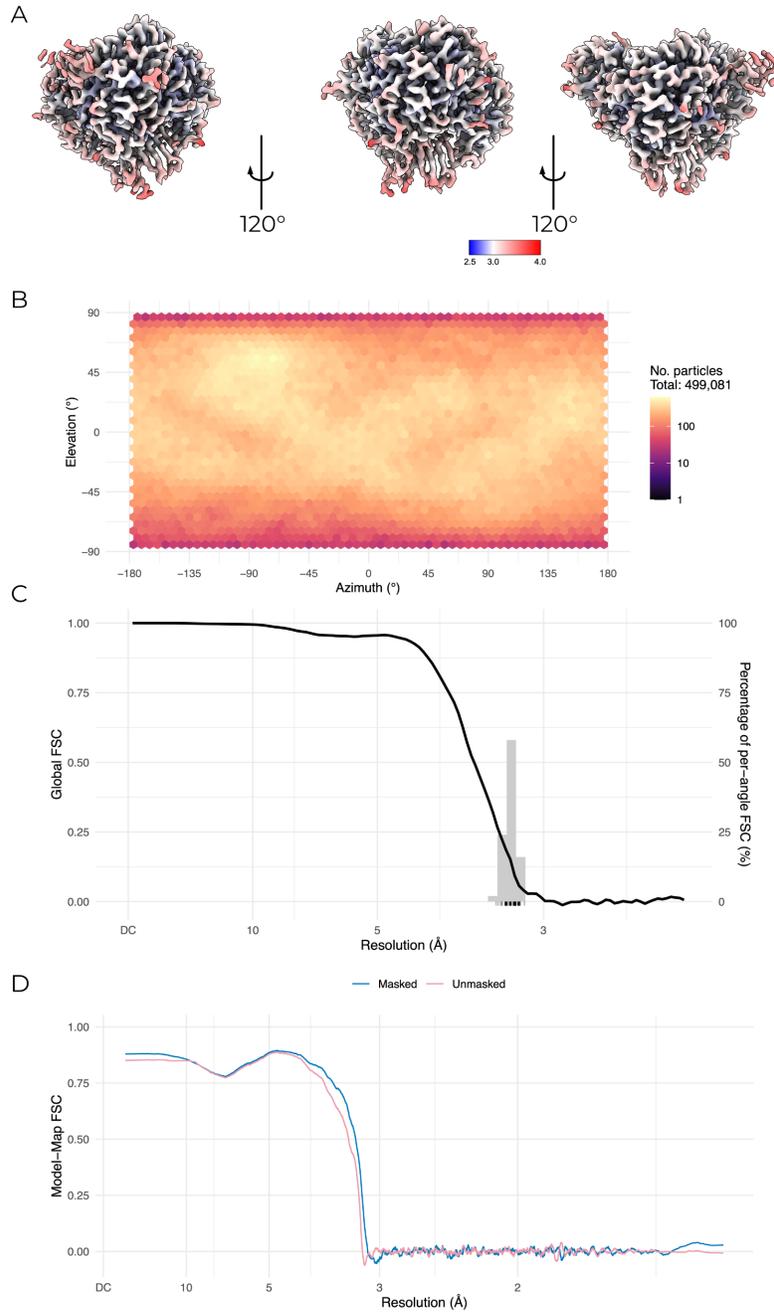Figure D.4.: Validation of human CKO nanodisc map and model.

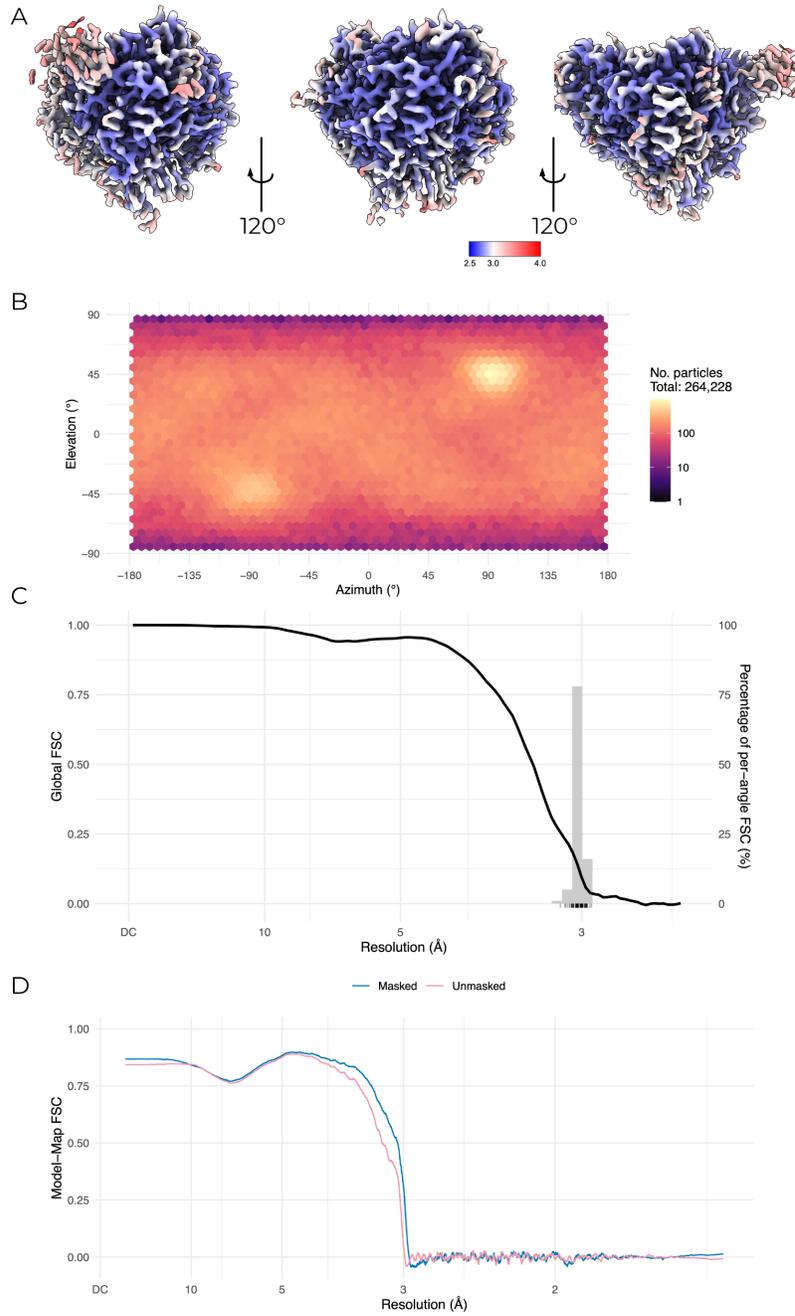Figure D.5.: Validation of mouse uncleaved map and model.

Figure D.6.: Validation of trypsin-cleaved mouse map and model.

E. Code and Computation

E.1. Appia

Modern structural biology makes extensive use of size-exclusion chromatography (SEC). The two types of SEC I encountered most often were *analytic chromatography*, in which samples are assessed for monodispersity and relative amount; and *preparative chromatography*, in which samples are purified based on their size. In an environment where only a heuristic assessment of these parameters is important (e.g., assessing whether a sample is homogeneous enough to make grids of, or whether a protein interacts with another) these parameters can be assessed by eye (Figure E.1). However, chromatography instrument manufacturers must include capacity for more complex analyses in their software. This necessarily makes the software more complex and arcane in the service of features that biochemists rarely need. To solve this mismatch I created Appia, a web-based chromatography visualization package[258]. In this section I will provide a brief summary of Appia's functionality and intended use, the installation process, and then some guidance for adding support for new chromatography instruments.

Appia can be installed via `pip`, or the source can be inspected at my github.

E.1.1. Structure

Appia is divided into two conceptual parts: the local processor and the web interface. The local processor is written entirely in python and processes all supported data formats into a unified Appia experiment. Several options are available at processing time, such as applying a scaling factor for various manufacturers or automatic trace plotting. Additionally, the local processor includes a user settings system. This system stores information such as flow rates to apply to a specific chromatography method and database login information. Experiments, to Appia, are collections of analytic and preparative traces.
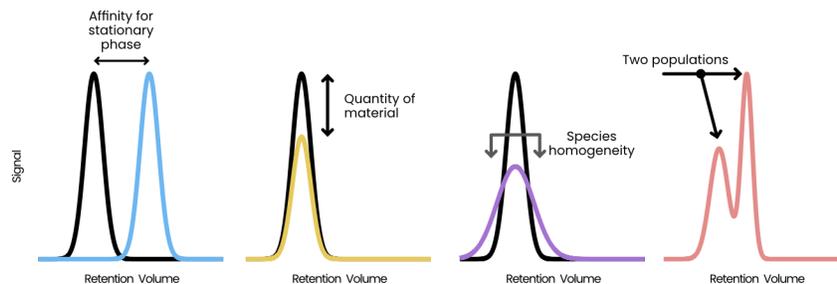
Figure E.1.: Heuristic chromatography parameters are easily as-
        sessed by eye. Users can approximate affinity for the
        stationary phase (size, in the case of SEC), quantity, ho-
        mogeneity, and the number of distinct species by inspect-
        ing peak shifts, peak height, peak width, and number of
        peaks respectively.

Importantly, Appia is agnostic as to the origins of the data in a sin-
gle experiment — experiments may contain traces from any number
of manufacturers and/or instruments, provided Appia has a proces-
sor for that manufacturer. The experiments are stored on the local
machine in both long (appropriate for ggplot2 and other grammar-of-
graphics plotting systems) and wide (appropriate for, e.g., Excel or
Prism) formats (Figure E.2). These experiments are packaged with
an experiment ID and uploaded to the other half of Appia, Appia
Web.

Appia Web provides a browser-based GUI and centralized trace
database. The database is a CouchDB database containing a simple
dictionary of experiments stored under their experiment IDs. The
browser-based GUI is written in python and plotly dash, and loads
user-requested data from the database and presents it using a series
of line plots. Analytic data is presented with one line per sample
per channel, while preparative data is presented as a single line
per injection with fractions highlighted by fill. Analytic data is also
presented with a normalization applied, such that the maximum of
each trace is 1 and the minimum is 0. The user may select a region
of the analytic traces and re-normalize them to set the maximum
over that range to 1, scaling the rest of the trace linearly (Figure E.3).
This normalization process is intended to aid in comparison of
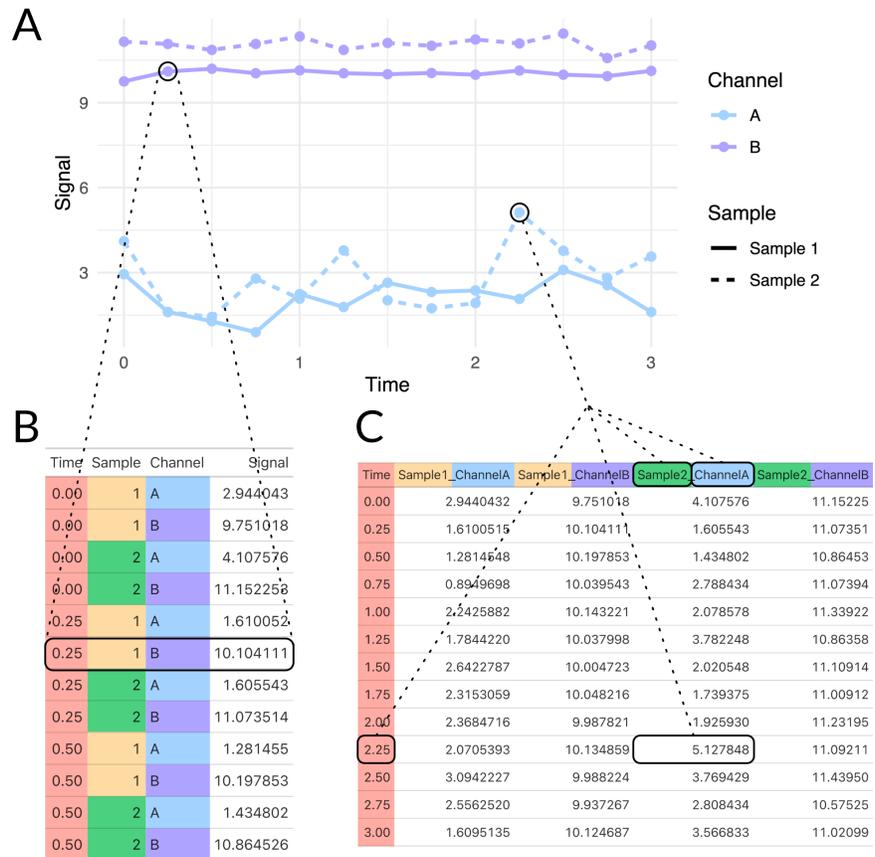relative peak heights between different samples which may have

Figure E.2.: Data formats saved by Appia and available for user download. Traces made up of individual samples (A) are represented as a single row in the long format (B). The wide format (C) instead represents the independent variable with its own column (Time, red), the response variable with the table body (Signal, white), and all other variables in column headers (various colors).

a different total amount of material, or to compare peaks within a trace compared to some standard peak height. Importantly, this process uses the simple readout of peak height. More complex analyses or analyses requiring quantitative accuracy are outside the
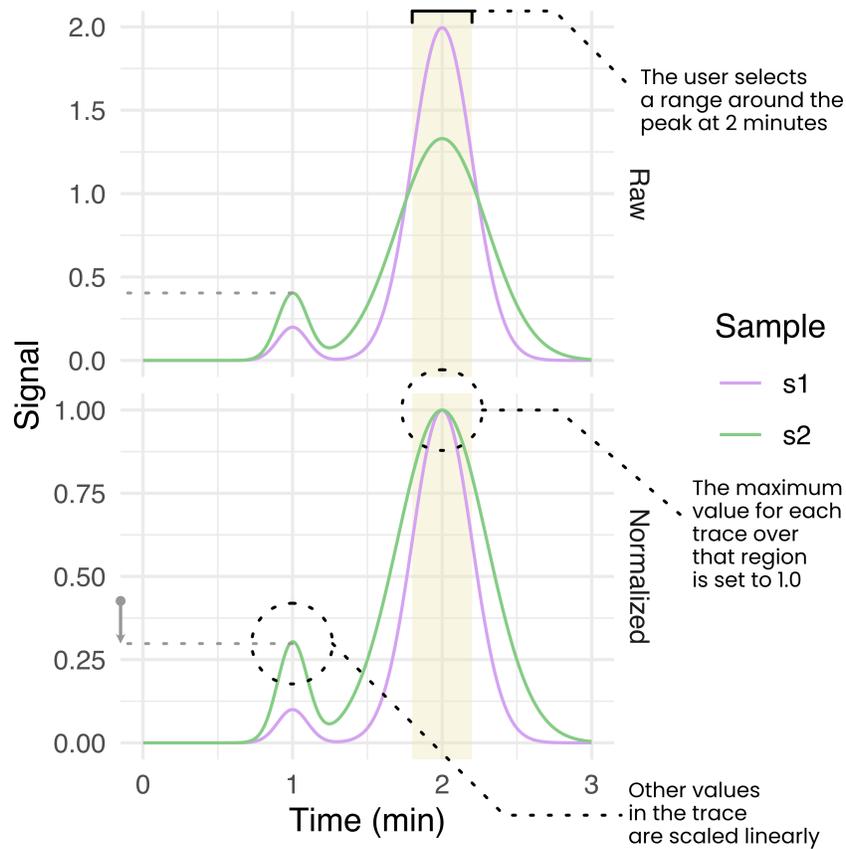

Figure E.3.: Appia's normalization process. A user-selected region is used to linearly scale all traces such that their maximum value over that region is 1.

E.1.2. Installation

Appia can be used solely to locally process chromatography data into a standard format for later plotting. However, we recommend installing a processing installation on each instrument computer and a single centralized Appia Web installation on some networked computer. This allows for single-click processing and upload of data to a central repository which users can then inspect, manipulate, and download from their personal computers without installing Appia. To facilitate this process, I have created Docker images for Appia Web. Images are available for both x86-64 and ARM architectures, and docker-compose templates are available in the project repository. Running one of these templates creates and networks the database and Appia Web automatically, requiring only that the user expose the correct ports (5984 for CouchDB and 8080 for Appia Web).

Below is an example process for installing Appia Web on a Windows PC which is accessible at `example.ohsu.edu`:

1. Install docker desktop
2. Download `install-appia-web_pc.ps1` and run it. Provide the desired configuration information
3. Run `docker-compose up -d`
4. Ensure that ports 5984 (database) and 8080 (web interface) are accessible

The Appia Web interface would now be available at example.ohsu.edu:8080/traces. All that is left is installing the processor on the instrument computer, a much simpler process:

1. Install python
2. Run `python -m pip install appia`
3. Run `appia utils --database-setup` and provide the information set up during Appia Web installation.

Now when a user finishes a chromatography experiment, they first export it to whatever format Appia expects (typically the default text format) and run (assuming the files end in .txt) `appia process *.txt -d` to upload the data to the web interface. The files will automatically be organized and stored on the local computer as well. This command can be wrapped in a script to avoid the need for users to interact with the command line.

E.1.3. Peak fitting with Gaussian Mixture Models

One useful form of analysis that Appia cannot perform on its own, but that can be performed with Appia's data output, is a Gaussian Mixture Model (GMM). In GMMs, we (perhaps obviously) treat our signal as a mixture of pure gaussian processes. This is especially useful when analyzing chromatography of species with known retention times. For instance, suppose that we know that a Fab binds a target, which shifts the target's retention time from 10 minutes to 9.8 minutes. The Fab's retention time is well outside this region, perhaps at 24 minutes, and so we can ignore unbound Fab. If we mix these proteins and look at the signal around 10 minutes, we might observe a peak like Figure E.4. We want to know what proportion of the target has shifted to the 9.8 minute retention time, since that will tell us how much has bound. However, it's impossible to tell this by looking at the data, or even by using manufacturer-written peak integrating algorithms. However, since we know the retention times of each component, we can model the mixture ourselves. I'll work this example in R, but it could just as easily be done in python, Matlab, or whatever modeling software the reader prefers.
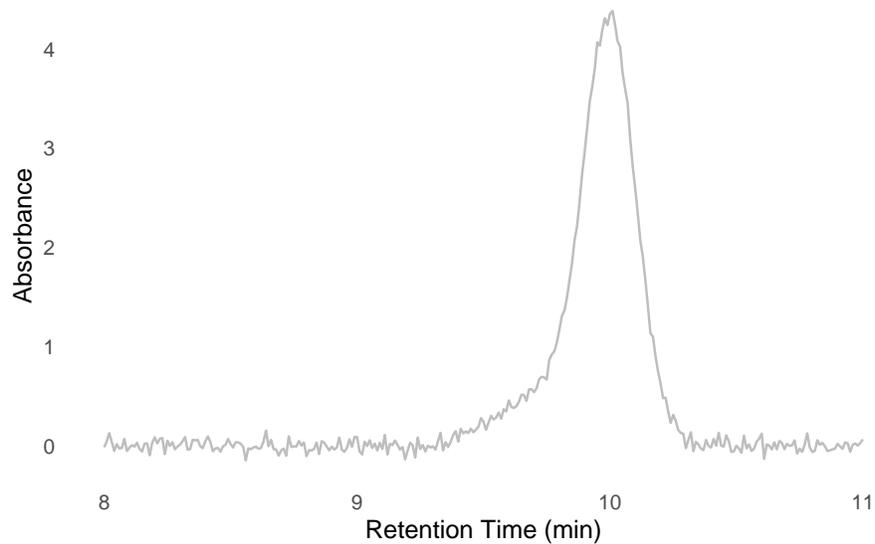

Figure E.4.: Example data of a mixture between a protein and a Fab.

Gaussian curves have two components: the mean and the standard deviation. In a chromatography context, the mean is the retention

time and the standard deviation the monodispersity of the peak (i.e., its width). We also need to model the amount of the component, which we can model with a simple scalar for each component. Performing a non-linear least squares fit to the data should give us these parameters

```r
# ub for unbound, b for bound
ub_rt <- 10
b_rt <- 9.8

# nls needs initial starting values,
# which we can eyeball.
# In this case it looks like our
# peak is mostly the unbound part
guesses <- list(
    'ub_amount' = 0.8, # real: 1.0
    'b_amount' = 0.4, # real: 0.3
    'ub_sd' = 0.15, # real: 0.1
    'b_sd' = 0.3 # real: 0.2
)

results <- nls(
    # This is the mixture model
    formula =
        signal
        ~ ub_amount * dnorm(
            rt, mean = ub_rt, sd = ub_sd
        )
        + b_amount * dnorm(
            rt, mean = b_rt, sd = b_sd
        ),
    data = example_trace,
    start = guesses
)
```

The `results` variable now contains the fitted values for each component. To see how well the data have been fit, we can plot each component separately, or their sum, as in Figure E.5.

```r
# helper function to extract values
get_val <- function(val_name) {
    coef(results)[[val_name]]
}
# function generator for the gaussians
plot_gauss <- function(scale, mean, sd) {
    \(x) scale * dnorm(x, mean = mean, sd = sd)
}
fit_unbound <- plot_gauss(
    get_val("ub_amount"),
    ub_rt, get_val("ub_sd")
)
fit_bound <- plot_gauss(
    get_val("b_amount"),
    b_rt, get_val("b_sd")
)

data_plot +
    geom_function(
        fun = fit_unbound,
        color = "blue",
        linetype = "dotted",
        n = 1000,
        linewidth = 1
    ) +
    geom_function(
        fun = fit_bound,
        color = "forestgreen",
        linetype = "dotted",
        n = 1000,
        linewidth = 1
    ) +
    geom_function(
        fun = \(x) fit_unbound(x) + fit_bound(x),
        color = "black",
        n = 1000
    )
```
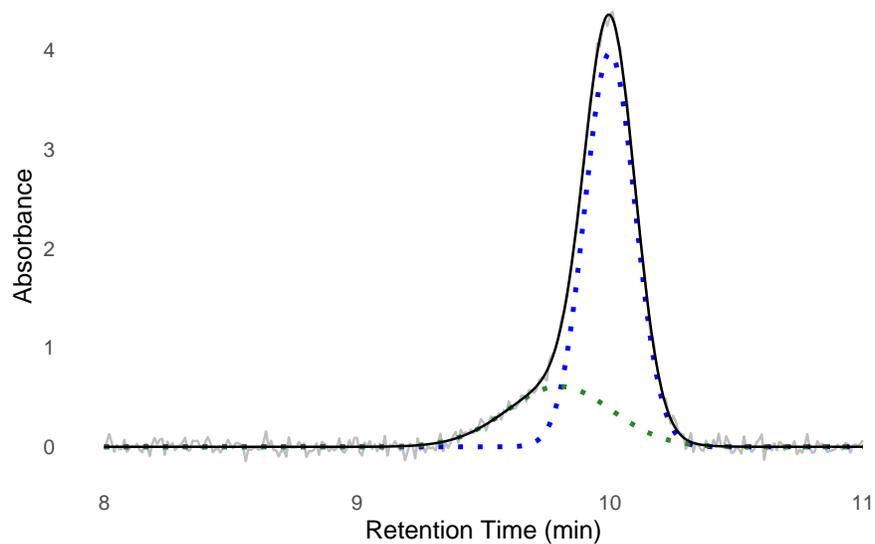
Figure E.5.: Fitted values plotted atop data. Bound and unbound are green and blue respectively, with the additive model in black.

We see the data fit well — we now have a model for the components of our experiment. To assess, for instance, the amount of protein in each peak, we could from here use the well-known equations for the area of a gaussian to find the peak area for each population, or just take their height as a heuristic. If this simple sum of gaussians model does not fit, you could consider adding a constant (for a constant non-zero baseline) or parameters for a linear function (for a linearly changing baseline) to the fit formula.

E.1.4. Writing a new processor

This section is intended for the advanced reader who wishes to add support for a chromatography instrument to Appia.

Processors are each a class which inherits from either `HplcProcessor` or `FplcProcessor` (for analytic or preparative data, respectively). At the time of writing, Appia supports the following data formats:

- Waters Empower `.arw` files
- Shimadzu `.asc` files

- Shimadzu `.txt` files
- Agilent `.csv` files
- Cytiva/GE `.csv` files

Your processor can perform any necessary setup in `__init__()`, but it must eventually run

```
super().__init__(
    filename,
    manufacturer = {appropriate_string},
    **kwargs
)
```

When Appia processes files, for each file, it creates an instance of every `Processor` child. These `Processors` all decide whether they can process a file using their `claim_file()` method, which you must implement. This method should accept a filename and return `True` if the processor thinks that is a type of file it can process and `False` otherwise. For instance, here is `WatersProcessor.claim_file()`:

```
@classmethod
def claim_file(cls, filename) -> bool:
    return filename[-4:].lower() == '.arw'
```

It simply checks whether the file ends in `.arw`. Depending on the data format for the new manufacturer, the method may require more complex checks, or you may have to add more specificity to other `claim_file()` methods.

If your processor claims the file, it will *automatically* run two methods: `prepare_sample()` and `process_file()`. The distinction between these is arbitrary, as they are both always run in sequence. It is intended that `prepare_sample()` collects metadata about the sample (method name, flow rate, sample set name, etc.) and `process_file()` creates the actual data frame. The data frame *must be in the long format*, should be stored in your processor's `df` attribute, and should have exactly the following column names:

- **mL**: the retention volume in mL.
- **Time**: the retention time in minutes.
- **Sample**: the sample name.

- **Channel**: the signal channel. Values in this column are arbitrary but should follow some kind of internal logic.
- **Normalization**: whether this row is normalized ("Normalized") or raw ("Signal").
- **Value**: the y-axis position for this row.

At this point, your `Processor` is done. As long as only one `Processor` claimed a file, the Appia `parser` will handle concatenation, plotting, and upload for you.

The parent classes provide a few conveniences for you. For example, the `flow_rate` and `column_volume` getters will prompt the user for the relevant info, if necessary, and then offer to store it in the user settings. It will also handle overrides of various parameters, which are accepted through `kwargs`. Additionally, `appia.processors.core` provides the `normalize()` function, which handles trace normalization. I encourage you to take a look at the `Processors` I've already written before embarking on writing your own.

I would encourage you to write a test as well, of course.

E.2. Model-building tools

I've written a few tools to aid with model building and general structure analysis. They're all available on my github.

`ca_bilder.py` creates a `.bild` file visualizing Cα shifts between two given models. Cylinders are drawn between each pair of Cα atoms, colored by the distance. The colors are scaled per-model, with the darkest color corresponding to the greatest shift. The models must be aligned before they are run through the script. If the models are multi-chain, cylinders will be drawn between the same chain ID. If the models are of two different proteins, you must provide a FASTA alignment and indicate which chain belongs to which sequence. These visualizations can be useful to highlight when certain domains move while others stay still, such as ASIC1's gating cycle (Figure E.6).

`check_for_glyc.py` searches a PDB model for the sequence NXS/T, the canonical N-linked glycosylation sequence. All asparagines matching this requirement are added to a ChimeraX command HTML file. Opening this file with ChimeraX creates a list of clickable asparagine names. Clicking these links orients the camera on the appropriate residue and removes the link from the list, creating a
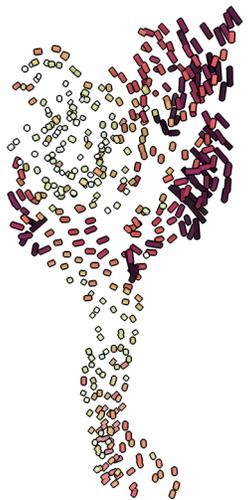

Figure E.6.: An image from `ca_bilder.py` highlighting the movement of the finger and thumb between the resting and desensitized states of ASIC1.

checklist of sorts. If the model and map are both open, this is a convenient way to step through all potential glycosylation sites in a model and assess whether they are indeed glycosylated. The user may then add sugars via the normal commands.

`model_map.py`, `orientation_plotter.py`, `phenix-table-reader.py`, and the three R scripts all read information from PHENIX or 3DFSC output and produce more aesthetically appealing plots. `phenix-table-reader.py` is a convenient way to automatically update a Table 1 (for instance, Table A.4) during the model building process. Output from the other scripts can be seen in Appendix D.

`mutator.py` checks the sequence of a model against a FASTA sequence and alerts the user to any mismatches. It also creates a ChimeraX command file which can be run to mutate the model to match the FASTA file. Any known deviations can be passed to the script as a `.txt` file with one mutation per line in a ChimeraX-like format. For instance, if chain A has a C→K mutation at position 260, the `.txt` file should have a line reading `/A:C260K`.

`translator.py` is currently ENaC specific, but could be generalized by a user. It is a simple script to translate residue numbers between the same gene of different organisms using a FASTA file. It is mostly useful when reading or writing and trying to incorporate data from multiple organisms. An example of this script in use:

```
$ translator.py mA260
Mouse αK260 => Human αK233
```

At time of writing, PHENIX adds waters to a seemingly random chain (perhaps based on proximity?) and with a number overlapping other residue numbers. This makes analysis extremely frustrating, since waters have the exact same atom specifier as other residues and are spread over the chains. `water_fixer.py` solves this problem by reading through a PDB file and moving all waters to chain H and numbering them starting at 1. This has the unfortunate side effect of waters not being numbered in a spatially coherent way, but it's better than nothing.